PERFORMANCE OF LAYERED STEERED SPACE-TIME CODES IN WIRELESS SYSTEMS

BY

AHMAD S. SALIM

A Thesis Presented to the

DEANSHIP OF GRADUATE STUDIES

KING FAHD UNIVERSITY OF PETROLEUM & MINERALS

DHAHRAN, SAUDI ARABIA

In Partial Fulfillment of the
Requirements for the Degree of

MASTER OF SCIENCE
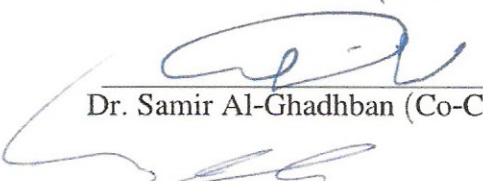
In

TELECOMMUNICATION ENGINEERING

January 2010

KING FAHD UNIVERSITY OF PETROLEUM AND MINERALS

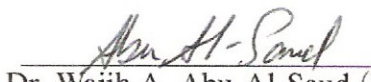## DHAHRAN 31261, SAUDI ARABIA

DEANSHIP OF GRADUATE STUDIES

This thesis, written by **Ahmad S. Salim** under the direction of his thesis advisor and approved by his thesis committee, has been presented to and accepted by the Dean of Graduate Studies, in partial fulfillment of the requirements for the degree of **MASTER OF SCIENCE In TELECOMMUNICATION ENGINEERING.**

THESIS COMMITTEE

Dr. Salam A. Zummo (Chairman)

Dr. Samir Al-Ghadhban (Co-Chairman)

Dr. Maan A. Kousa (Member)

Dr. Wajih A. Abu-Al-Saud (Member)

Dr. Yahya S. Al-Harthi (Member)

Department Chairman, Dr. Samir H. Abdul-Jauwad

Dean of Graduate Studies, Dr. Salam A. Zummo

26/1/10

Date

Dedicated to

My Late Father, Mother, Brothers, Sisters

and

Teachers

ACKNOWLEDGEMENTS

In the name of Allah, the Most Gracious and the Most Merciful

All praise is due to Allah (Subhanahu wa-ta'ala) who gave me the knowledge, courage and patience to accomplish this research, and I ask Him to accept it as an act of worship. I ask for His blessings, mercy, and forgiveness. May the peace and blessings of Allah be upon Prophet Muhammad (Peace Be upon Him).

My deep appreciation goes to my advisor Dr. Salam Zummo. He was always there when I needed him, and even with his tight schedule, he has always found time for me. I am extremely grateful to him for his prompt replies and his numerous proofreads. Also, I acknowledge, with deep gratitude the guidance of Dr. Samir Al-Ghadhban, my co-advisor. His support and guidance were very important, especially in Matlab. Dr. Samir has provided me with many subroutines that were essential to my work. I am also very grateful to my thesis committee members, Dr. Maan Kousa, Dr. Wajih Abu-Al-Saud, and Dr. Yahya Al-Harthi, for their care, cooperation and constructive advice.

I would like to express my deepest indebtedness to my late father, and to my mother, sisters and brothers for their constant prayers, guidance, encouragement and support throughout my career. They are the source of power, inspiration, and confidence in me. I also like to thank my colleagues and friends for their concern and help.

Acknowledgement is due to the King Fahd University of Petroleum and Minerals and the Department of Electrical Engineering, for the support and the excellent facilities given for this research, and for granting me the opportunity to pursue my graduate studies with financial support.

Contents

List of Tables

List of Figures

Nomenclature

Abbreviations

4G	Fourth generation
ISI	Inter symbol interference
AA	Antenna arrays
AA-RR	Antenna assisted round robin scheduling
AWGN	Additive white Gaussian noise
BER	Bit error rate
BLAST	Bell labs layered space-time architecture
BPSK	Binary phase shift keying
CCDF	Complementary cumulative distribution function
CDF	Cumulative distribution function
CIR	Channel impulse response
CSI	Channel state information
EGC	Equal gain combining
EPA-LSSTC	Equal power allocation LSSTC

FDMA	Frequency division multiple access
FEC	Forward error correction
FN	Frobenius norm
GLST	Generalized layered space-time coding
GSC	Generalized side lobe canceller
J	Number of users
LOS	Line of sight
LSSTC	Layered steered space time codes
MAP	Maximum Aposteriori Probability
MIMO	Multiple-Input Multiple-Output
ML	Maximum-Likelihood
MLSTBC	Multi-layered space time block codes
MLSTTC	Multi-layered space-time trellis codes
MMSE	Minimum mean square error
MRC	Maximal ratio combining
MRRC	Maximal-ratio receiver combining
N-MUST	Neural multiple source tracking
OBF	Opportunistic beamforming
OFDM	Orthogonal frequency division multiplexing
OPA-LSSTC	Optimum power allocation LSSTC
ORR	Opportunistic round robin

OSTBCs	Orthogonal space-time block codes
PA-LSSTC	Power allocation scheme for LSSTC
PDF	Probability density function
PF	Proportional fair
PGIC	Parallel group interference cancellation
PIC	Parallel interference cancellation
PSK	Phase shift keying
QAM	Quadrature amplitude modulation
QOS	Quality of service
RR	Round robin
RV	Random variable
SA-BTS	Smart antenna base station system
SDMA	Spatial domain multiple access
SGIC	Serial group interference cancelation
SIC	Successive interference cancellation
SINR	Signal-to-interference plus noise ratio
SISO	Single-input single-output
SLC	Side lobe canceller
SNR	Signal to noise ratio
ST	Space time
STBC	Space time block code

STTC	Space time trellis code
TDMA	Time division multiple access
VBLAST	Vertical Bell labs space-time
WLAN	Wireless local area network
ZF	Zero-forcing

Symbols

R_s	Rate of the STBC
H	Channel matrix
H̃	The reconstructed channel matrix
N_0	One-side power spectral density of the AWGN process
σ	Standard deviation
e_k	Estimation error
T	Symbol duration I_m
C_A	Alamouti's two-branch coding matrix
N_T	Number of transmit antennas
N_R	Number of receive antennas
M	Number of antenna arrays
K	Number of layers (groups)
m_k	Number of antenna arrays associated each STBC in a layer
P_T	Total transmission power

P_i	The transmit power of the ith sub-stream
$P_{L,i}$	The transmit power of the ith layer
P_s	The average transmit power per modulation symbol
L	Number of antenna elements per antenna array
τ_k	Delay of the kth signal
$\Psi_{n,m}$	The nm^{th} link's DOA
$d(m)$	The Distance between the elements of the mth antenna array
$\mathcal{CN}(0,1)$	circular-complex normal random variables with zero-mean
	And 0.5 variance per dimension
$\mathbf{Y}$	Received baseband data matrix
$\mathbf{W}$	$M \times M$ diagonal weight matrix
b_{mi}	The ith weighting gain of the mth antenna array
$\mathbf{c}_k$	The component STBC used at layer k
Ω	The optimum ordered detection set
$g_k(.)$	A map function defined to accommodate for any injection
	of i errors in the $k-1$ detected symbols
A_{k-1}^i	The event of having i errors in the symbols $\hat{S}_1 \sim \hat{S}_{k-1}$
$\mathbf{N}^{i,k}$	Equivalent noise random variable given that i detection errors
	exist in $k-1$ detected symbols
P_{e_k}	The probability of error on the kth layer
C_{LSSTC}	Instantaneous capacity of LSSTC

r	Spatial multiplexing gain
d	The diversity gain
$\mathbf{K}$	Sub-stream power allocation vector
$\mathbf{K}_L$	Layer power allocation vector
D_i	The SNR of the ith layer
ρ_i	The diversity order and of the ith layer
σ_t^2	The variance of the approximated Gaussian noise variable
$DRCi(t)$	Instantaneous Data Rate Of User i At The tth Time Slot
$R_{k,n}(t)$	Data rate of the nth channel for the kth user at the tth time slot
$\Gamma(k)$	The layer from which the kth symbol is transmitted
λ	The wavelength

Operators

$E[\cdot]$	Expectation operator
$Var[\cdot]$	Variance operator
$\lvert \cdot \rvert$	Matrix determinant
$(\cdot)^H$	Hermitian
$(\cdot)^T$	Transpose
$(\cdot)^*$	Conjugate
$I_0(\cdot)$	The modified Bessel function of first kind and order zero

General Notation

Vectors   Bold-Face, Lower-Case Letters

Matrices   Bold-Face, Capital Letters

THESIS ABSTRACT

Name: AHMAD S. SALIM

Title: PERFORMANCE OF LAYERED STEERED
        SPACE-TIME CODES IN WIRELESS SYSTEMS

Degree: MASTER OF SCIENCE

Major Field: TELECOMMUNICATION ENGINEERING

Date of Degree: January 2010

As the amount of applications and subsequent users grows for limited bandwidth channels, more reliable and spectrally efficient communication methods are needed. In this work we study a recently proposed multiple-input multiple-output (MIMO) system called the Layered Steered Space-Time Codes (LSSTC) that combines the benefits of vertical Bell Labs space-time (VBLAST) scheme, space-time block codes (STBC) and beamforming. The aim of this research is to investigate the analytical error performance of single-user LSSTC. The analysis will result in a very accurate analytical approximation of the symbol error probability of LSSTC systems for several modulation techniques. Also, we study the error performance when using power allocation in LSSTC. The analytical results is supported by computer simulations. It is shown that there is a good match between the theoretical and simulated results. In addition, the tradeoff between several parameters of LSSTC is analyzed. Finally, we investigate the use of LSSTC system in multi-user environments, in which the multi-user diversity will result in improving the system's capacity and error performance. It is shown the most suitable scheduling criteria for LSSTC is the one that maximizes its capacity

Keywords*: MIMO, Diversity, Multiplexing, Beamforming, VBLAST, STBC, Antenna Arrays, LSSTC, Tradeoff.*

King Fahd University of Petroleum and Minerals, Dhahran.

January 2010

Abstract (Arabic)
ملخص الرسالة

الإسم: أحمد سهيل سليم سليم

عنوان الرسالة: أداء الشيفرات المكانية-الزمانية الطبقية الموجهة في النظم الاسلكية

الدرجــــــــــــــة: الماجستير في العلوم

التخصص الرئـيسي: هندسة الإتصالات

تاريخ الدرجة العلمية يناير - ٢٠١٠ م

إنّ ازديادعدد التطبيقات و المستخدمين في نطاق ترددي ضيق أدى إلى إزدياد الحاجة لأنماط إتصالات ذات كفاءة عالية. في هذا البحث ندرس نموذج جديد للنظم متعددة المدخلات والمخرجات (MIMO) يسمى الشيفرات المكانية-الزمانية الطبقية الموجهة (LSSTC) والذي يجمع إيجابيات ثلاثة من الأنظمة المقترحة في أبحاث سابقة، وهي الشيفرات المكانية-الزمانية (STBC) و نظام مختبرات بيل العمودي للشيفرات المكانية-الزمانية (VBLAST) و نظام توجيه الهوائيات. ويهدف هذا البحث إلى بحث نسبة الخطأ في الإرسال للنظام المقترح بالنسبة لمستخدم منفرد، حيث تم إشتقاق معادلات لحساب نسبة الخطأ. أيضاً تم بحث نسبة الخطأ في حالة التوزيع الغير المتكافئ للطاقة بين طبقات النظام المتعددة. بالإضافة إلى ذلك، تم دراسة موازنة بين خصائص النظام المختلفة. وتم اختبار هذا النظام بإستخدام محاكاة حاسوبية، كان من نتائجها، إثبات صحة النتائج النظرية لمطابقتها لنتائج المحاكاة.

كما تم تقييم أداء النظام في بيئة متعددة المستخدمين ومايتعلق بذلك من جدولة المستخدمين الذي يعمل على تحسين سرعة و أداء النظام، و قد تبين أن الطريقة الأنسب لجدولة المستخدمين في النظام المقترح تكون بإختيار المستخدم الأعلى سرعةً.

درجة الماجستير في العلوم
جامعة الملك فهد للبترول والمعادن
الظهران، المملكة العربية السعودية
يناير - ٢٠١٠ م

Chapter 1

Introduction

Wireless devices such as mobile phones have been gaining more and more popularity mainly because of their mobility. Though voice was the only service available on early phones, more recently internet and multimedia services including pictures and videos have started to emerge. The demand for these services is on the rise. At the same time wireless networks still have to compete with their wired counterparts mainly because of their high data rates. Wireless networks are attractive for their mobility, but the high data rates available on the wired networks still seem to be unreachable in wireless networks. A requirement for high data rates directly translates into a wider bandwidth requirement which is not feasible because of the limited radio spectrum. The increasing adoption of multimedia and demand for mobility in computer networks have resulted in a huge wireless research effort in the recent years. Given the limited radio spec-

trum and unfriendly propagation conditions, designing reliable high data rate wireless networks has lots of problems.

The maximum capacity of a radio channel with a given bandwidth is limited by the Shannon formula [1]. The Shannon limit gives the maximum limit on transmission rate but does not say anything about how to achieve that limit. Various techniques have been proposed to counter the problem of propagation conditions, and to achieve data rates that are very close to the Shannon limit. One of these techniques is using multiple-input multiple-output (MIMO) systems which uses antenna arrays at both the transmitter and the receiver. Wolniansky *et al*. has proposed in [2] the well-known MIMO scheme, known as vertical Bell Labs space-time (VBLAST). In VBLAST architecture, parallel data streams are sent via the transmit antennas at the same carrier frequency. Given that the number of receive antennas is greater than or equal to the number of transmit antennas, the receiver employs a low complexity method based on successive interference cancellation (SIC) to detect the transmitted data streams. In this manner, VBLAST can achieve high spectral efficiencies without any need for increasing the system's bandwidth or transmitted power.

While MIMO systems such as VBLAST can improve the system capacity greatly [3], it is difficult to implement antenna arrays on hand-held terminals due to size, cost and hardware limitation[4], also it has poor energy performance and does not fully exploit the available diversity. In order to overcome these problems,

Alamouti has presented in [4] a new scheme called space-time block codes (STBC) with two transmit and one receive antennas that provides the same diversity order as maximal-ratio receiver combining (MRRC) with one transmit and two receive antennas. This scheme can be generalized to two transmit antennas and M receive antennas to provide a diversity order of $2M$. Similar work was considered in [5] where space-time trellis codes (STTC) were used as the component codes. With the tempting advantages of VBLAST and STBC, many researchers have attempted to combine these two schemes to result in a multilayered architecture called MLSTBC [6] with each layer being composed of antennas that correspond to a specific STBC. This combined scheme arises as a solution to jointly achieve spatial multiplexing and diversity gains simultaneously. With MLSTBC scheme, it is possible to increase the data rate while keeping a satisfactory link quality in terms of symbol error rate (SER) [7].

Another powerful scheme called beamforming, has been combined with MLSTBC in [8] to produce a hybrid system called the layered steered space time codes(LSSTC), in which beamforming was added to MLSTBC to improve the performance of the system by focusing the energy towards one direction, where the antenna gain is increased in the direction of the desired user, whilst reducing the gain towards the interfering users. In multi-user systems, scheduling can be used to increase the system capacity as in [9], where it was shown that the independence of fading among users in multi-user environments that results in

multi-user diversity is capable of increasing the system capacity. The outline of this chapter is as follows. Section 1.1 addresses a general background on wireless channels, and starts by discussing the characteristics of radio channels such as attenuation, multipath, the Doppler effect and fading, followed by an introduction to transmit diversity techniques. A detailed literature survey on the subject is presented in Section 1.2. In Section 1.3, we list the thesis contributions. Finally, Section 1.4 gives an outline for the rest of the thesis.

1.1 Background

1.1.1 Propagation Characteristics of Wireless Channels

In a real environment radio waves from mobile devices travel through the air, buildings and other obstacles. Reflections from different objects cause the waves to travel via multiple paths to the receiver. The movement of objects in the channel or that of the receiver cause an apparent shift in the carrier frequency. A reliable communication system tries to overcome or take advantage of these channel perturbations. In the following subsections, we will discuss some of those perturbations as follows.

Attenuation

Attenuation is the loss of the average received signal power [10]. Factors respon-
sible for attenuation are the distance between the transmitter and receiver, the
obstacles in between, their physical properties, etc. The presence of very large
obstacles such as buildings, hills, etc. causes another type of attenuation known
as log-normal shadowing [11]. Geometric models have been proposed to explain
these large-scale power losses but statistical models are often used because of
their accurate description of particular real environments. Statistically, the atten-
uation is considered as a random variable having a well known distribution. A
common formula used to model attenuation is [3]

$$PL(d)[dB] = \overline{PL}(d_0) + 10n \log \left(\frac{d}{d_0} \right) + X_\sigma \tag{1.1}$$

where X_σ is a zero mean Gaussian distributed random variable (in dB) with stan-
dard deviation σ (also in dB) and accounts for the log normal shadowing effect.
The path loss at any arbitrary distance d is statistically described relative to the
close-in reference point d_0, the path loss exponent n, and the standard deviation
σ. The exponent n can have values from 1.6 (in indoor line of sight) up to 6 (in
highly builtup cites).

The Doppler Effect

When there is a relative movement between the transmitter and receiver, the carrier frequency, as perceived by the receiver, gets shifted by some amount; this is known as the Doppler effect [3]. The amount of frequency shift depends on the relative mobility, the direction of movement and the frequency of the carrier. Another parameter, often used to characterize the time varying nature of the channels is the coherence time which is related to the Doppler shift [3].

Multipath Fading

Radio waves traveling along different paths arrive at the receiver at different times with random phases and combine constructively or destructively. The net result is a rapid fluctuation in the amplitude of the received signal in a short period of time or distance travelled. However, the large-scale average path loss remains constant. Multipath propagation had previously been considered a problem, but in MIMO systems it is exploited to achieve higher capacity. The multipath structure of a channel is quantified by its delay spread or by its root-mean-square (RMS) value [3]. A channel having delay spread less than the symbol period of transmission offers frequency-nonselective attenuation, and a larger value of delay spread means there is a frequency-selective variation in the channel. Another parameter, the coherence bandwidth is also often used to describe the frequency selectivity [3].

The result of multipath and the Doppler shift is fading. Fading is the rapid variation in signal strength over a short distance or time interval where the large scale attenuation is constant. A fade can be flat or frequency selective depending on the multipath structure of the channel, and slow or fast depending on the Doppler effect.

Slow fading describes the channel where the symbol transmission time T_s is less than the channel coherence time. In this regime, the amplitude and phase change imposed by the channel can be considered roughly constant over the period of use. Slow fading can be caused by events such as shadowing, where a large obstruction obscures the main signal path. The amplitude change caused by shadowing is often modeled using a log-normal distribution with a standard deviation according to the log-distance path loss model. Fast fading occurs when the coherence time of the channel is small relative to T_s. In this regime, the amplitude and phase change imposed by the channel vary considerably over the period of use.

A fade can be flat or frequency selective depending on the multipath structure of the channel [3]. In flat fading, the coherence bandwidth of the channel is larger than the bandwidth of the signal. Therefore, all frequency components of the signal will experience the same magnitude of fading. In frequency-selective fading, the coherence bandwidth of the channel is smaller than the bandwidth of the signal [12]. Different frequency components of the signal therefore experience

decorrelated fading.

Fading Distributions

The fading effect is usually described statistically using the Rayleigh distribution. The amplitude of the sum of two quadrature Gaussian signals follows the Rayleigh distribution whereas the phase follows a uniform distribution. The probability distribution function (PDF) of a Rayleigh distribution is given by

$$p(r) = \frac{r}{\sigma^2} \exp\left(-\frac{r^2}{2\sigma^2}\right), \tag{1.2}$$

where σ^2 is the average power of the received signal. In environments where the chance of a line-of-sight path is high, the fading follows a Ricean distribution with PDF given by:

$$p(r) = \frac{r}{\sigma^2} \exp\left(-\frac{(r^2 + A^2)}{2\sigma^2}\right) I_0\left(\frac{Ar}{\sigma^2}\right), \tag{1.3}$$

where A is the peak amplitude of the dominant path and $I_0(.)$ is the modified Bessel function of the first kind and order zero. Figure 1.1 shows the PDFs of Rayleigh and Ricean distributions.
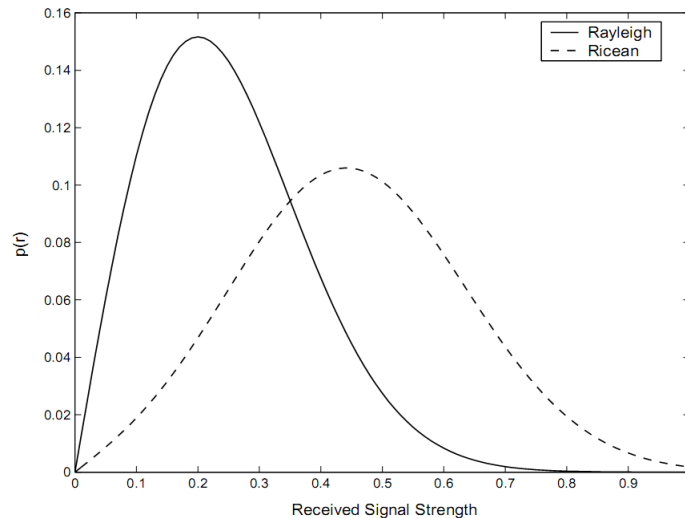
Figure 1.1: PDFs of Rayleigh and Ricean distributions.

1.1.2 Diversity

Diversity is a powerful technique that provides link improvement at low cost. In fading channels, there is a high probability that a path will be in a deep fade at a time instant, thus the path will suffer from errors. A natural way to suppress these errors is to reduce the probability of signal fading at any time instant. This is done by providing multiple independently faded versions of the transmitted signal (diversity branches) at the receiver in order to produce a better version of the transmitted signal, thus ensuring more reliable communication as long as one of the received versions is not in a deep fade. Consider two independently faded versions of the transmitted signal. The probability distribution of the fading determines the probability of outage, which is defined as the probability of the signal envelope falling below a certain threshold [3]. If the probability of sig-

nal outage i.e., $P(r_i < R_{th}) = 0.2, i = 1, 2$ then the probability that both signals will

fade simultaneously is $P(r_1 < R_{th}, r_2 < R_{th}) = 0.2^2 = 0.04$.

There are many ways of combining the diversity branches [3]. In selection diversity (SC), the best diversity branch is selected for detection. In maximal ratio combining (MRC), the signals from each diversity branch are aligned in phase, and weighted by their channel gains before adding them coherently. If the weights used in MRC is set to be the same for all the branches, then the resulting combining scheme is called equal gain combining (EGC) [13]. Different diversity branches can be provided using one of the following techniques:

- Time diversity: Because the channel characteristics change with time, another replica of the signal can be sent after a certain time interval. This time interval must be longer than the coherence time of the channel [3]. This time separation is required in order to ensure that the channel characteristics have changed enough so that they can be uncorrelated. While highly effective in fast fading environments, time diversity is not as effective in slow fading channels unless a large decoding delay can be tolerated. A coding structure known as interleaving is often used to realize time diversity where the receiver knows the code before any transmission takes place.

- Frequency diversity: In this technique, the signal is transmitted over more than one frequency which are separated by more than the channel coherence bandwidth which is the bandwidth over which the channel response

is highly correlated [3].

- Space diversity: Here, multiple antennas can be used at the transmitter and/or the receiver. The separation between the antennas must be more than the coherence distance, which is about half of the signal's wave length [14]. In this case, the channel gains between different antenna pairs fade independently and independent signal paths are created at the receiver.

1.2 Literature Survey

1.2.1 Multi-Antenna Systems

Recent research on wireless communication systems has shown that using multiple antennas at both the transmitter and the receiver offers the possibility of higher data rates compared to single antenna-systems. The information-theoretic capacity of MIMO channels was shown to grow linearly with the minimum of the numbers of transmit and receiver antennas in rich scattering environments, and at sufficiently high signal-to-noise (SNR) ratios [15]. However, for single-input single-output (SISO) channels, the capacity increases logarithmically with SNR. Thus, a significant capacity increase can be achieved using MIMO systems without any increase in transmit power or expansion in the bandwidth [16]. In the following, we will review some of the major contributions in multi-antenna systems.

Diversity-Based Systems

In 1998, Alamouti designed a simple transmission diversity technique for systems having two transmit antennas called space-time block codes (STBC) [4]. This method provides full diversity and requires simple linear operations at both transmission and reception side. The encoding and decoding processes are performed with blocks of transmission symbols. The Alamouti's simple transmit diversity scheme was extended in [17] and [18] with aid of the theory of orthogonal designs to larger number of transmit antennas. These codes are referred to in the literature as orthogonal space-time block codes (OSTBCs).

Multiplexing-Based Systems

The Bell Labs Layered Space-Time Architecture (BLAST) is a narrowband point-to-point communication architecture for achieving high spectral efficiency. BLAST architecture was one of the first spatial multiplexing systems; it is also called layered space-time (LST).

Flat fading MIMO channels having multiple transmit and receive antennas were shown to offer relatively huge spectral efficiencies compared to SISO channels [19, 20]. To achieve this capacity, diagonal BLAST (DBLAST) was proposed by Foschini in [19], which utilizes multi-element antenna arrays at both ends of wireless link. However, the complexity of D-BLAST implementation led to the vertical BLAST (VBLAST) which is a modified version of BLAST [2]. Two nulling

criteria, namely zero-forcing (ZF) [21] and minimum mean squared error (MMSE) are utilized as detection algorithms. Originally, the BLAST detection scheme was based on a successive interference cancellation (SIC) [2, 21, 22], and later on, a parallel interference cancellation (PIC) scheme was proposed in [23].

BLAST detectors including both SIC and PIC suffer from the error propagation problem, so that they lead to the poor energy efficiency which can be improved if the previously detected layers were perfectly canceled because the following layers depend highly on the result of the previous detected signals. The error propagation problem of BLAST detectors can be reduced with channel coding and interleaving [24, 25]. In [6], decoding algorithms for multi-layered space time block codes (MLSTBC) were compared. In addition, a scheme that combines serial group interference cancellation (SGIC) and parallel group interference cancellation (PGIC) was proposed. It was shown in [6] that the optimal performance of MLSTBC can be achieved by using sphere decoding (SD).

Beamforming-Based Systems

In adaptive antenna systems multiple antennas are used to receive (or transmit) the same information. Instead of using only one antenna to receive (or transmit) the radio signal, combinations of multiple antennas output (or input) are used to focus the energy towards one direction. The adequate combination of the signals received by the different antennas results in a better link quality for a given

transmitted power, or a lower transmitted power required for a given link quality [26]. The same concept of adaptive antennas can be found under different names such as smart antennas, or adaptive beamforming [27]. The basic concept behind adaptive antennas is to change the standard antenna that has an omnidirectional radiation pattern for a new one with a directive radiation pattern that is continuously adapted to the environment [26].

Engineers in the second-generation cellular systems were aware of the capacity gain of using directional antennas and they mostly implemented three directional antennas covering a $120°$ sector each instead of an omnidirectional unique one [27]. The utilization of three sectors multiplied the cell capacity by a factor close to three. In this case three is an upper bound for the capacity improvement. In a general case with N sectors, the upper bound for the capacity gain is N [26]. Actual figures are always lower than that, but for the case of three sectors of $120°$-sectors and uniformly distributed users the actual capacity gain is quite close to the upper bound [26]. Adaptive antennas go a step further; they provide as many radiation patterns (sectors) as users in the cell. Each radiation pattern, usually named as beam, is steered toward one user to maximize its signal-to-Interference plus noise ratio (SINR).Antenna Arrays (AAs) do not maintain fixed beams, but they are adapted continuously to match the dynamics of the environment. Because of its capability of following the users and maximizing their quality of service (QoS), AAs are also referred to as smart antennas [27]. Because

of the duality of the antennas, which states that the transmission and reception behaviour of an antenna are equal, adaptive antennas can be used in transmission or reception [26].

Many authors have contributed to the field of adaptive antenna arrays for wireless communications. Godara's papers [28, 29] form an excellent review and introduction to the topic in a comprehensive way with many references. The paper by W.F Gabriel [30] provide excellent introductions to the general theory of adaptive antenna arrays. A lot of research is going on in implementing smart antennas in the existing and future generations of mobile communication systems. In [31] a brief description of the technical challenges facing wireless services providers is presented, along with that, historical attempts to address the challenges and proposing smart antenna technology as a solution for them were presented. In [32] some experimental results demonstrating the efficacy of smart antenna technology involving spatial domain multiple access SDMA in improving the capacity and coverage is given. The use of spatial and temporal processing in improving the performance in mobile radio communications is presented in [33, 34].

The application of smart antennas in wireless systems using CDMA[1], GSM and IS-136 in different environments and performance analysis is presented by Winters in [35]. Rappaport and Liberti Jr. in [36] gave in-depth concepts on the

---

[1]Code Division Multiple Access

use of smart antennas in IS-95 and third-generation CDMA applications. A thorough investigation of the comparison of tracking beam array and switching beam array is done by Choi *et al*. in [37].

Various beamforming and null-steering strategies have been proposed to combat interference. One of the earliest forms of quasi-adaptive generic arrays is the side lobe canceller (SLC) presented in [38]. Sng *et al*. in [39] suggested a new generalized side lobe canceller (GSC) beamforming structure, in which the weight updates are calculated based on the steering vectors responding to be DOA[2] of the jammers. This research was further extended in [40] to reduce the adaptive dimension of the array. Zooghby *et al*. in [41] carried out multiple source tracking with neural network based smart antennas. The proposed neural multiple source tracking (N-MUST) algorithm is used to perform DOA, and the experimental validation of this proposed work is presented in [42]. Zetterberg and Ottersen in [43] investigated the spectral efficiency gain using transmit antenna arrays at the base station. The proposed system estimates the angular positions of the mobiles from the received data and allows multiple mobiles to be allocated to the same channel within the cell. Ponnikanti and Sali [44] devised an effective adaptive antenna scheme to prevent the desired signal cancellation in optimal weight vector computation of the beamformer. Kozick *et al*. [45] investigated the effect of steering the individual element patted along with adjusting complex weights to improve

---

[2]Direction of Arrival

the performance of adaptive arrays. Choi *et al.* in [46, 47] proposed a novel adaptive beamforming algorithm for a smart antenna base station system (SA-BTS). The new technique is based on the eigen-space method for computing the optimal weight vector which does not degrade the receiving performance even in wide angle-spread circumstances.

Hybrid Systems

Several systems that combine two or more MIMO schemes have been proposed in order to satisfy certain tradeoffs.

In [48], Meixia *et al.* has implemented a combination of BLAST and space-time coding (STC) for MIMO systems which they called generalized layered space-time coding (GLST). In [48] post-ordered detection algorithm is introduced based on the generalization of the original BLAST ordering detection algorithm. The performance is analyzed through a comparison to that of pre-ordered decoding with and without power allocation. In [6], the combination of V-BLAST and STBC is referred to as multi layer space-time block codes (MLSTBC). The basic idea of this scheme is to partition the transmit antennas into different groups and assign each group to a layer of VBLAST. Within each group, the signals are space-time block coded. So the transmit diversity of the layered architecture increases. Also, exploiting the orthogonal nature of STBC, the number of received antennas can be reduced compared to traditional VBLAST. The combination of VBLAST and

STBC has been also proposed in [49], in which STBC is associated with each layer of VBLAST as a way of improving its energy efficiency. At the receiver, a reduced number of antennas are used to take advantage of the delay structure of STBCs.

Chong *et al.* in [7] considered the combination of VBLAST and STBC by proposing an algorithm that combines the algorithm of successive interference cancellation zero-forcing (SIC-ZF) and successive interference cancellation zero-forcing with maximum aposteriori probability (SIC-ZF-MAP). The proposed algorithm (SIC-ZF-MAP) reduces the complexity if compared with using the individual algorithms alone.

In [5], Tarokh *et al.* proposed using a combined scheme that is called multi-layered space-time trellis code (MLSTTC), in which space-time trellis code (STTC) is used in each layer of VBLAST with different transmission power. In other words, the decoding order is pre-determined based on the power level. One advantage of using MLSTBC over MLSTTC is that the orthogonal structure and the short code length can be exploited at the receiver to reduce the minimum required number of receive antennas [50]. For MLSTTC [5, 51], the number of receive antennas should be at least equal to the total number of transmit antennas, while for MLSTBC, it should be at least equal to the number of layers [51].

In [52], the authors proposed a scheme that combines VBLAST with beamforming, this is carried out by using an *L*-element beamformer with each layer of VBLAST. This scheme utilizes the uplink direction of arrival (DOA), and it was

shown that this scheme provides ($10log(L)$ dB) performance enhancement to the traditional VBLAST scheme.

Recently, many researches have focused on combining beamforming and STBC techniques [53, 54, 55]. The combining techniques usually require more than one AA at the transmitter. The transmitted signal is encoded by STBC and precoded by beamforming weights independently before transmitting on different antenna arrays [27]. One way to obtain the beamforming weights is through eigen decomposition of the estimated channel covariance matrix as in [53]. Another way is to utilize the direction of arrival information (DOA) to calculate the beamforming weights as conducted in [53, 54]. In addition, a transmission scheme that effectively combines conventional transmit beamforming with orthogonal spacetime block coding was proposed in [56], in which the side information was utilized for improving a pre-determined orthogonal STBC by means of a linear transformation that leads to the optimal solution.

Upon Combining beamforming and STBC, it was able to achieve both diversity and beamforming gain that can improve the system performance but it cannot improve the system spectral efficiency, since these two techniques are mainly meant to combat fading. Therefore, there is a need for a scheme that adds spectral efficiency improvement to the combined system of STBC and beamforming, which was achieved in [8], namely, a multi-functional MIMO scheme was proposed in [8], that combines the benefits of STBC, beamforming, as well as

VBLAST to further enhance the system performance and maximize the coding advantage of the transmission scheme. In addition, the capacity limits for this novel scheme were derived in [8].

Analytical performance evaluation of VBLAST systems employing zero-forcing successive interference cancellation (ZF-SIC) without ordering and using BPSK over Rayleigh-fading channel was presented in [57]. Further, a general recursive procedure to calculate the bit error rate (BER) of each sub-stream with arbitrary number of transmit and receive antennas was proposed. Similar work but with different approach has been conducted in [58]. It would be interesting and novel to extend this analysis to the case of LSSTC.

1.2.2 Scheduling

In systems with a single base station antenna, it was shown in [59] that transmitting to the user with the strongest channel at any given time achieves the sum rate capacity, which is the sum-of rates of all the users [59]. The resulting multi-user diversity is expected to be present as well in the multiantenna case. In [9], multi-user diversity resulting from independence of fading among users in multi-user environments was shown to be capable of increasing the system capacity. Motivated by information-theoretic results, an approach to increase the throughput of multi-user systems is proposed in [60] that takes advantage of the independence of the fading statistics of the different users. This requires a packet scheduler to

preferentially allocate radio resources to users in good channel conditions. Two critical targets of packet scheduling are to maximize the system rate and to offer fairness among users.

In [9], the scheduling scheme maximizes the system capacity through the use of multi-user diversity. Specifically, each spatial channel is allocated to a user with the best channel condition for each time slot. Therefore, some users in adverse channel conditions may not be served, causing unfairness among users. In [61], the round robin (RR) scheduling scheme was studied for MIMO cellular systems. In RR scheduling channel is assigned in a cyclic fashion regardless of the channel conditions, and thus achieves fairness among users. However, the RR scheme does not use multi-user diversity, resulting in the same capacity as a single user system. In order to exploit the multi-user diversity and at the same time maintain fairness across the users, two other scheduling schemes have been proposed. In [62] the antenna assisted round robin scheduling (AA-RR) scheme has been proposed, which is an improved version of RR scheme that exploits multiple antennas to achieve a diversity effect from multiple users.

In situations where minimal channel variation is experienced, opportunistic beamforming (OBF) has been proposed in [63] to create artificial channel variation where it might not otherwise exist. Proportional fair (PF) scheduling was also investigated in [63] as a way to ensure that users are treated fairly over some time interval. The PF scheduler assigns a user for transmission when its

instantaneous channel capacity is high relative to its average channel condition. As such, the benefit of multi-user diversity can be exploited and fairness among users can be maintained. Some work has been done in extending the opportunistic beamforming idea to the case where base station and mobile stations all have multiple antennas [9], but this has not been yet studied extensively. Multiple random beams are used in [64] with limited feedback to communicate with many users. Further work on feedback reduction has been conducted in [65], where it is shown that the feedback rate can be minimized without losing the gains due to adaptive modulation and multi-user diversity. Along with that the authors in [65] present an in-depth study of the literature in the area, and evaluate the performance of several state-of-the-art channel quality feedback schemes.

1.3 Thesis Contributions

The contributions of this thesis can be summarized as follows:

- We investigate the analytical error performance of single user LSSTC, and recursive expressions for the probability of error is obtained starting from previously obtained results for VBLAST; our work extends that work to the LSSTC case where beamforming and STBC are involved. The analytical results are supported by simulation results. In addition, a formula for the instantaneous capacity of single-user LSSTC is derived.

- We analyze the diversity, multiplexing, and beamforming tradeoff curve for LSSTC. This curve relates these three extremes, where increasing one parameter causes the other parameters to decrease and vice versa.

- We propose a multi-configuration transmission scheme based on LSSTC and VBLAST systems. This scheme suggests the configuration and the modulation scheme in order to improve the performance. The main results of this study showed that combining beamforming, STBC, and VBLAST has better performance than VBLAST at high SNR range.

- We suggest a power allocation scheme for LSSTC that is based on the results of [66] for VBLAST. Also we obtain formulas for the symbol error rate for M-ary PSK and M-ary QAM. This system enhances the performance and capacity by assigning power to the layers in an optimum manner.

- Finally, we evaluate LSSTC in multi-user environments. This is done by comparing the capacity and the probability of error for several combinations of algorithms and criteria for scheduling the users' data. Also we derive a formula for the PDF of the maximum pre-processing SNR for a Greedy-based multi-user LSSTC.

1.4 Thesis Outline

In Chapter 2 we describe a number of multi-antenna systems, namely, STBC, VBLAST, and beamforming. The system model of each of those systems is introduced with necessary details.

Chapter 3 introduces the system model of single-user LSSTC, where we show in detailed mathematical steps the benefit of combining STBC, VBLAST, and beamforming. Also we find formulas for the instantaneous capacity and the probability of bit error. Along with that we discuss the tradeoff between diversity, multiplexing, and beamforming.

In 4 we suggest a modified scheme for LSSTC that enhances the capacity by assigning power to the layers in an optimum manner. We investigate the performance of this scheme for different modulation schemes, namely, BPSK, M-ary PSK and M-ary QAM. also, we use numerical methods for finding the optimum power conditions.

Chapter 5 addresses the use of LSSTC in multi-user environments where scheduling techniques can be applied to improve the performance of LSSTC systems.

Finally in Chapter 6, the main conclusions from the thesis and possible future research directions are discussed.

Chapter 2

Multi-Antenna Systems

In this chapter we will discuss a number of multi-antenna systems, namely, STBC, VBLAST, and beamforming. These systems are the components that constitute the LSSTC. Therefore a detailed description of each system is essential for the complete understanding of the topic. The Chapter is organized as follows. Section 2.1 gives a description of STBC and presents the system model of Alamouti's transmit technique. The system model of VBLAST is presented in Section 2.2, where the vertical encoding process of VBLAST is also discussed. Finally, Section 2.3 introduces the system model of adaptive antenna arrays.

2.1 Space-Time Block Codes (STBC)

The challenge of communication over Rayleigh fading channels is that the error probability decays only inversely with SNR, compared with the exponential de-

cay observed on AWGN channels. STBC [4] is a simple method that enhances the reliablility by increasing the decay of error probability through diversity.

The encoder of an STBC can be described as follows. The symbols $(x_1, x_2, \ldots, x_n)$ arrive at the encoder which are mapped to an $m \times l$ orthogonal transmission matrix, where the ith row represents the transmitted symbols from the ith antenna and the jth column represents the transmitted symbols in the jth time slot. Since n symbols are transmitted during l time slots, the rate (R_s) of STBC is

$$R_s = \frac{n}{l} \quad \text{symbols/time slot.} \tag{2.1}$$

The maximum transmission rate of STBC is equal to one symbol/time slot. For orthogonal STBC, the maximum rate is achieved only for the two transmit antennas case which is Alamouti's scheme [17].

Alamouti's Transmit Technique

Historically, the transmit diversity technique proposed by Alamouti was the first STBC. The encoding and decoding operation is carried out in sets of two modulated symbols. These two symbols are transmitted at two consecutive time instances t_1 and t_2. The times t_1 and t_2 are separated by a constant time duration T.

The encoding operation for Alamouti's $2T_x - 1R_x$ scheme is shown in Figure 2.1. The following notation will be used throughout this thesis. $\mathbf{s} = [x_1, x_2]^T$ is an

STBC block that consists of two symbols. The transmission rate is equal to the transmission rate of a SISO system. The space-time encoding mapping of Alamouti's two-branch transmit diversity technique can be represented by the coding matrix

$$\mathbf{C}_A = \begin{pmatrix} x_1 & -x_2^* \\ x_2 & x_1^* \end{pmatrix}. \tag{2.2}$$

The above coding matrix is orthogonal because $\mathbf{C}_A \cdot \mathbf{C}_A^H$ is a diagonal matrix according to $\mathbf{C}_A \mathbf{C}_A^H = \left[\sum_{i=1}^{n} |x_i|^2 \right] \cdot I_m$, where C_A^H is the hermitian of C_A, I_m is the identity matrix of size $m \times m$, where m represents the number of transmit antennas, and n is the number of symbols transmitted per transmission block in C_A.

The decoding operation assumes that the fading channel coefficients during the two consecutive transmission time periods, t_1 and t_2, are to remain constant. In other words, the channel coefficients from the first antenna to the jth receiver antenna $\alpha_{j,1}$ and those from the second antenna to the jth receiver antenna $\alpha_{j,2}$ must satisfy the following set of equations:

$$\alpha_{j,1} = \alpha_{j,1}(t) = \alpha_{j,1}(t+T) = \alpha_{j,1}(t_1) = \alpha_{j,1}(t_2)$$
$$\alpha_{j,2} = \alpha_{j,2}(t) = \alpha_{j,2}(t+T) = \alpha_{j,2}(t_1) = \alpha_{j,2}(t_2). \tag{2.3}$$

The receiver observes the received signals for the whole block length l. Assuming that the MIMO channel is constant during the transmission of one block, the
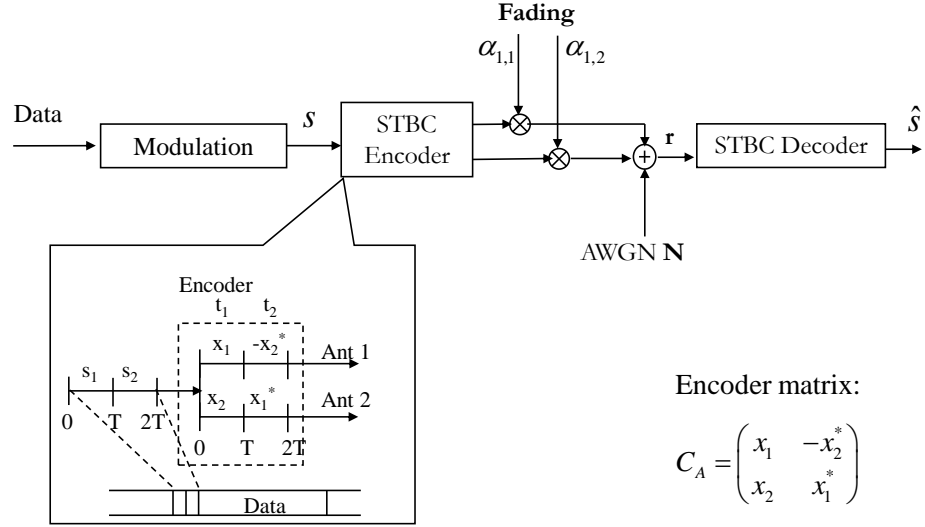
Figure 2.1: STBC Block Diagram (Alamouti's $2T_x - 1R_x$ scheme) .

discrete-time received signals over the l time slots can be written as [6]

$$\underbrace{\mathbf{Y}}_{n \times l} = \underbrace{\mathbf{H}}_{n \times m} \underbrace{\mathbf{C}_A}_{m \times l} + \underbrace{\mathbf{N}}_{n \times l}. \tag{2.4}$$

To illustrate the decoding algorithm, consider transmitting over 2×2 MIMO channel using C_A transmission matrix, the received signal over two time slots is given by

$$\begin{bmatrix} y_1^1 & y_1^2 \\ y_2^1 & y_2^2 \end{bmatrix} = \begin{bmatrix} h_{1,1} & h_{1,2} \\ h_{2,1} & h_{2,2} \end{bmatrix} \begin{bmatrix} x_1 & -x_2^* \\ x_2 & x_1^* \end{bmatrix} + \begin{bmatrix} z_1^1 & z_1^2 \\ z_2^1 & z_2^2 \end{bmatrix}. \tag{2.5}$$

A transformation of the channel matrix into a virtual matrix was proposed in [6], where the received vectors from the l time slots are rearranged into one vector

using the virtual MIMO model [16], resulting in (2.5) rewritten as

$$
\begin{bmatrix} y_1^1 \\ y_2^1 \\ y_1^{2*} \\ y_2^{2*} \end{bmatrix} = \begin{bmatrix} h_{1,1} & h_{1,2} \\ h_{2,1} & h_{2,2} \\ h_{1,2}^* & -h_{1,1} \\ h_{2,2}^* & -h_{2,1}^* \end{bmatrix} \begin{bmatrix} x_1 \\ x_2 \end{bmatrix} + \begin{bmatrix} z_1^1 \\ z_2^1 \\ z_1^{2*} \\ z_2^{2*} \end{bmatrix}
\tag{2.6}
$$

$$
\mathbf{y}_v = \mathbf{H}_v \mathbf{s} + \mathbf{z}_v,
\tag{2.7}
$$

where v refers to the virtual representation, and y_i^t and z_i^t indicate the received signal and the AWGN at receive antenna i at time t, respectively. Since $\mathbf{H}_v$ is orthogonal, the transmitted symbols could be easily estimated by decoupling the received signals after multiplying $\mathbf{y}_v$ by $\mathbf{H}_v^H$, and thus the estimated symbols can be written as [16]

$$
\hat{\mathbf{s}} = \mathbf{H}_v^H \mathbf{y}_v = \mathbf{H}_v^H \mathbf{H}_v \mathbf{s} + \mathbf{H}_v^H \mathbf{z}_v,
\tag{2.8}
$$

and since

$$
\mathbf{H}_v^H \mathbf{H}_v = \left[|h_{1,1}|^2 + |h_{1,2}|^2 + |h_{2,1}|^2 + |h_{2,2}|^2 \right] \cdot I_2 = b \cdot I_2,
\tag{2.9}
$$

where b is constant, then

$$
\begin{bmatrix} \hat{x}_1 \\ \hat{x}_2 \end{bmatrix} = \begin{bmatrix} b & 0 \\ 0 & b \end{bmatrix} \begin{bmatrix} x_1 \\ x_2 \end{bmatrix} + \mathbf{H}_v^H \mathbf{z}_v.
\tag{2.10}
$$

We notice that the decision statistics are composed of an amplified version of

the transmitted signals and a noise component. The signal amplification is equal to the sum of the amplitudes of all channel coefficients. The noise component is a sum of the receiver antenna noises multiplied by channel fading components. The combined signals are then sent to the maximum likelihood detector [4] which, for each of the signals x_1 and x_2 uses the maximum likelihood decision rule that operates on each estimated symbol separately. For example, for detecting x_1 the detector will choose symbol x_i if the following condition is satisfied

$$
\begin{aligned}
&\left[|h_{1,1}|^2 + |h_{1,2}|^2 + |h_{2,1}|^2 + |h_{2,2}|^2 - 1\right] |x_i|^2 + d^2(\hat{x}_1, x_i) \\
\leq\ &\left[|h_{1,1}|^2 + |h_{1,2}|^2 + |h_{2,1}|^2 + |h_{2,2}|^2 - 1\right] |x_k|^2 + d^2(\hat{x}_1, x_k) \quad \forall i \neq k,
\end{aligned}
\tag{2.11}
$$

where $d^2(\hat{x}_1, x_i)$ is the squared Euclidian distance between $\hat{x}_1$ and x_i. For equal-energy signals, such as PSK, the above decision criterion simplifies to the following

$$
d^2(\hat{x}_1, x_i) \leq d^2(\hat{x}_1, x_k) \quad \forall i \neq k;
\tag{2.12}
$$

2.2 Vertical Bell Labs Layered Space-Time Architecture

A high-level block diagram of a single user VBLAST system is shown in Figure 2.2 where the number of transmit antennas is N_T and the number of receive antennas is N_R. A single bit stream is demultiplexed into several layers, and each

layer is then modulated independently and sent through a separate transmit antenna. The condition of operation for the VBLAST system is that N_R is equal or greater than N_T, so if that is satisfied, and there is rich scattering in the channel such that the layer channel vectors are independent, one can use the V-BLAST detection algorithm to demodulate the layers, which is based only on the spatial characteristics formed by the antenna array.
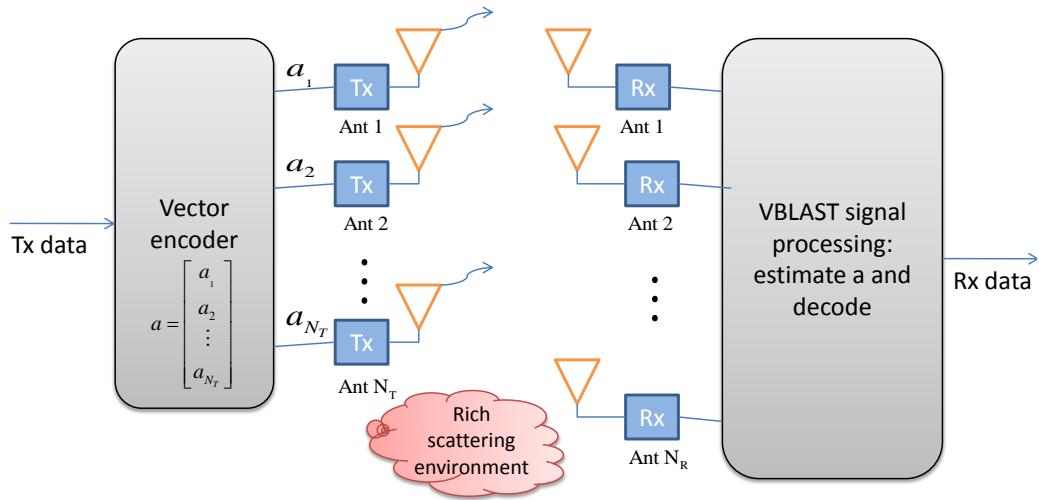
Figure 2.2: high-level block diagram of a single user VBLAST system.

Although V-BLAST, as shown above, is essentially a single-user system which uses multiple transmitters, it was shown in [2] that it differs from traditional multiple-access techniques. Some of the differences are as follows. First, unlike CDMA or other spread-spectrum multiple access techniques, the total channel bandwidth utilized in a BLAST system is only a small fraction in excess of the symbol rate. Second, unlike frequency division multiple access (FDMA), each transmitted signal occupies the entire system bandwidth. Finally, unlike time

division multiple access (TDMA), the entire system bandwidth is used simulta-

neously by all of the transmitters all of the time.

A block diagram of a VBLAST transmitter with four antennas is shown in

Figure 2.3. A single data stream is demultiplexed into 4 sub-streams, and each

sub-stream is then encoded into symbols and fed to its respective transmitter.

Transmitters 1 to 4 operate using the same channel at a symbol rate of $1/T_s$ sym-

bols/sec, where T_s is the symbol duration, where the symbol timing is synchro-

nized.
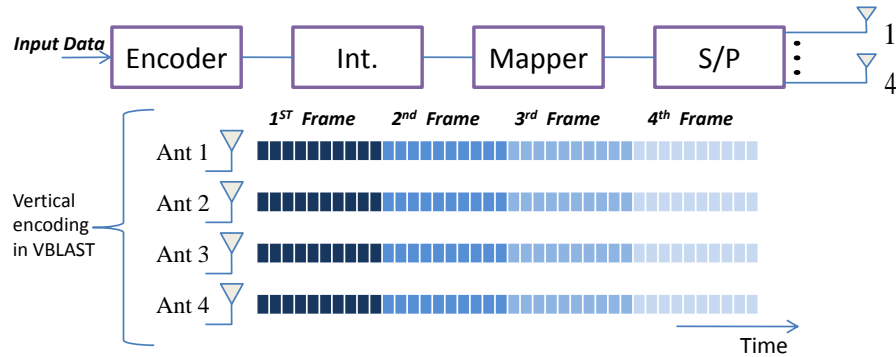
Figure 2.3: Block diagram of a VBLAST transmitter.

Figure 2.3 also shows the vertical encoding in VBLAST where each frame is

partitioned over the transmit antennas and sent in a vertical manner. The vector

encoding process is simply a demultiplex operation followed by independent bit-

to-symbol mapping of each layer. No inter-layer coding, or coding of any kind,

is required, though conventional coding of the individual layers may certainly be

applied. For the remainder of this work, we will assume that the layers comprise

uncoded, independent data symbols.

2.3   Adaptive Antenna Arrays

According to Sections 2.1 and 2.2, it becomes clear that multiple antennas can be used for the sake of attaining either spatial diversity or spatial multiplexing gains. However, multiple antennas can also be used in order to improve the SNR at the receiver or the SINR in a multi-user scenario. This can be achieved by employing adaptive antenna arrays (AAs) techniques [67].

In order to implement an antenna with multiple beams and with the capability of dynamically changing the radiation pattern of each beam, AAs are constructed as a digital combination (in baseband) of an array of elementary antennas. Because of this implementation, AAs are also named adaptive antenna arrays and the elementary antennas composing the array are called antenna elements. Techniques used to compute the optimal combination of the antenna elements are referred to as array processing algorithms.

Beamforming is an effective technique for reducing the multiple-access interference, where the antenna gain is increased in the direction of the desired user, whilst reducing the gain towards the interfering users [68]. If the directions of the different propagation paths are known at the transmitter or the receiver, then beamforming techniques can be employed in order to direct the received beam pattern in the direction of the specified antenna or user [28, 29]. Hence, signifi-

cant SNR gains can be achieved in comparison to a single-antenna system. On the transmitter side, when the DOA of the dominant paths at the receiver is known for the transmitter, then the transmit power is concentrated in the direction of the target user, and less power is wasted in the other directions. On the other hand, beamforming can be used in order to reduce the co-channel interference or multi-user interference [68]. When using beamforming, each user adjusts their beam pattern to ensure that there are nulls in the directions of the other users, while there is a high directivity in the direction of the desired receiver. Hence, the system attains an SINR gain.

Basic block diagram for the AA architecture is depicted in Figure 2.4. the AA consists of L elements that are spaced at a distance of $d = \lambda/2$ for the sake of achieving beamforming, where λ is the signal's wavelength. The AA algorithm defines the weight vector w_i which determines the radiation pattern of the overall antenna. The array processing algorithm considered in this work will be described in Section 3.1 where transmit beamforming is used.
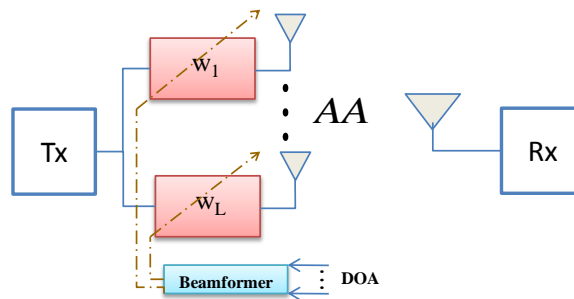
Figure 2.4: Block diagram for the AA architecture.

2.4 Chapter Conclusions

In this Chapter we described the system models of STBC, VBLAST, and beamforming. These systems are the components of LSSTC, therefore, understanding the system model of each of those systems is essential in this thesis. It was shown that STBC introduces diversity by providing redundancy in both time and space. VBLAST can increase the data rate by providing spatially-multiplexed channels that operates with same frequency. On the other hand, beamforming can provide a direct SNR gain by steering the radiation pattern toward the desired user.

Chapter 3

LSSTC in Single-User Systems

In this chapter we introduce of the layered steered space-time codes (LSSTC) in single-user systems. We will show the benefit of combining STBC, VBLAST, and beamforming in a detailed mathematical approach. Also, we investigate the error performance and capacity of single-user LSSTC. The Chapter is organized as follows. Section 3.1 gives a detailed description of our system model considering its components VBLAST, beamforming, and STBC. Section 3.2 presents the detector used in this thesis which is the serial group interference cancelation (SGIC) [48]. Section 3.3 presents the performance analysis of LSSTC, in which we derive a formula for the probability of bit error. In Section 3.4, we derive a formula for the instantaneous capacity of single-user LSSTC. In Section 3.5 the tradeoff between several advantages of LSSTC is analyzed. Section 3.6 presents the simulation results conducted to evaluate the LSSTC system. Finally, Section 3.7 presents the

chapter's conclusions.

3.1 System Model

Figure 3.1 shows the block diagram of a single-user LSSTC system proposed in [8]. The system has N_T total transmitting antennas and N_R receiving antennas and is denoted by an $N_T \times N_R$ LSSTC. The antenna architecture employed in Figure 3.1 has M transmit adaptive antenna arrays (AAs) spaced sufficiently far apart in order to experience independent fading and hence achieve transmit diversity. Each of the AAs consists of L elements that are spaced at a distance of $d = \lambda/2$ to ensure achieving beamforming. A block of B input information bits is sent to the
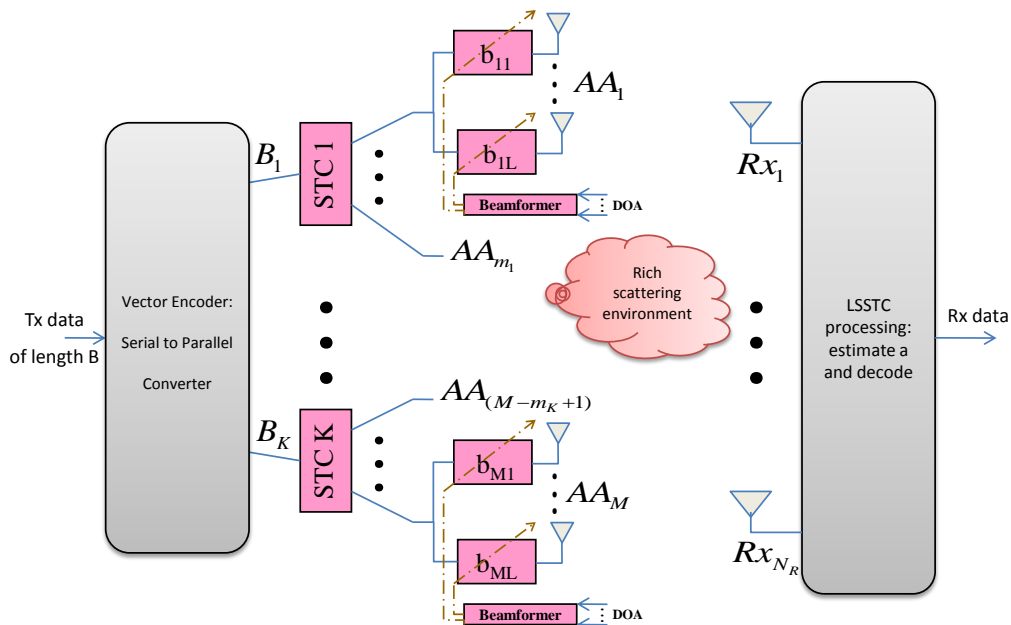
Figure 3.1: Block diagram of a single user LSSTC system.

vector encoder of LSSTC and serial-to-parallel converted to produce K streams

(layers) of length $B_1, B_2, \ldots, B_K$, where $B_1 + B_2 + \cdots + B_K = B$. Each group of B_k bits, $k \in [1, K]$, is then encoded by a component space-time code STC_k associated with m_k transmit AAs, where $m_1 + m_2 + \cdots + m_K = M$. The output of the kth STC encoder is a $m_K \times l$ codeword, $\mathbf{c}_i$, that is sent over l time intervals. The space-time coded symbols from all layers can be written as $\mathbf{C} = [\mathbf{c}_1, \mathbf{c}_2, \ldots, \mathbf{c}_K]^T$, where $\mathbf{C}$ is an $M \times l$ matrix.

The coded symbols from $\mathbf{C}$ are then processed by the corresponding beamformers, and then transmitted simultaneously over the wireless channels. The transmit antennas of all the groups are synchronized and allocated equal power. Moreover, the total transmission power is fixed, where the transmitted symbols have an average power of $P_T = 1$, where the average is taken across all codewords over both spatial and temporal components. For the LSSTC system to operate properly, the number of receive antennas N_R should be at least equal to the number of layers K.

We formulate the system model as follows. The channel model is a MIMO quasi-static Rayleigh flat-fading channel with N_T transmit antennas and N_R receive antennas. The quasi-static assumption indicates that the channel gain coefficients remain constant for the duration of the STBC block and change independently for each STBC block. The flat-fading assumption allows each transmitted symbol to be represented by a single-tap in the discrete-time model with no inter-symbol interference (ISI). We assume independent Rayleigh coefficients,

i.e.,fading coefficients are independent and identically distributed (i.i.d.) circular-complex normal random variables with zero-mean and 0.5 variance per dimension, abbreviated as $\mathcal{CN}(0,1)$. The correlation caused by the small distance separation is approximately removed using the beamforming processing as we will show in this Section. At the receiver, White Gaussian noise is added. The system model also assumes that the receiver has perfect channel state information (CSI), whereas the transmitter does not have any knowledge of the channel.

Denote the L-dimensional channel impulse response (CIR) vector spanning the mth AA, $m \in [1,\dots,M]$ and the nth receiver antenna, $n \in [1,\dots,N_R]$ as $\mathbf{h}_{n,m}(t)$. Over flat fading channels $\mathbf{h}_{n,m}$ can be expressed as [52]

$$\mathbf{h}_{n,m}(t) = [\mathbf{d}_{n,m}]^T \cdot \alpha_{n,m}(t), \tag{3.1}$$

where $\alpha_{n,m}$ is the rayleigh faded coefficient coupling the mth AA to the nth receiver antenna, and $\mathbf{d}_{n,m}$ is the adaptive antenna array response corresponding to the mth AA and the nth receiver antenna, defined as [52]

$$\mathbf{d}_{n,m} = \left[1, e^{-j2\pi d(m)\sin(\Psi_{n,m})/\lambda}, \dots, e^{-j2\pi(L-1)d(m)\sin(\Psi_{n,m})/\lambda}\right]^T, \tag{3.2}$$

where $d(m)$ is the distance between the elements of the mth AA, $\Psi_{n,m}$ is the nm^{th} link's DOA, and superscript $'T'$ denotes the matrix transposition.

The system model can be described in matrix notation, where the received

baseband data matrix $\mathbf{Y}$ can be expressed as

$$\mathbf{Y} = \mathbf{HWC} + \mathbf{N}, \tag{3.3}$$

where $\mathbf{Y}$ is the received signal over l time intervals and has a dimension of $N_R \times l$, and $\mathbf{H}$ is an $N_R \times M$ matrix whose entries are $\mathbf{h}_{n,m}$ defined in (3.1), and $\mathbf{N}$ is an $N_R \times l$ matrix that characterizes the additive white Gaussian noise (AWGN). The nth row of $\mathbf{N}$ denoted as $\mathbf{z}_n$, where $n \in [1,\ldots,N_R]$, is a row vector of l columns, the ith entry of $\mathbf{z}_n$ is a spatially uncorrelated circular-complex normal random variable, and can be written as $z_n^i = z_{I,n}^i + j z_{Q,n}^i$, where $z_{I,n}^i$ and $z_{Q,n}^i$ are two independent zero-mean Gaussian random variables having a variance of $N_0/2$, we will represent z_n^i as $\mathcal{CN}(0, N_0)$. Furthermore, $\mathbf{W}$ is an $M \times M$ diagonal weight matrix, whose diagonal entry $\mathbf{w}_{m,m}$ is the L-dimensional beamforming weight vector for the mth beamformer AA and the nth receive antenna, and can be written as $\mathbf{w}_{m,m} = [b_{m1}, \cdots, b_{mL}]$, where b_{mi}, $i \in [1,\ldots,L]$, is the ith weighting gain of the mth AA. The received signal Y can be written in matrix form as

$$
\begin{bmatrix} \mathbf{y}_1 \\ \mathbf{y}_2 \\ \vdots \\ \mathbf{y}_{N_R} \end{bmatrix} = \begin{bmatrix} \mathbf{h}_{1,1}\mathbf{w}_{1,1} & \cdots & \mathbf{h}_{1,M}\mathbf{w}_{M,M} \\ \mathbf{h}_{2,1}\mathbf{w}_{1,1} & \cdots & \mathbf{h}_{2,M}\mathbf{w}_{M,M} \\ \vdots & \ddots & \vdots \\ \mathbf{h}_{N_R,1}\mathbf{w}_{1,1} & \cdots & \mathbf{h}_{N_R,M}\mathbf{w}_{M,M} \end{bmatrix} \begin{bmatrix} \mathbf{c}_1 \\ \mathbf{c}_2 \\ \vdots \\ \mathbf{c}_K \end{bmatrix} + \begin{bmatrix} \mathbf{z}_1 \\ \mathbf{z}_2 \\ \vdots \\ \mathbf{z}_{N_R} \end{bmatrix}. \tag{3.4}
$$

Throughout this thesis, the LSSTC model presented in this section will be used to design single and multiple user transmission systems. Also, whenever the phrase "sub-stream" is mentioned it refers to the data stream of each AA, which we denote as x, whereas, the term "layer", denoted by $\mathbf{s}$, represents the data stream to be encoded by STBC. In the case of Alamouti's $2T_x - 1R_x$ scheme, $\mathbf{s} = [x_1, x_2]^T$ where x_i is the symbol of the ith AA substream.

The beamforming vector $\mathbf{w}_{m,m}$ is given by [52] as $\mathbf{w}_{m,m} = \mathbf{d}_{n,m}^*$, where the superscript * represents the conjugate of the matrix. Refering to (3.4), we define a modified channel matrix as

$$
\hat{\mathbf{H}} = \begin{bmatrix}
\mathbf{h}_{1,1}\mathbf{w}_{1,1} & \cdots & \mathbf{h}_{1,M}\mathbf{w}_{M,M} \\
\mathbf{h}_{2,1}\mathbf{w}_{1,1} & \cdots & \mathbf{h}_{2,M}\mathbf{w}_{M,M} \\
\vdots & \ddots & \vdots \\
\mathbf{h}_{N_R,1}\mathbf{w}_{1,1} & \cdots & \mathbf{h}_{N_R,M}\mathbf{w}_{M,M}
\end{bmatrix}, \tag{3.5}
$$

where $\hat{\mathbf{H}}$ is the reconstructed channel matrix comprising the MIMO fading channel and the DOA information. Note that we assumed that the nulling vector for all the paths corresponding to one AA ($\mathbf{w}_{m,m}$) is the same. This follows from the assumption that the separation between the receive antennas is much less than the distance between the AA and the receiver, then roughly speaking, they will have the same direction of arrival, which will result in having the same nulling vector.

According to Equation (3.4) $\mathbf{Y}$ can be rewritten as:

$$\mathbf{Y} = \hat{\mathbf{H}}\mathbf{C} + \mathbf{N}. \tag{3.6}$$

The channel coefficient $\hat{\mathbf{H}}_{n,m}$ can roughly expressed as

$$
\begin{aligned}
\hat{\mathbf{H}}_{n,m} &= \mathbf{h}_{n,m}\mathbf{w}_{m,m} \\
&= \alpha_{n,m} \cdot [\mathbf{d}_{n,m}]^T [\mathbf{d}_{n,m}]^* \tag{3.7} \\
&= L \cdot \alpha_{n,m}.
\end{aligned}
$$

Therefore the received signal can be expressed as in [8]:

$$\mathbf{Y} = L\tilde{\mathbf{H}}\mathbf{C} + \mathbf{N}, \tag{3.8}$$

where $\tilde{\mathbf{H}}$ is an $(N_R \times M)$ matrix whose entries are $\alpha_{n,m}$. Looking at (3.8), the effect of beamforming can be clearly seen, which is a direct SNR gain. Expressing $\tilde{\mathbf{H}}\mathbf{C}$ in terms of the layers components we get

$$\mathbf{Y} = L \sum_{k=1}^{K} \tilde{\mathbf{h}}_k \mathbf{c}_k + \mathbf{N}, \tag{3.9}$$

where $\mathbf{c}_k$ represents the component STBC used at layer k, where $k \in [1,\dots,K]$, and

$$\tilde{\mathbf{H}} = \begin{bmatrix} \alpha_{1,1} & \cdots & \alpha_{1,m_1} & \alpha_{1,m_1+1} & \cdots & \alpha_{1,M} \\ \vdots & \ddots & \vdots & \vdots & \ddots & \vdots \\ \alpha_{N_R,1} & \cdots & \alpha_{N_R,m_1} & \alpha_{N_R,m_1+1} & \cdots & \alpha_{N_R,M} \end{bmatrix}. \tag{3.10}$$

Partitioning $\tilde{\mathbf{H}}$ into groups corresponding to each layer, the channel matrix can be rewritten as in [6]:

$$\tilde{\mathbf{H}} = \left[\tilde{\mathbf{h}}_1, \ldots, \tilde{\mathbf{h}}_K \right], \tag{3.11}$$

where the kth vector in (3.11) represents the channel matrix of each layer, which can be written as:

$$\tilde{\mathbf{h}}_k = \begin{bmatrix} \alpha_{1,m_{k-1}+1} & \cdots & \alpha_{1,m_{k-1}+m_k} \\ \vdots & \ddots & \vdots \\ \alpha_{N_R,m_{k-1}+1} & \cdots & \alpha_{N_R,m_{k-1}+m_k} \end{bmatrix}, \tag{3.12}$$

where $m_0 = 0$.

3.2 Serial Group Interference Cancelation (SGIC)

The detection process can be classified into two types [48]. The first type is the non-ordered detection, in which choosing the layer to be detected does not depend on the power of the layer, and the detection order is predetermined before the signal is received. The second type is the post-ordered detection, where the

detection order is not known until the channel realization is perfectly estimated at the receiver. The steps of post-ordered SGIC proposed in [6, 48] can be summarized as follows:

1. Ordering: Determining the group (layer) with the maximum SNR to optimize performance. Since the average power of the codeword in each group is assumed to be the same, the post-detection SNR of the ith layer is proportional to the squared Frobenius norm (FN) of the channel matrix of the corresponding layer [6]. Therefore, the optimal ordering is based on simply selecting the group $\tilde{\mathbf{h}}_i$ from the channel matrix $\tilde{\mathbf{H}}$ that has the highest FN at each stage of the detection. In fact, the transmitted symbol with the smallest post-detection SNR will dominate the error performance of the system. So, we decode first the streams which exhibit highest SNR so as to minimize propagating errors in later stages. According to [6] the detection order at the ith layer k_i is given by

$$k_i = \arg\max_i \{\|\mathbf{h}_i\|_F\}, \qquad\qquad 1 \leqslant i \leqslant K. \qquad\qquad (3.13)$$

The squared FN that measures the MIMO fading power is given by:

$$\|\mathbf{h}_i\|_F^2 = \text{trace}\left(\mathbf{h}_i \mathbf{h}_i^H\right), \qquad\qquad (3.14)$$

where $\{\}^H$ is the Hermitian operator.

2. Group interference nulling: interference from yet-to-be-detected groups is nulled out by projecting the desired group on their null space, resulting in nulling out all the other streams for each transmit antenna.

3. Slicing: estimating the detected group.

4. Symbol canceling: To improve the performance subtract the detected group from received signal vector and return to the nulling step.

Steps $\{1\text{-}4\}$ will be repeated until all symbols that have been transmitted from all layers are detected. Note that the detection here is serial, i.e., layer-by-layer detection. The optimum ordered set $\Omega = \{k_1, k_2, \ldots, k_K\}$ is chosen such that the post detection SNR is maximized in each iteration of the LSSTC detection algorithm. Components of the transmitted symbol vector will be extracted according to Ω. In contrast, for non-ordered decoding the order set is just $\{1, 2, \ldots, K\}$. Figure 3.2 shows how the optimal detection ordering operates in LSSTC receivers.

The procedure described above can be implemented in the LSSTC using the following algorithm[5, 6, 48]:

1. The layer that has the maximum post-detection SNR (or highest FN) is assigned to the index "1", and the detection will start from this layer, and therefore $\mathbf{Y}$ is assigned to $\mathbf{r_1}$.

2. Assuming the desired layer is k. Let $\mathcal{N}(\mathbf{c}_k)$ be the left null space of $\Lambda(\mathbf{c}_k)$
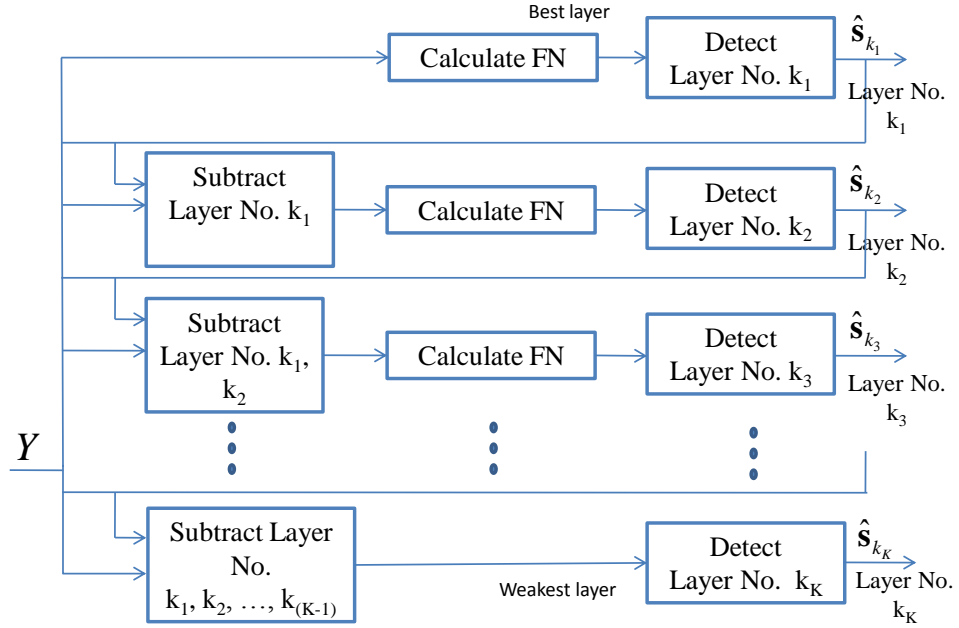
Figure 3.2: General block diagram of LSSTC receiver.

where

$$\Lambda(\mathbf{c}_k) = \left[\tilde{\mathbf{h}}_1, \ldots, \tilde{\mathbf{h}}_{k-1}, \tilde{\mathbf{h}}_{k+1}, \ldots, \tilde{\mathbf{h}}_K\right]. \tag{3.15}$$

3. The detector of layer k finds the $(N_R - M + m_k) \times N_R$ matrix $\Theta(\mathbf{c}_k)$, whose rows form a set of orthonormal vectors in $\mathcal{N}(\mathbf{c}_k)$.

4. The detector left multiplies the received signal $\mathbf{r}_1$ by $\Theta(\mathbf{c}_k)$, and the decision statistics for $\mathbf{c}_k$ are found as

$$\check{\mathbf{r}}_1 = \Theta(\mathbf{c}_k)\mathbf{Y} = \check{\mathbf{h}}_k\mathbf{c}_k + \check{\mathbf{n}}, \tag{3.16}$$

where $\check{\mathbf{h}}_k$ is the $(N_R - M + m_k) \times m_k$ modified channel matrix, and $\check{\mathbf{n}}$ is the

$(N_R - M + m_k) \times l$ modified noise matrix. Hence $\mathbf{c}_k$ can be decoded using the STBC maximum likelihood decoder.

5. Once $\mathbf{c}_k$ is decoded, its contribution is subtracted out from the original received signal $\mathbf{r_1}$ as follows

$$\mathbf{r_2} = \mathbf{r_1} - \check{\mathbf{h}}_k \check{\mathbf{c}}_k, \tag{3.17}$$

where $\check{\mathbf{c}}_k$ is the estimated STBC block of the kth layer.

6. The nulling and cancellation procedure in steps (2) to (5) are repeated serially until all the layers are detected.

3.3 Performance Analysis of LSSTC

In this section we derive a nearly exact error probability analysis for the LSSTC with SGIC receiver employing Binary Phase-Shift Keying (BPSK) modulation. In the analysis we will consider the effect of errors propagating from the previous erroneous layers. We will analyze the system assuming that the power is equally splitted among the AAs at the transmitter. Therefore it is denoted as equal power LSSTC (EPA-LSSTC). Our analysis gives recursive expressions for the error probability of each symbol which is evaluated using a recursive procedure [57]. In our analysis we assumed Alamouti's encoding matrix expressed in (2.2) where two symbols are transmitted over two time slots from each layer.

For the purpose of finding the probability of error we will use the virtual

MIMO model discussed in Section 2.1, where the system will be equivalent to an M-branch VBLAST system, where M is the number of AAs. For convenience the received signal obtained from (3.8) is re-written as

$$\underbrace{\mathbf{y}}_{(N_R*l)\times 1} = L \underbrace{\mathbf{H}_v}_{(N_R*l)\times M} \underbrace{\mathbf{s}}_{M\times 1} + \underbrace{\mathbf{n}}_{(N_R*l)\times 1}, \tag{3.18}$$

where $\mathbf{y}$ and $\mathbf{n}$ denotes the virtual matrices of $\mathbf{Y}$ and $\mathbf{N}$ respectively as defined in Section 2.1. Further, $\mathbf{H}_v$ can be partitioned into groups corresponding to each substream as $\tilde{\mathbf{H}}_v = [\mathbf{h}_1, \ldots, \mathbf{h}_M]$. Using the received signal, the detector will perform non-ordered SGIC since the post-ordered scheme will make our analysis more complicated. In addition, in [69] it was shown that the post-ordering does not increase diversity order, but only increases the SNR gain. The detector applies the algorithm discussed in Section 2.1. At the end of each stage and after subtracting the contribution of $\{x_1, \ldots, x_k\}$ the updated received signal becomes:

$$
\begin{aligned}
\mathbf{Y}_v^k &= \mathbf{Y}_v - \sum_{j=1}^{k} \mathbf{h}_j \hat{x}_j \\
&= \underbrace{\sum_{j=k+1}^{M} \mathbf{h}_j x_j}_{\text{faded target signal with interference}} + \underbrace{\left(\mathbf{n} + \sum_{j=1}^{k} \mathbf{h}_j \cdot (x_j - \hat{x}_j) \right)}_{\text{equivalent noise}},
\end{aligned} \tag{3.19}
$$

$\mathbf{y}^k$ is composed of three parts: the yet-to-be-detected symbols, the noise vector and the potential error propagation signal. We refer to the last two terms of (3.19) as the equivalent noise.

Assuming a total transmit power of P_T, each AA will have (P_T/M) as a transmit power. Since each AA results in a scalar $\alpha_{i,j}$ after multiplying by the weight matrix $\mathbf{W}$, each AA will be treated as a single antenna for the purpose of calculating transmit power and received SNR. According to [13], if a system has M independent sub-channels, the exact probability of bit error on the kth symbol when using BPSK modulation can be expressed as

$$P_{e_k} = \left[\frac{1}{2}(1-\mu)\right]^{D_k} \sum_{t=0}^{D_k-1} \binom{D_k - 1 + t}{t} \left[\frac{1}{2}(1+\mu)\right]^t, \qquad (3.20)$$

where $\mu = \sqrt{\dfrac{\rho}{1+\rho}}$, ρ is the sub-stream SNR, $\rho = \dfrac{(L^2 P_T/N_T)}{N_0}$, and D_k is the diversity order of the layer $\Gamma(k)$ from which the kth symbol is transmitted, and of course, all sub-streams associated with the same layer have the same diversity order, for instance, if we used Alamouti's STBC, the first and second sub-streams will have the same diversity order. We write the diversity order of the kth sub-stream as $D_k = m_k(N_R - K + \Gamma(k))$. This definition is quite reasonable and proven to be valid by the simulation results. It can be noted that STBC increases the diversity order of each layer. It is clear to see that the generalization of this procedure to M-ary PSK, or M-ary QAM can be done simply by replacing (3.20) with the formulas corresponding to these modulation schemes. Note that all the sub-streams of a layer employing STBC have the same probability of error. For instance, if $m_k = 2$, then $\text{Prob}\{x_1 \neq \hat{x}_1\} = \text{Prob}\{x_2 \neq \hat{x}_2\}$.

The sub-stream error will depend on the number of errors that occurred in the sub-stream itself and on the errors propagating from the previous layers, and will not depend the errors occurring in the other sub-streams of the same layer. Therefore, we will calculate the layer probability of error, which will be equal to the probability of sub-stream error of the sub-streams sent from that layer. Therefore throughout this thesis we will express the layer performance in terms of that of one of its substreams. For the ith layer the latter will be denoted as s_i. Since Equation (3.20) will be used very often in our analysis, and for the sake of simplicity, we define the function

$$P_e(D_k, \rho) = \left[\frac{1}{2}(1-\mu) \right]^{D_k} \sum_{t=0}^{D_k-1} \binom{D_k - 1 + t}{t} \left[\frac{1}{2}(1+\mu) \right]^t. \qquad (3.21)$$

It is clear that in the absence of error propagation, the layer probability of error of the kth layer for $k = 1, \ldots, K$, can be expressed as

$$P_{e_k} = P_e(D_k, \rho). \qquad (3.22)$$

But when considering the presence of error propagation, the probability of error can be expressed as

$$
\begin{aligned}
P_{e_k} &= \text{Prob}\{s_k \neq \hat{s}_k\} \\
&= \sum_{i=0}^{k-1} \text{Prob}\{s_k \neq \hat{s}_k \mid A_{k-1}^i\} \text{Prob}\{A_{k-1}^i\}, \qquad (3.23)
\end{aligned}
$$

where A_{k-1}^i defines the event of having i errors in the symbols $\hat{s}_1 \sim \hat{s}_{k-1}$. Now in order to find P_{e_k}, we need to find $\text{Prob}\{s_k \neq \hat{s}_k \mid A_{k-1}^i\}$ and $\text{Prob}\{A_{k-1}^i\}$ first, which is discussed in the following sections.

3.3.1 Calculation of $\text{Prob}\{s_k \neq \hat{s}_k \mid A_{k-1}^i\}$

Define the equivalent noise as a new random variable $\mathbf{N}^{i,k}$ given by

$$
\begin{aligned}
\mathbf{N}^{i,k} &= \mathbf{n} \mid A_{k-1}^i \\
&= \mathbf{n} + \sum_{j=1}^{k-1} \mathbf{h}_j \cdot \left(s_j - \hat{s}_j\right).
\end{aligned}
\tag{3.24}
$$

given that i detection errors exist in $k-1$ symbols that were detected in the first $k-1$ layers, then there will be $(k-1-i)$ correct decissions in which s_j and $\hat{s}_j$ are equal. To generalize our work as in [57], we didn't restrict the order of errors. Instead, a map function $g_k(\cdot)$ is defined to accommodate for any injection of i errors, and therefore the equivalent noise can be written as

$$
\mathbf{n} + \sum_{j=1}^{i} \mathbf{h}_{g_k(j)} \cdot \left(s_{g_k(j)} - \hat{s}_{g_k(j)}\right).
\tag{3.25}
$$

Since we assume BPSK modulation, $s_{g_k(j)}$ will take one of the values in the set $\{-\sqrt{P_T/M}, +\sqrt{P_T/M}\}$, and therefore, $\left(s_{g_k(j)} - \hat{s}_{g_k(j)}\right)$ given that $s_{g_k(j)} \neq \hat{s}_{g_k(j)}$, will take a value from the set $\{-2\sqrt{P_T/M}, +2\sqrt{P_T/M}\}$. Note that the equivalent noise given in (3.25) is not Gaussian [57] since the event A_{k-1}^i will bring restrictions on

$\mathbf{n}$ and $\mathbf{h}_{g_k(j)}$. However, in the analysis of [57] it was assumed that $\mathbf{N}^{i,k}$ is white Gaussian, which turned out to be a valid assumption when comparing with the simulation results. In order to completely express $\mathbf{N}^{i,k}$ assuming it is a white Gaussian random variable (RV), we need to find its mean and variance. First, let's calculate the mean of the RV $\mathbf{N}^{i,k}$:

$$\mathrm{E}\left[\mathbf{n} \mid A_{k-1}^i\right] = \mathrm{E}[\mathbf{n}] + \sum_{j=1}^{i} \mathrm{E}\left[\mathbf{h}_{g_k(j)}\right] \cdot \mathrm{E}\left[s_{g_k(j)} - \hat{s}_{g_k(j)}\right]. \tag{3.26}$$

Since $s_{g_k(j)}$ and $\hat{s}_{g_k(j)}$ are taken from the same constellation then they have same expected value, which is zero, and therefore

$$\mathrm{E}\left[\mathbf{n} \mid A_{k-1}^i\right] = E[\mathbf{n}] = 0. \tag{3.27}$$

We calculate the covariance matrix of $\mathbf{N}^{i,k}$ in Appendix A as

$$\mathrm{Cov}\left[\mathbf{N}_m^{i,k}, \mathbf{N}_n^{i,k}\right] = \left[N_0 + \frac{4P_T i L^2}{M}\right] I_{N \times N}, \tag{3.28}$$

and thus $\mathrm{Prob}\{s_k \neq \hat{s}_k \mid A_{k-1}^i\}$ in (3.23) can be expressed as

$$\mathrm{Prob}\{s_k \neq \hat{s}_k \mid A_{k-1}^i\} = P_e\left(m_k(N_R - K + k), \frac{P_T L^2}{M N_0 + 4 P_T i L^2}\right). \tag{3.29}$$

3.3.2 Calculation of $\text{Prob}\{A^i_{k-1}\}$

In this section we will summarize the formulas used to find $\text{Prob}\{A^i_{k-1}\}$ for three cases using the approach adopted in [57]. The details of the derivation can be reviewed from Appendix B.

$$\text{Prob}\{A^i_{k-1}\} = \begin{cases} \left[1 - P_e\left(m_{k-1}(N_R - K + k), \frac{P_t L^2}{MN_0}\right)\right] \times \text{Prob}\{A^0_{k-2}\}, & i = 0 \\[2em] P_e\left(m_{k-1}(N_R - K + k), \frac{P_t L^2}{MN_0 + 4P_t(k-2)L^2}\right) \times \text{Prob}\{A^{k-2}_{k-2}\}, & i = k-1 \\[2em] \text{Prob}\{s_{k-1} \neq \hat{s}_{k-1} \mid A^{i-1}_{k-2}\}\text{Prob}\{A^{i-1}_{k-2}\} \\[1em] + \left[1 - \text{Prob}\{s_{k-1} \neq \hat{s}_{k-1} \mid A^i_{k-2}\}\right]\text{Prob}\{A^i_{k-2}\}, & 0 < i < k-1 \end{cases}$$

3.3.3 Calculation of P_{e_k}

After finding $\text{Prob}\{s_k \neq \hat{s}_k \mid A^i_{k-1}\}$ and $\text{Prob}\{A^i_{k-1}\}$, the probability of error on the kth layer denoted as P_{e_k} can be evaluated directly using (3.23). From that we can find the probability of error of the individual sub-streams by

$$\text{Prob}\{x_k \neq \hat{x}_k\} = P_{e_{\Gamma(k)}}, \tag{3.30}$$

where $\Gamma(k)$ is the layer from which the kth sub-stream is sent. The average proba-

bility of error over all M sub-streams can be written as

$$P_{av} = \frac{1}{M} \cdot \sum_{k=1}^{M} \text{Prob}\{x_k \neq \hat{x}_k\}. \tag{3.31}$$

3.4   Capacity of LSSTC

To derive a formula for the capacity of LSSTC per user, we will follow the deriva-

tion of [50]. First, the instantaneous capacity was found in [70] for an orthogonal

STBC with M_s transmit antennas and R_s code rate,

$$C_{STBC} = R_s \cdot \log_2 \left(1 + \frac{P_T}{M_s} \|\mathbf{H}\|^2 \right) \tag{3.32}$$

In MLSTBC which is a combination of VBLAST and STBC, an outage occurs if an

outage happens in any layer because all the STBC encoders (layers) are transmit-

ting at the same rate. The layer that is the most probable to fall in an outage is the

weakest layer, i.e. the one that has the least value of $\|\mathbf{H}_i\|^2$, $i = 1, 2, \ldots, K$, where $\mathbf{H}_i$

is the ith matrix of $\mathbf{H}$. Therefore, the instantaneous capacity of a K layered STBC

system with a sub-stream SNR of ρ can be written as:

$$
\begin{aligned}
C &= K \cdot R_s \cdot \log_2 \left(1 + \rho \cdot \min_{k=1,2,\ldots,K} \left\{ \|\mathbf{H}_i\|^2 \right\} \right) \\
&= K \cdot R_s \cdot \min_{k=1,2,\ldots,K} \left\{ \log_2 \left(1 + \rho \cdot \|\mathbf{H}_i\|^2 \right) \right\}.
\end{aligned} \tag{3.33}
$$

Extending the last results, the instantaneous capacity of LSSTC can be expressed as:

$$C_{LSSTC} = K \cdot R_s \cdot \min_{k=1,2,\ldots,K} \left\{ \log_2 \left(1 + \frac{L^2 \cdot P_T}{M \cdot N_0} \cdot \|\mathbf{H}_{PP,k}\|^2 \right) \right\} \qquad (3.34)$$

where $\mathbf{H}_{PP,k}$ is the Post-Processing (PP) matrix corresponding to the kth layer after nulling out the interference from the yet-to-be-detected layers. It is clear that the LSSTC capacity is dominated by the worst group which has the minimum value of $\mathbf{H}_{PP,k}$, $k = 12,\ldots,K$.

3.5 Diversity, Multiplexing, and Beamforming Trade-off in LSSTC

In [71] the authors have found the tradeoff curve for a MIMO system that has the capability of providing both diversity and multiplexing advantage. In this section, we add to that the beamforming advantage of LSSTC by providing a comparison among the LSSTC system configurations. A system is said to have a diversity gain of d if the error probability decays as $(SNR)^{-d}$ [71] , and a spatial multiplexing gain of r if the rate of the scheme is $(r \log SNR)$.

In an LSSTC system with N_T transmit and N_R receive antennas, assuming the path gains between individual antenna pairs are i.i.d. Rayleigh faded, the maximum diversity gain ignoring the antennas assigned for beamforming is $\left(\frac{N_T N_R}{L} \right)$, which is the total number of fading realizations over which system performance

is averaged.

The tradeoff curve shows the diversity advantage achievable by the LSSTC system for each multiplexing gain r, and beamforming gain which we define as the number of beamforming elements (L). Clearly, L cannot exceed the total number of transmit antennas N_T. On the other hand, r cannot exceed the total number of degrees of freedom provided by the channel $min\left(\frac{N_T N_R}{L}, N_R\right)$; and $d(r,L)$ cannot exceed the maximum diversity gain of the channel $\left(\frac{N_T N_R}{L}\right)$. The tradeoff curve links between these three extreme limits. The tradeoff curve is found in a similar manner to [71], and is given by the piecewise-linear function connecting the points $(r, d(r,L))$, $r = 0, 1, \ldots,$ $min\left\{\frac{N_T N_R}{L}, N_R\right\}$. For each possible value of L, the diversity gain $d(r)$ is given by

$$d(r,L) = \left(\frac{N_T}{L} - r\right)\left(N_R - r\right) \tag{3.35}$$

3.6 Numerical Results

In all the Monte-Carlo simulations conducted in this work, we used Alamouti's STBC matrix of unity rate expressed in (2.2) for the STBC encoders in each layer. In addition, unless otherwise mentioned, the SGIC detector does not perform ordering, rather it performs detection starting from the first layer in the $\tilde{\mathbf{H}}$ matrix, which is not necessarily the best decoding order.

Figure 3.3 compares the symbol error rate of an LSSTC system with different

number of receive antennas, and 16-QAM modulation is used. The transmiter sends the symbols on two layers ($K = 2$) each of which consists of two sub-streams ($m_k = 2$) that corresponds to Alamouti's STBC encoder. Each of those sub-streams is then transmitted through the corresponding AA of two elements ($L = 2$). It is clear to see that increasing N_R will improve the performance since increasing N_R will result in higher diversity order, which will lead to having a steeper slope of the error probability curve versus SNR.

Figure 3.4 shows the effect of increasing the downlink beamforming gain by increasing the number of beam-steering elements L in each AA, while maintaining the same number of layers ($K = 2$) and AAs ($m_k = 2$), also the number of receive antennas is the same ($N_R = 2$). As shown in the Figure, when the number of beam-steering elements L increases, the achievable SER performance significantly improves.
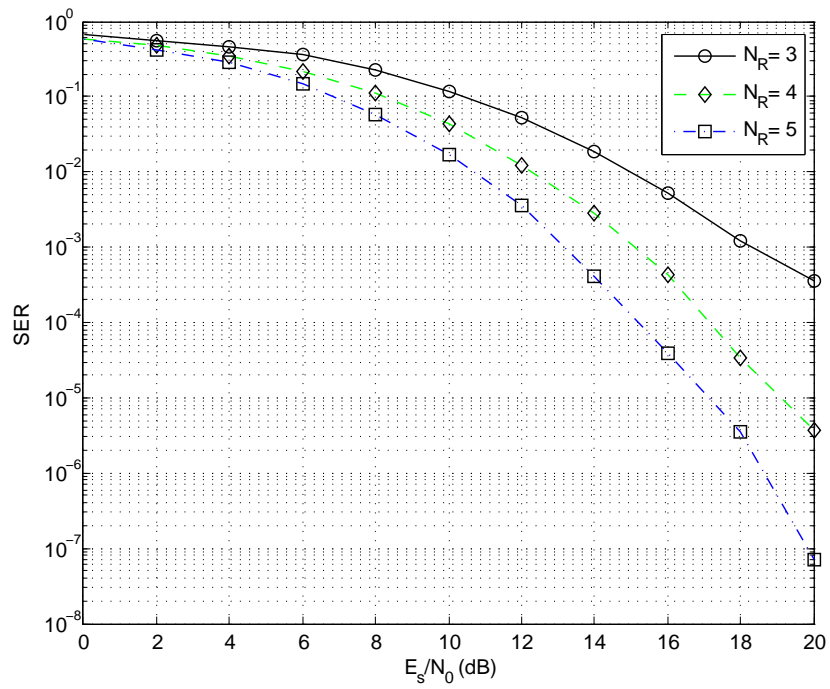
Figure 3.3: SER of LSSTC employing non-ordered SGIC and using 16-QAM modulation with $K = 2$ & $L = 2$ (comparing different number of receive antennas).
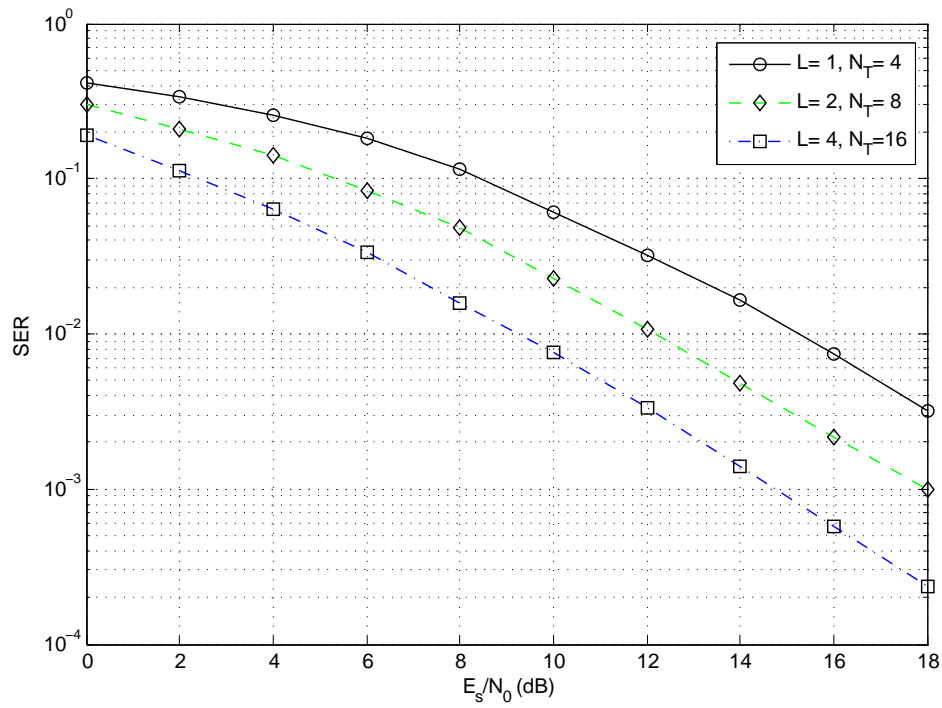
Figure 3.4: SER of LSSTC employing non-ordered SGIC and using 16-QAM modulation with $K = 2$ & $N_R = 2$ (comparing different number of beam-steering elements).

Now a fair comparison between LSSTC and VBLAST is conducted. This fairness is achieved by structure and spectral efficiency fairness, that means that the total number of antennas at the transmitter N_T and the number of symbols sent every time slot are the same for both systems.

Figure 3.5 shows a comparison between LSSTC and VBLAST in terms of the symbol error rate. The two systems use a total number of transmit antennas, $N_T = 8$, and the receiver is equipped with 4 antennas. In this comparison we have also compared many transmitter configurations, in each a different modulation scheme is used such that the spectral efficiency would be the same for all of them, which is set to 4 bps/Hz. From Figure 3.5 it can be clearly seen that VBLAST outperforms LSSTC in the low range of SNR, whereas for values of SNR that exceed 9 dB, the LSSTC outperforms VBLAST because it has a higher diversity order resulting from using STBC, which drives the SER to decay sharply.
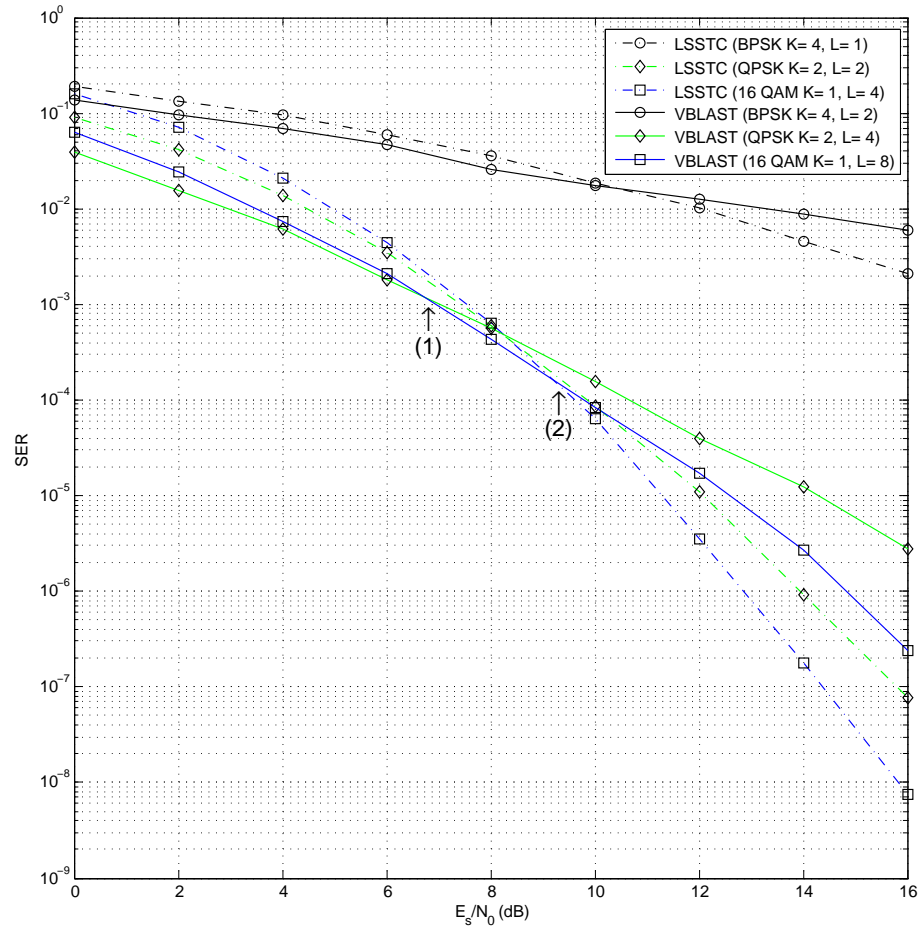
Figure 3.5: SER of LSSTC employing non-ordered SGIC at 4 bps/Hz and different modulation schemes with $N_T = 8$ & $N_R = 4$ (comparing VBLAST to LSSTC fairly).

Next, we propose a multi-configuration transmission scheme based on LSSTC and VBLAST systems. This scheme suggests the configuration and the modulation scheme in order to improve the performance. Table 3.1 lists the proposed transmitter configuration and modulation scheme depending on the SNR level in the system.

For example if the SNR in a wireless system ranges from (6.6 dB-9.2 dB), then the performance will be better if VBLAST scheme with 16-QAM modulation is used, while if it lies in the range(>9.2 dB) then it is better to use LSSTC scheme with 16-QAM modulation.

One might say, why do not we design an adaptive system that chooses between VBLAST and LSSTC? This can be done using an antenna array with the capability of electronically activating specific antenna elements and deactivating the remaining ones. This is done to meet the antenna separation conditions of each mode in the multi-configuration system. In LSSTC, there are two conditions for the antenna element separation. (1) The AAs should be sufficiently far apart in order to experience independent fading. (2) Beamforming elements within each AA should be spaced at small distance that is less than $\lambda/2$ for the sake of achieving beamforming. On the other hand, VBLAST requires all the antennas to be spaced

Table 3.1: Proposed transmitter configuration and modulation schemes.

SNR level (dB)	Transmitter configuration	Modulation scheme
< 6.6	VBLAST	QPSK
$6.6 - 9.2$	VBLAST	16-QAM
> 9.2	LSSTC	16-QAM

sufficiently far from each other. In Figure 3.6, the SER performance of LSSTC employing non-ordered SGIC is compared to LSSTC employing post-ordered SGIC, where QPSK modulation with $K = 3$ and $N_R = 4$ is used. As shown in the Figure, employing post-ordered SGIC will improve the SER performance, and this improvement can be seen more clear at high values of SNR. In addition, it can be noted that while increasing the SNR, the difference between non-ordered and post-ordered SGIC will increase.

Figure 3.7 compares the simulation results to the analysis results for the symbol error rate of an LSSTC system employing non-ordered SGIC and BPSK modulation with $K = 2$ and $N_R = 2$. It can be seen that the simulation and analysis results match quite well, which proves the validity of the analysis. Figure 3.7 proves the validity of approximating the equivalent noise $\mathbf{N}^{i,k}$ to a white gaussian random variable
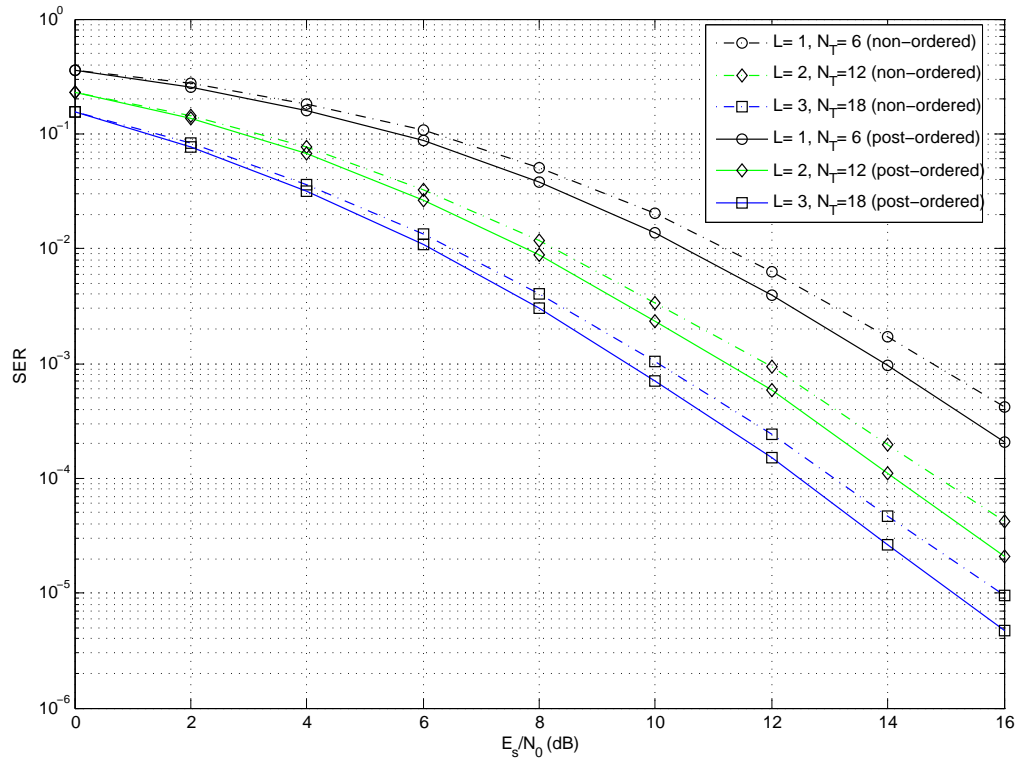
Figure 3.6: SER of LSSTC employing SGIC and QPSK modulation with $K = 3$ & $N_R = 4$ (comparing non-ordered SGIC to post-ordered SGIC).
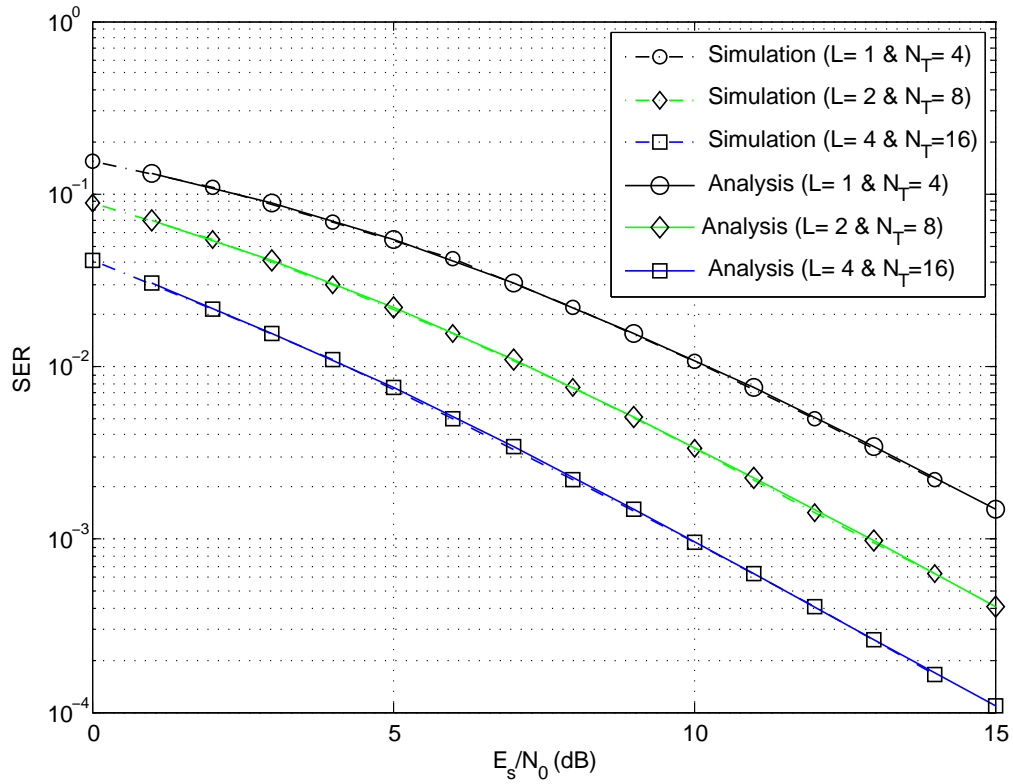
Figure 3.7: SER of LSSTC employing non-ordered SGIC and BPSK modulation with $K = 2$ & $N_R = 2$ (comparing analysis to simulation results).
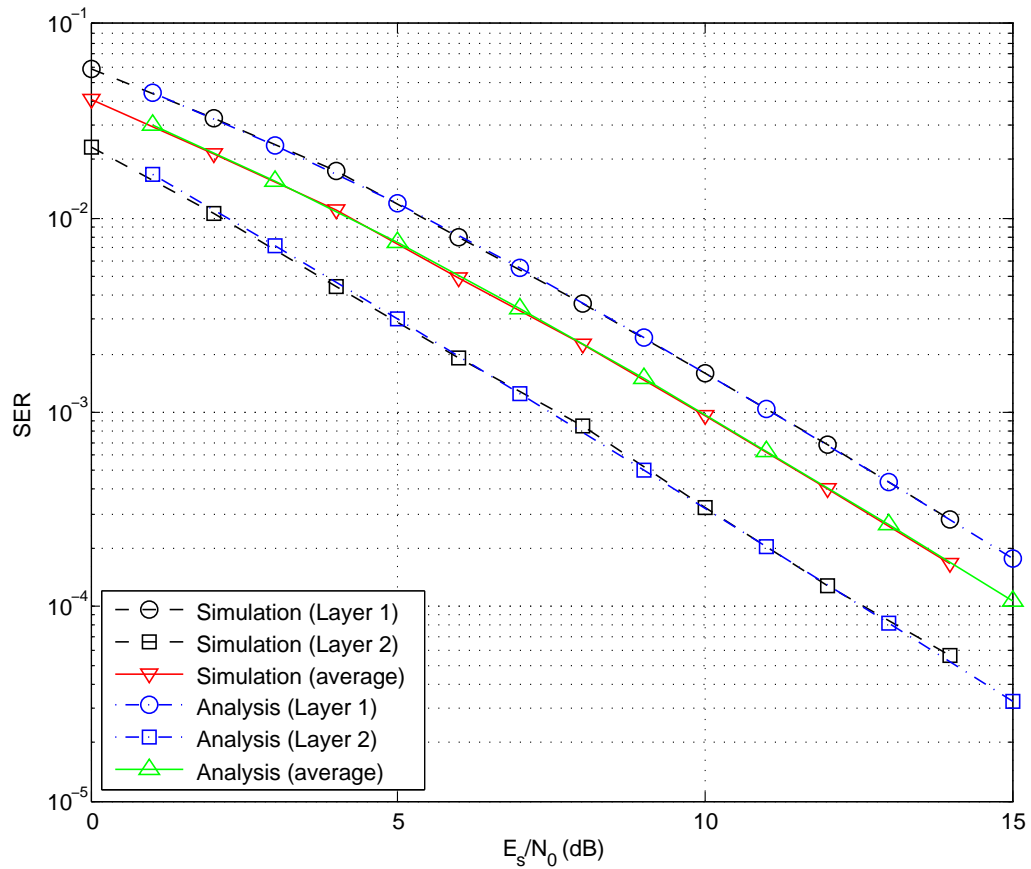
Figure 3.8: SER of the individual layers of a 16×2 LSSTC employing non-ordered SGIC and BPSK modulation with $K = 2$ & $L = 4$ (comparing analysis to simulation results).

Figure 3.8 shows the SER of the individual layers of a 16×2 LSSTC using non-ordered SGIC detector employing BPSK modulation with $K = 2$ and $L = 4$ obtained from both the simulation and the analysis. The Figure compares the analytical results obtained for the EPA-LSSTC to those obtained from the simulation results with equal power allocation. It is clear that the Monte Carlo simulation makes a nearly perfect match to the analysis methods, which demonstrates the validity of the analysis proposed in this chapter.

Figure 3.9 fairly compares LSSTC to VBLAST in terms of the ergodic capacity of an 8×4 MIMO using non-ordered SGIC at 15 dB average SNR. Several configuration are considered, and the capacity is plotted versus E_s/N_0. As it can be seen from the figure, the capacity is approximately linearly increasing with increasing E_s/N_0. It is clear to see that VBLAST outperforms LSSTC, which is actually expected, since VBLAST is a pure spatial multiplexing unlike LSSTC, where some antennas are assigned for diversity.
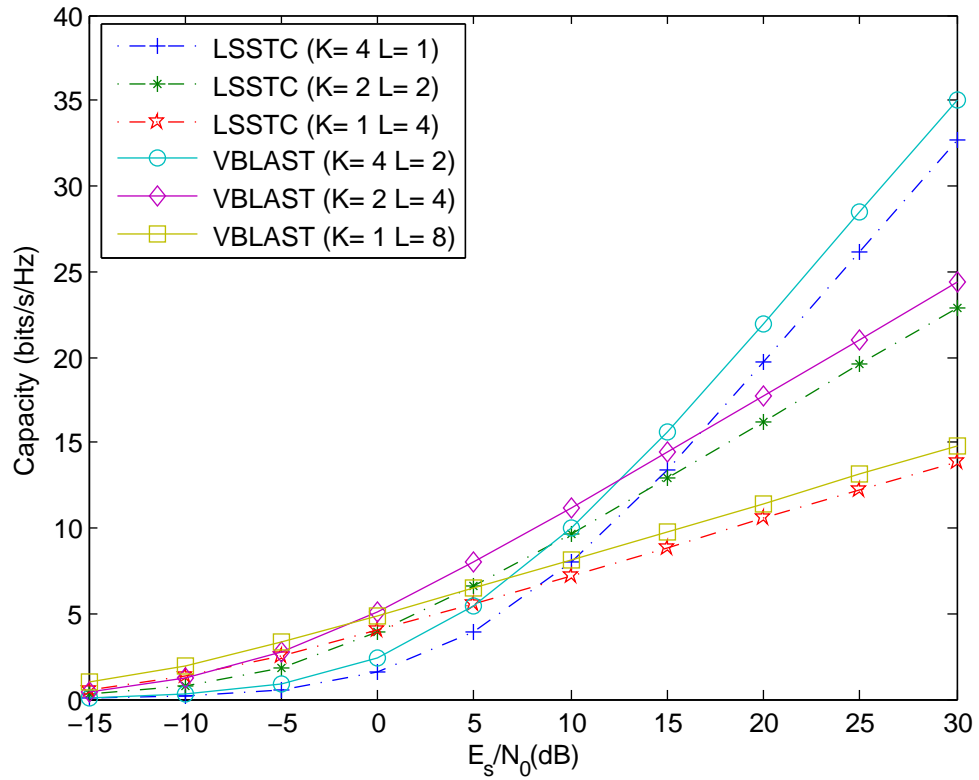
Figure 3.9: Ergodic Capacity vs. E_s/N_0 for an 8×4 MIMO at 15 dB average SNR (comparing VBLAST to LSSTC fairly).

Figure 3.10 compares the outage capacity of LSSTC to that of VBLAST for an 8×4 MIMO at 10% Outage probability and 15 dB average SNR. The different configurations behave in a similar manner to that in Figure 3.9. For the 4-layer case, we see that LSSTC approaches VBLAST, one possible reason for that is that the STBC processing will tend to average the channel, and as a result LSSTC will be less probable to fall in an outage. On the other hand, VBLAST doesn't have such a capability. Figure 3.10 shows that we can design a multi-configuration system, such that to maximize the capacity for all values of SNR. For the forementioned configuration we choose the single-layer VBLAST system for the first range (-15 dB up to 1 dB), and for the second range (1 dB up to 20 dB) the dual-layer VBLAST system gives the highest capacity. If the SNR lies in the last range(>20 dB), then using either LSSTC or VBLAST with 4 layers will have approximately the same capacity. However, Figure 3.5 shows that LSSTC has a lower SER in the last range, and therefore, we choosing LSSTC is better. Figure 3.11 shows similar results to those of Figure 3.10 but with using an 8×8 MIMO at 90% Outage probability. There is a huge jump in the capacity due to increasing the number of receive antennas, and consequently increasing the spatial multiplexing gain.
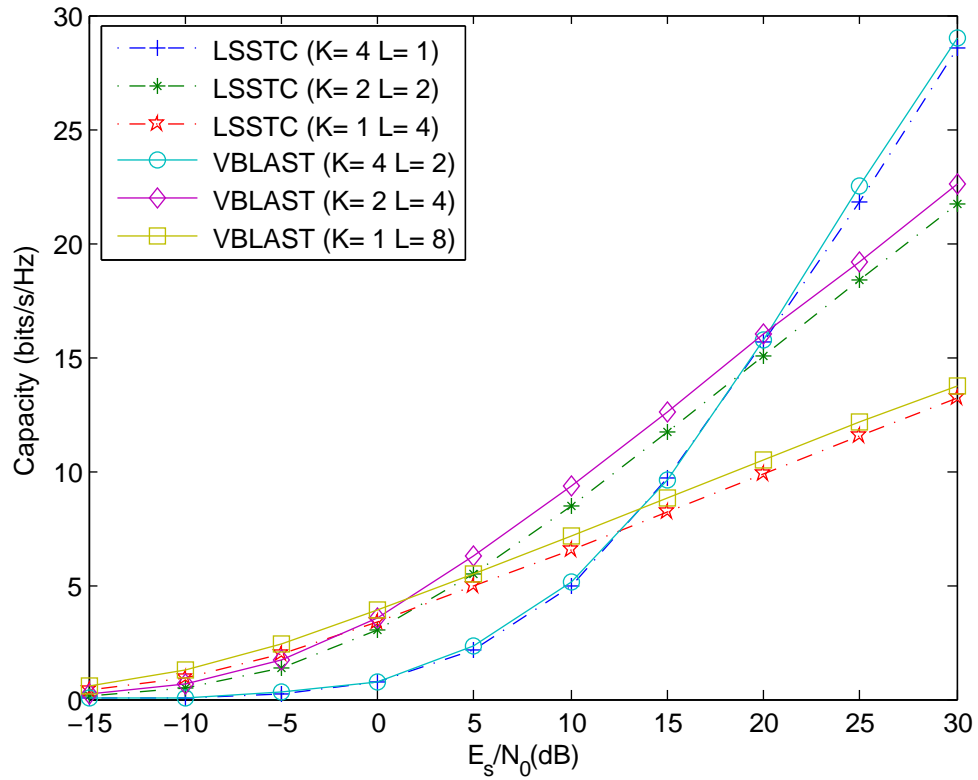
Figure 3.10: Outage Capacity vs. E_s/N_0 for an 8×4 MIMO at 10% Outage probability, and 15 dB average SNR (comparing VBLAST to LSSTC fairly).
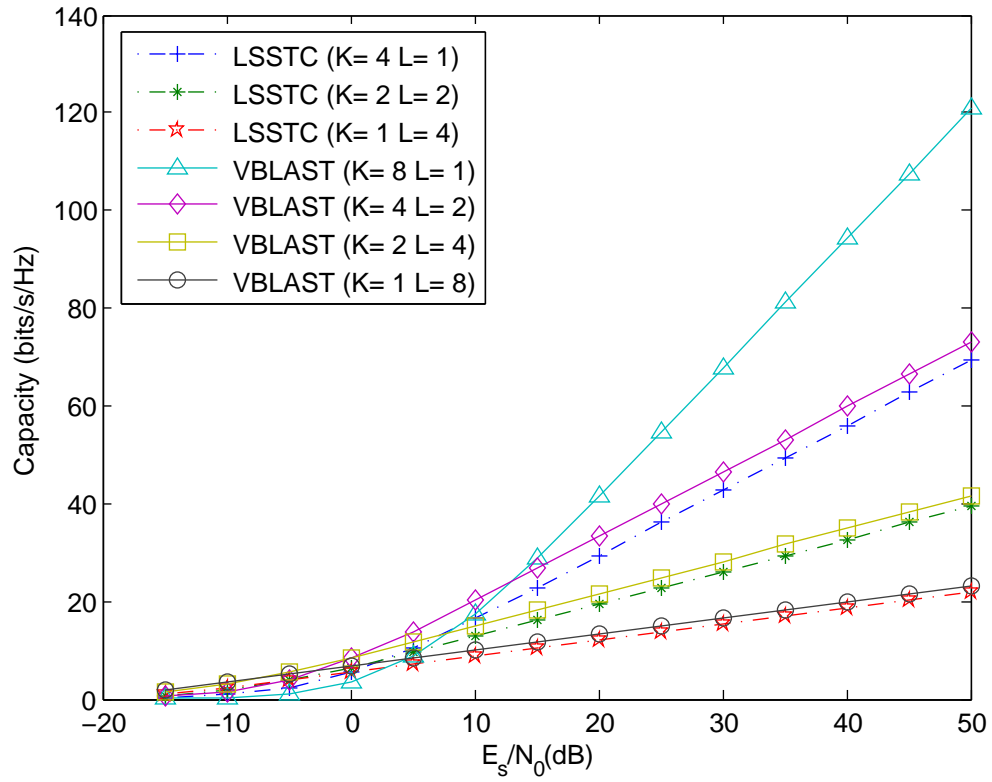
Figure 3.11: Outage Capacity vs. E_s/N_0 for an 8×8 MIMO at 90% Outage probability, and 15 dB average SNR (comparing VBLAST to LSSTC fairly).

Figure 3.12 shows the diversity-multiplexing tradeoff curve of a 16×8 LSSTC system. As we can see from the figure, two points of interest can be identified

$$
\begin{aligned}
d_{max} &= d(r_{min}, L_{min}) = d(0,1) = \frac{N_T N_R}{L} \qquad &(3.36)\\
r_{max} &= \min\left\{\frac{N_T N_R}{L}, N_R\right\} \qquad &(3.37)
\end{aligned}
$$

It can be noted that increasing the diversity advantage at a specific beamforming gain comes at a price of decreasing the spatial multiplexing gain, and vice versa. Figure 3.13 shows the same tradeoff of a 64×32 LSSTC system. Figure 3.14 shows the diversity-beamforming tradeoff of a 16×8 LSSTC system. In Figure 3.12 it should be noted that the points to the left of each curve represent an achievable diversity gain for that specific configuration, whereas the points to the right are not achievable. This means that we may find systems that has a trade-off curve to the left of the optimum trade-off curve, but not to his right.

Figure 3.15 shows the diversity-multiplexing-beamforming tradeoff of a 16×8 LSSTC system plotted in $3 - D$ format. In the figure, it can be noted that increasing one parameter causes the other parameters to decrease and vice versa.
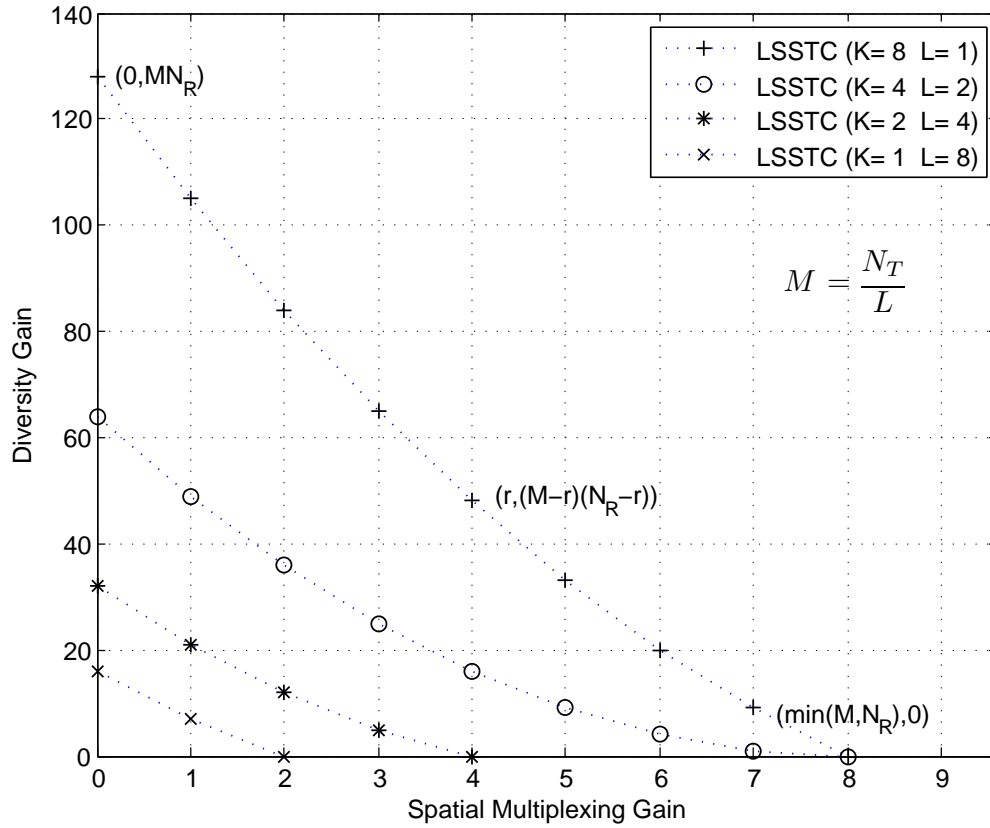
Figure 3.12: Diversity-multiplexing tradeoff of LSSTC ($N_T = 16$ & $m_k = 2$ & $N_R = 8$).
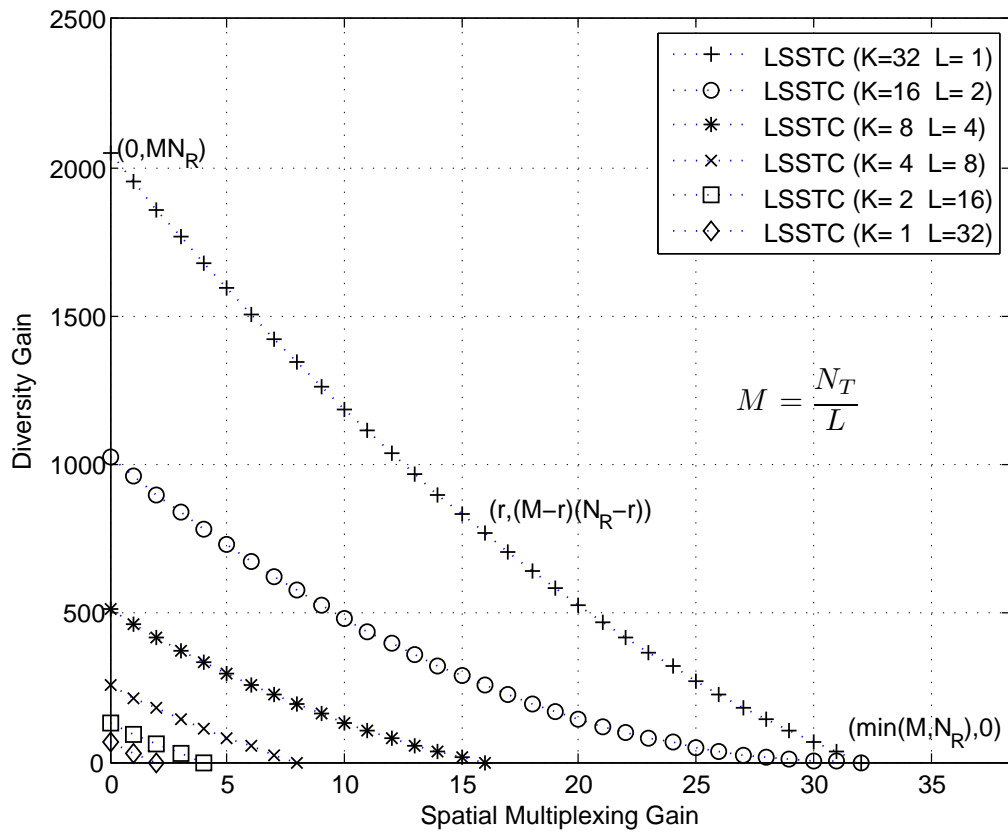
Figure 3.13: Diversity-multiplexing tradeoff of LSSTC ($N_T = 64$ & $m_k = 2$ & $N_R = 32$).
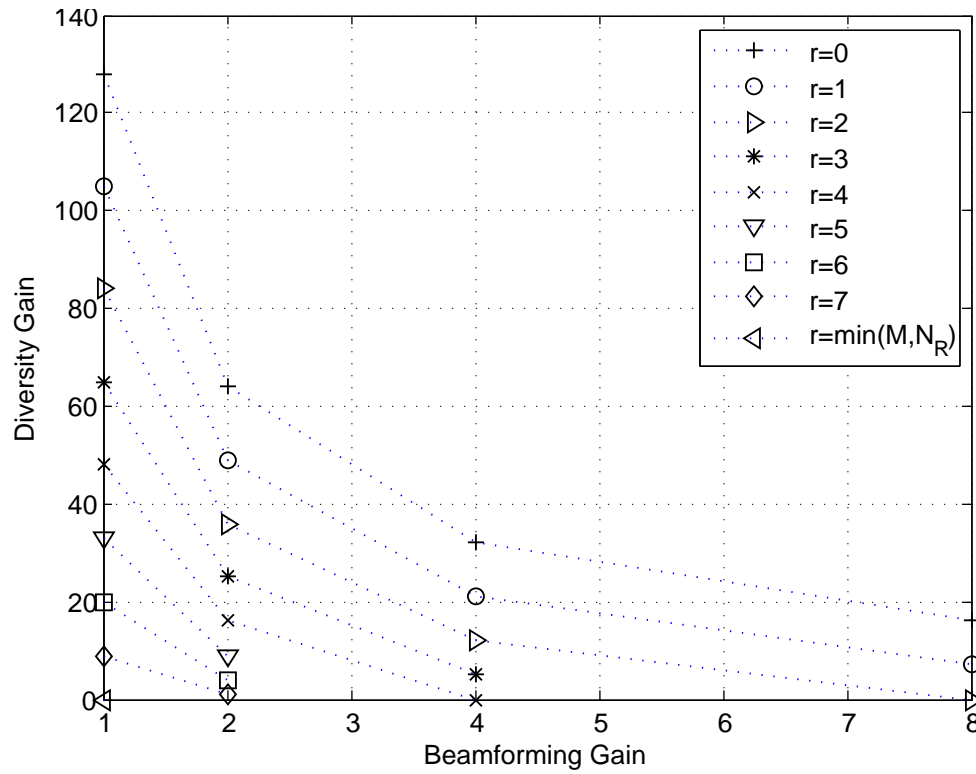
Figure 3.14: Diversity–beamforming tradeoff of LSSTC ($N_T = 16$ & $m_k = 2$ & $N_R = 8$).
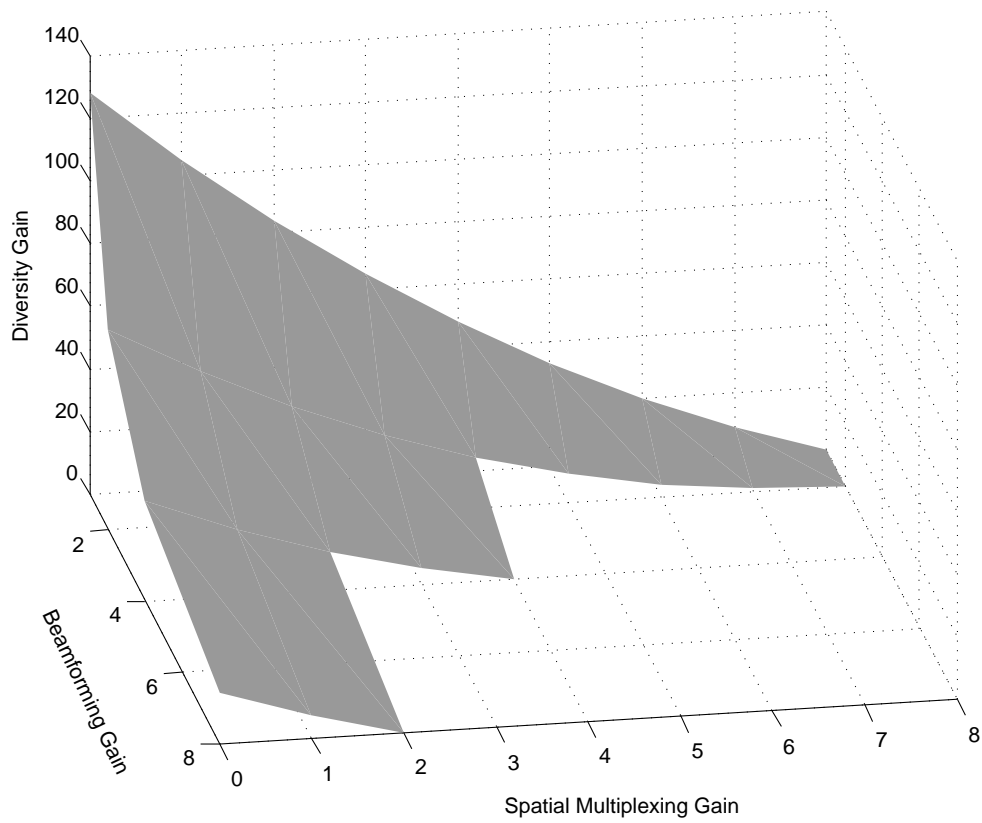
Figure 3.15: Diversity-multiplexing–beamforming tradeoff of LSSTC ($N_T = 16$ & $m_k = 2$ & $N_R = 8$).

3.7   Chapter Conclusions

In this chapter we investigated the performance of single-user LSSTC. A brief mathematical description on beanmforming was explained. We extended the derivation of the probability of error for VBLAST system employing BPSK to include the effect of beamforming and STBC. We showed that using antenna arrays results in a direct SNR gain. On the other hand, using STBC increases the diversity order of each layer. The analytical results were verified by the simulation results. Also, a formula for the instantaneous capacity of single-user LSSTC was derived. Additionally, the diversity, multiplexing, and beamforming tradeoff curve for LSSTC was investigated. This curve provided a deeper insight to the system where it was found that increasing one parameter causes the other parameters to decrease and vice versa. Finally, we proposed a multi-configuration transmission scheme based on LSSTC and VBLAST systems. This scheme showed that LSSTC has better performance than VBLAST at high SNR range.

Chapter 4

Power Allocation in LSSTC

In this chapter we suggest a new scheme for LSSTC, in which we have modified the LSSTC system model presented in Section 3.1 by assuming that the user feeds the BS with the average SNR per layer through the uplink feedback channel. The reason for designing such a system is to enhance the performance and capacity by assigning power to the layers in an optimum manner. Our analysis is based on the results of [66] for VBLAST applying the power allocation scheme and extends to the LSSTC case where beamforming and STBC are involved. We refer to the system proposed in this chapter as the power allocation LSSTC (PA-LSSTC). We also investigate the performance of PA-LSSTC, and extend the results to M-ary PSK and M-ary QAM.

The Chapter is organized as follows. Section 4.1 presents the notation used for the power allocation scheme. Section 4.3 shows the performance analysis of PA-

LSSTC, in which we derive a formula for the probability of error of the individual layers employing different modulation schemes, Furthermore, we formulate the the average SER of the LSSTC system. In Section 4.4, the optimum PA scheme for LSSTC is derived so that the probability of error is minimized. Section 4.6 presents the simulation results conducted to evaluate the PA-LSSTC system. Finally, Section 4.7 presents the chapter's conclusions.

4.1 The Power Allocation Scheme

The PA pattern for the PA-LSSTC scheme is defined in a similar manner as for VBLAST in [66]. The system is characterized by the vector $\mathbf{K} = [K_1, K_2, \cdots, K_{M-1}]$ where K_i is defined as the transmit power ratio of the ith sub-stream to the sum of sub-stream $i+1, \cdots, M$. K_i is defined by

$$K_i = \frac{P_i}{\sum_{j=i+1}^{M} P_j}, \quad i = 1, 2, \cdots, M-1, \tag{4.1}$$

where P_i denotes the transmit power of the ith sub-stream. Similarly, we define the layer PA pattern as $\mathbf{K}_L = [K_{L,1}, K_{L,2}, \cdots, K_{L,K-1}]$ where K is the number of layers, and $K_{L,i}$ is defined as the transmit power ratio of the ith layer to the sum of layer $i+1, \cdots, K$. $K_{L,i}$ is defined by

$$K_{L,i} = \frac{P_{L,i}}{\sum_{j=i+1}^{K} P_{L,j}}, \quad i = 1, 2, \cdots, K-1, \tag{4.2}$$

where $P_{L,i}$ denotes the transmit power of the ith layer. For fair comparison among different energy allocation patterns, P_i must satisfy the energy conservation constraint, $P_T = \sum_{i=1}^{M} P_i = P_s$, where P_s denotes the average transmit power per modulation symbol.

The reason for defining **K** is intended to reduce the hardware complexity because we use Newton's method to find the optimum power allocation in Section 4.4. Using **K** reduces the number of equations by one since we express it in terms of of the total power, otherwise, we would have to write K equations corresponding to the power of the layers, where K is the number of layers.

4.2 System Model

The system model we use in this chapter is built on that proposed in Section 3.1, with an exception that the BS of PA-LSSTC prompts the user to feedback the CSI per layer via the feedback channel along with the DOA data. Also the transmitter is capable of performing PA processing. The system model of PA-LSSTC is shown in Figure 4.1

4.3 Performance Analysis

In this section, the performance of LSSTC systems employing PA scheme and SGIC receivers with a fixed detection ordering is analyzed. The analysis is car-
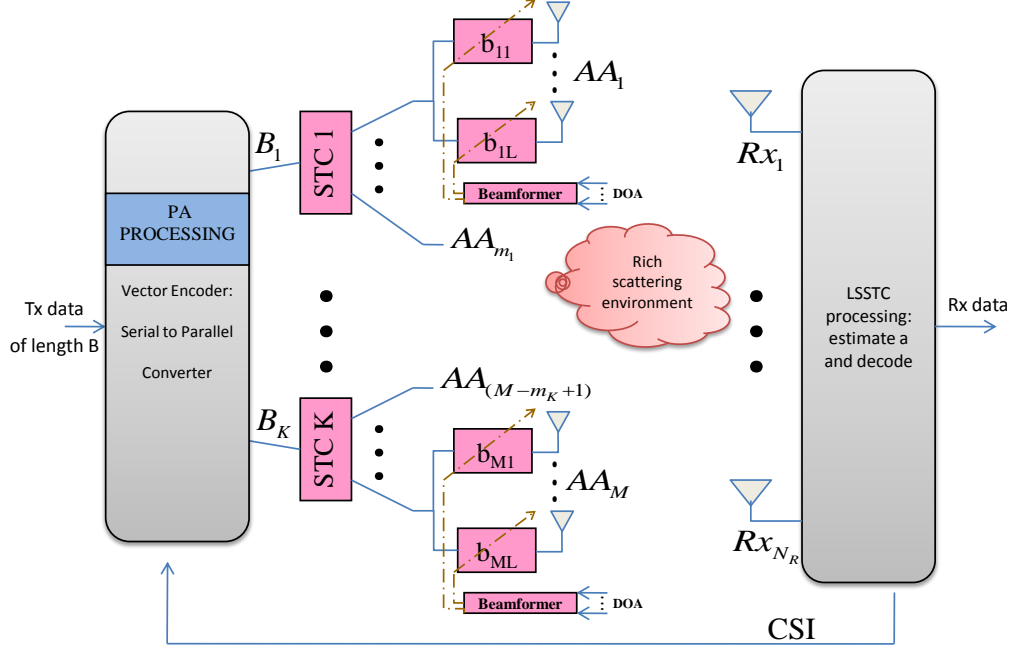
Figure 4.1: Block diagram of a single user PA-LSSTC system.

ried out for slow Rayleigh fading channels, in which we assume that the channel remains constant for many STBC blocks. Thus the transmitter obtains the estimates of the average SNR per layer from the receiver, finds the optimum power allocation, and uses the same power allocation pattern till the channel changes. Using this assumption minimizes the feedback load by a significant amount. We first denote the SER of the ith sub-stream under PA pattern $\mathbf{K}_L$ and noise of variance N_0 as $P_{e_i|(\mathbf{K}_L,N_0)} = P\{\hat{s}_i \neq s_i \mid \mathbf{K}_L,N_0\}$. The SER of the ith layer has the form

$$P_{e_i|(\mathbf{K}_L,N_0)} = \sum_{l=0}^{i-1} P\{s_i \neq \hat{s}_i, A_{i-1}^l \mid \mathbf{K}_L,N_0\}, \qquad (4.3)$$

where the event A_{i-1}^l is defined in Section 3.3. Let V_m denote one of the $\binom{i-1}{l}$ events which has detection errors at certain l layers among the $i-1$ processed layers at each time slot. Thus V_m is a set that contains the layer indices for one of the $\binom{i-1}{l}$ combinations of choosing l error symbols among the $i-1$ layers [66], where $m = 1, 2, \cdots, \binom{i-1}{l}$. We can express V_m as a set $V_m = \{v_{m,1}, v_{m,2}, \cdots, v_{m,l}\}$ where $v_{m,k}$ denotes the index of the layer in which the kth error has occurred. For instance, if $V_m = \{1, 3, 4\}$ then the first error was in the first layer, while the second was in the third layer, and the third was in the fourth layer. Also, we assume that $v_{m,1} < v_{m,2} < \cdots < v_{m,l}$, $v_{m,k} \in \{1, 2, \cdots, i-1\}$. Further more, the complement set of V_m is defined as

$$W_m = \{1, 2, \cdots, i-1\} - V_m = \{w_{m,1}, w_{m,2}, \cdots, w_{m,i-1-l}\}$$

where $w_{m,1} < w_{m,2} < \cdots < w_{m,i-1-l}$, $w_{m,k} \in \{1, 2, \cdots, i-1\}$. Similar to [66] we define $e_{V_m}^i$ as the event of having the ith layer in error and having l erroneous layers indicated by V_m given a specific PA pattern $\mathbf{K}_L$ and noise of variance N_0

$$e_{V_m}^i = \left\{ s_i \neq \hat{s}_i \bigcap_{\forall v_{m,k} \in V_m} \{s_{v_{m,k}} \neq \hat{s}_{v_{m,k}}\} \right.$$
$$\left. \bigcap_{\forall w_{m,k} \in W_m} \{s_{w_{m,k}} = \hat{s}_{w_{m,k}}\} \;\middle|\; \mathbf{K}_L, N_0 \right\}. \tag{4.4}$$

Then, then the probability that the ith layer along with l proceeding layers defined by V_m given $\mathbf{K}_L$ and N_0 can be found by simply summing the probability of all the

possible combinations of V_m. Mathematically, we can write this as

$$P\{s_i \neq \hat{s}_i, A_{i-1}^l \mid \mathbf{K}_L, N_0\} = \sum_{m=1}^{\binom{i-1}{l}} P(e_{V_m}^i). \tag{4.5}$$

Moreover, $P(e_{V_m}^i)$ can be decomposed into a product of i components as follows

$$P(e_{V_m}^i) = P(e_{V_m}^{i,i}) \cdot P(e_{V_m}^{i,i-1}) \cdots P(e_{V_m}^{i,1}) = \prod_{t=1}^{i} P(e_{V_m}^{i,t}), \tag{4.6}$$

where $e_{V_m}^{i,t}$ is defined similar to $e_{V_m}^i$ except that it corresponds to the tth layer (whether erroneous or correct). In [66], $e_{V_m}^{i,t}$ was defined as

$$e_{V_m}^{i,t} = \begin{cases} \left\{ s_t \neq \hat{s}_t \mid \bigcap_{\forall v_{m,k} < t} \{s_{v_{m,k}} \neq \hat{s}_{v_{m,k}}\} \right. \\ \qquad \left. \bigcap_{\forall w_{m,k} < t} \{s_{w_{m,k}} = \hat{s}_{w_{m,k}}\}, \mathbf{K}_L, N_0 \right\}, \quad t \in V_m \\ \left\{ s_t = \hat{s}_t \mid \bigcap_{\forall v_{m,k} < t} \{s_{v_{m,k}} \neq \hat{s}_{v_{m,k}}\} \right. \\ \qquad \left. \bigcap_{\forall w_{m,k} < t} \{s_{w_{m,k}} = \hat{s}_{w_{m,k}}\}, \mathbf{K}_L, N_0 \right\}, \quad t \in W_m \end{cases} \tag{4.7}$$

Thus, using (4.6) in (4.5) the latter becomes

$$P\{s_i \neq \hat{s}_i, A_{i-1}^l \mid \mathbf{K}_L, N_0\} = \sum_{m=1}^{\binom{i-1}{l}} \prod_{t=1}^{i} P(e_{V_m}^{i,t}). \tag{4.8}$$

The exact SER of the ith layer without error propagation given the diversity order and the SNR for different modulation schemes have been derived in the

literature [13].As defined earlier in Section 3.3, we denote the SER of ith layer as $P_e(D_i, \rho_i)$, where D_i and ρ_i are the diversity order and the SNR of the ith layer, respectively. By approximating the symbol errors caused in the previous layers as Gaussian random variable, we can write the following

$$P(e_{V_m}^{i,t}) = \begin{cases} P_e(N - M + t, P_t/\sigma_t^2), & t \in V_m \\ \\ 1 - P_e(N - M + t, P_t/\sigma_t^2), & t \in W_m, \end{cases} \tag{4.9}$$

where σ_t^2 is the variance of the approximated Gaussian noise variable. The value of σ_t^2 depends on the modulation scheme and the symbol energy used in previous layers as will be described in the following subsections in which we will present the expression of σ_t^2 and $P_e(D_i, \rho_i)$ for the case of BPSK, M-QAM, and M-PSK.

4.3.1 BPSK

As defined earlier in section 3.3, the diversity order of the sub-streams of the ith layer is $D_i = m_i(N - K + \Gamma(i))$. According to [13], the exact SER of the ith layer without error propagation using BPSK modulation,

$$P_e(D_i, \rho_i) = \left[\frac{1}{2}(1 - \mu_i) \right]^{D_i} \sum_{\tau=0}^{D_i-1} \binom{D_i - 1 + \tau}{\tau} \left[\frac{1}{2}(1 + \mu_i) \right]^{\tau}, \tag{4.10}$$

where $\mu_i = \sqrt{\rho_i/(1 + \rho_i)}$ and ρ_i denotes the SNR of the ith layer. By applying Gaussian approximation to the error propagation component in (3.19), and extending

the results of [66] for LSSTC, the noise variance, σ_t^2 , can be approximated by

$$
\begin{aligned}
\sigma_t^2 &= N_0 + \sum_{\forall v_{m,k} < t} \mathrm{E}\left[\|\mathbf{h}_{v_{m,k}}\|^2\right] \cdot \mathrm{Var}\left[e_{v_{m,k}} \mid x_{v_{m,k}} \neq \hat{x}_{v_{m,k}}\right] \\
&= N_0 + \sum_{\forall v_{m,k} < t} L^2 \cdot 4P_{L,v_{m,k}} \\
&= N_0 + 4L^2 \cdot \sum_{\forall v_{m,k} < t} P_{L,v_{m,k}},
\end{aligned}
\tag{4.11}
$$

where $\|\mathbf{h}_{v_{m,k}}\|^2$, $P_{L,v_{m,k}}$, and $e_{v_{m,k}}$ denotes the FN, transmit power, and the error event of layer $v_{m,k}$ respectively. $E[.]$ is the expectation Operator, and $Var[.]$ is the variance operator.

4.3.2   M-QAM

For simplicity, we consider square M-QAM modulation schemes such as 16-QAM, 64-QAM, etc. Under a Rayleigh fading channel and with diversity order D_i, the SER of a square M-QAM can be written as follows [72]

$$
P_e(D_i, \rho_i) = 4\left(1 - \frac{1}{\sqrt{M}}\right) I_1 - 4\left(1 - \frac{1}{\sqrt{M}}\right)^2 I_2,
\tag{4.12}
$$

where the terms I_1 and I_2 are defined as

$$
I_1 = \left[\frac{1}{2}(1 - \mu_i)\right]^{D_i} \cdot \sum_{k=0}^{D_i - 1} \binom{D_i - 1 + k}{k}\left[\frac{1}{2}(1 + \mu_i)\right]^k,
\tag{4.13}
$$

$$I_2 = \frac{1}{4} - \mu_i \cdot \left(\frac{1}{2} - \frac{1}{\pi} \cdot \tan^{-1}(\mu_i)\right) \cdot \sum_{k=0}^{D_i-1} \binom{2k}{k} \cdot (4\tau_i)^{-k}$$

$$+ \frac{\mu_i}{\pi} \sin\left(\tan^{-1}(\mu_i)\right) \sum_{k=1}^{D_i-1} \sum_{i=1}^{k} \tau_i^{-k} \cdot T_{ik} \cdot \left(\cos\left(\tan^{-1}(\mu_i)\right)\right)^{2(k-i)+1}, \quad (4.14)$$

where

$$\mu_i \triangleq \sqrt{\frac{\rho_i}{\frac{2}{3}(M-1) + \rho_i}}, \quad (4.15)$$

$$\tau_i \triangleq \left(\frac{3\rho_i}{2(M-1)} + 1\right), \quad (4.16)$$

$$T_{ik} \triangleq \frac{\binom{2k}{k}}{\binom{2(k-i)}{k-i} 4^i \cdot (2(k-i)+1)}. \quad (4.17)$$

The variance of the effective noise affecting the tth layer is approximated by

$$\sigma_t^2 = N_0 + \frac{6L^2}{M-1} \cdot \sum_{\forall v_{m,k} < t} P_{L,v_{m,k}}. \quad (4.18)$$

4.3.3 M-PSK

Using the result of [72], the SER of ith layer assuming perfect interference cancellation and M-PSK modulation with diversity order D_i and layer SNR ρ_i is written as follows

$$P_e(D_i, \rho_i) = \frac{M-1}{M} - \frac{\mu_i}{\sqrt{\mu_i^2 + 1}} \left(\frac{1}{2} + \frac{\omega_i}{\pi}\right) \sum_{k=0}^{D_i-1} \binom{2k}{k} \left[4(\mu_i^2 + 1)\right]^{-k}$$

$$- \frac{\mu_i}{\sqrt{\mu_i^2 + 1}} \cdot \frac{1}{\pi} \sin(\omega_i) \sum_{k=1}^{D_i-1} \sum_{i=1}^{k} \frac{T_{ik}}{(\mu_i^2 + 1)^k} \left[\cos(\omega_i)\right]^{2(k-i)+1}, \quad (4.19)$$

where

$$\mu_i \triangleq \sqrt{\rho_i}\sin(\frac{\pi}{M}), \tag{4.20}$$

$$\omega_i \triangleq \tan^{-1}\left(\frac{\sqrt{\rho_i}\cos(\frac{\pi}{M})}{\sqrt{\mu_i^2+1}}\right), \tag{4.21}$$

$$T_{ik} \triangleq \frac{\binom{2k}{k}}{\binom{2(k-i)}{k-i}4^i\cdot(2(k-i)+1)}. \tag{4.22}$$

The variance of the effective noise affecting the tth layer is approximated by [66] as

$$
\begin{aligned}
\sigma_t^2 &= N_0 + \sum_{\forall v_{m,k}<t} \mathrm{E}\left[\|\mathbf{h}_{v_{m,k}}\|^2\right]\cdot\mathrm{Var}\left[e_{v_{m,k}}\mid x_{v_{m,k}}\neq\hat{x}_{v_{m,k}}\right] \\
&= N_0 + \sum_{\forall v_{m,k}<t} L^2\cdot 4\cdot\sin^2\left(\frac{\pi}{M}\right)P_{L,v_{m,k}} \\
&= N_0 + 4L^2\cdot\sin^2\left(\frac{\pi}{M}\right)\cdot\sum_{\forall v_{m,k}<t} P_{L,v_{m,k}}.
\end{aligned}
\tag{4.23}
$$

After finding the expressions of σ_t^2 and $P_e(D_i,\rho_i)$, they can be substituted into (4.9). The SER of the ith layer, $P_{e_i|(\mathbf{K}_L,N_0)}$, can be evaluated by combining (4.3), (4.8), and (4.9), and from that we can find the probability of error of the individual substreams by

$$P_{e_{x_i}|(\mathbf{K},N_0)} = \mathrm{Prob}\{x_i\neq\hat{x}_i\mid\mathbf{K},N_0)\} \tag{4.24}$$

$$= P_{e_{\Gamma(i)}|(\mathbf{K}_L,N_0)}, \tag{4.25}$$

and the average SER over all M sub-streams is simply written as

$$P_{av|(\mathbf{K},N_0)} = \frac{1}{M} \cdot \sum_{i=1}^{M} P_{e_{x_i}|(\mathbf{K},N_0)}. \tag{4.26}$$

4.4   Optimum Power Allocation

In this Section, we aim to find the optimum power allocation $\mathbf{K}$ that would result in optimizing the performance by minimizing the probability of error for the LSSTC system. To achieve this we need to differentiate the formula of the average SER $P_{av|(\mathbf{K},N_0)}$ with respect to $\mathbf{K}$ to find the minimum value of the SER. Clearly such analytical differentiation is very difficult, therefore we use a numerical approach applying Newton's method [66]. To minimize $P_{av|(\mathbf{K},N_0)}$, we need to find the value of $\mathbf{K} = [K_1, K_2, \cdots, K_{M-1}]$ that satisfies the following set of equations

$$\frac{\partial P_{av|(\mathbf{K},N_0)}}{\partial K_i} = 0, \quad i = 1, 2, \cdots, M-1. \tag{4.27}$$

To solve the set of equations in (4.27) by Newton's method [66], we first define the following parameters

$$
\begin{aligned}
f_i &\triangleq \frac{\partial P_{av|(\mathbf{K},N_0)}}{\partial K_i}, \\
f_{ij} &\triangleq \frac{\partial f_i}{\partial K_j} = \frac{\partial^2 P_{av|(\mathbf{K},N_0)}}{\partial K_i \partial K_j}, \\
\mathbf{K}_{i+\Delta} &\triangleq [K_1, \cdots, K_{i+\Delta}, \cdots, K_{M-1}], \\
\mathbf{K}_{i+\Delta,j+\Delta} &\triangleq [K_1, \cdots, K_{i+\Delta}, \cdots, K_{j+\Delta}, \cdots, K_{M-1}],
\end{aligned}
\tag{4.28}
$$

where $i, j \in \{1, 2, \cdots, M-1\}$. Given that the step size Δ is chosen to be small, then the partial derivatives in (4.28) can be found numerically by Newton's method by the following approximation

$$
\begin{aligned}
f_i &\simeq \frac{1}{\Delta} \left(P_{av|(\mathbf{K}_{i+\Delta},N_0)} - P_{av|(\mathbf{K},N_0)} \right), \\
f_{ij} &\simeq \frac{1}{\Delta^2} \left(P_{av|(\mathbf{K}_{i+\Delta,j+\Delta},N_0)} - P_{av|(\mathbf{K}_{i+\Delta},N_0)} - P_{av|(\mathbf{K}_{j+\Delta},N_0)} + P_{av|(\mathbf{K},N_0)} \right),
\end{aligned}
\tag{4.29}
$$

where $i, j \in \{1, 2, \cdots, M-1\}$. To use Newton's method we start with an initial guess $\mathbf{K}^{(0)} = [K_1^{(0)}, K_2^{(0)}, \cdots, K_{M-1}^{(0)}]$, after that we compute the corresponding partial derivatives $f_i^{(0)}$ and $f_{ij}^{(0)}$ using (4.30). To compute the power allocation at the

u^{th} iteration $\mathbf{K}^{(u)}$, we apply the following procedure

$$
\begin{aligned}
K_1^{(u+1)} &= K_1^{(u)} - \frac{|\mathbf{A}_1^{(u)}|}{|\mathbf{J}^{(u)}|}, \\
K_2^{(u+1)} &= K_2^{(u)} - \frac{|\mathbf{A}_2^{(u)}|}{|\mathbf{J}^{(u)}|}, \\
&\vdots \\
K_{M-1}^{(u+1)} &= K_{M-1}^{(u)} - \frac{|\mathbf{A}_{M-1}^{(u)}|}{|\mathbf{J}^{(u)}|},
\end{aligned}
\tag{4.30}
$$

where $|\cdot|$ denotes the matrix determinant, the matrix $\mathbf{J}^{(u)}$ is defined as

$$
\mathbf{J}^{(u)} = \begin{pmatrix}
f_{11}^{(u)} & f_{12}^{(u)} & \cdots & f_{1(M-1)}^{(u)} \\
f_{21}^{(u)} & f_{22}^{(u)} & \cdots & f_{2(M-1)}^{(u)} \\
\vdots & \vdots & \ddots & \vdots \\
f_{(M-1)1}^{(u)} & f_{(M-1)2}^{(u)} & \cdots & f_{(M-1)(M-1)}^{(u)}
\end{pmatrix},
\tag{4.31}
$$

the matrix $\mathbf{A}_v^{(u)}$ is defined to be the matrix obtained by replacing the vth column of $\mathbf{J}^{(u)}$ with $\left[f_1^{(u)}, f_2^{(u)}, \cdots, f_{(M-1)}^{(u)} \right]^T$. The optimum PA pattern $\mathbf{K}_{opt}$ can be obtained by repeating the procedure until $\mathbf{K}^u$ converges, which depends on the initial guess $\mathbf{K}^{(0)}$ and the step size Δ. We will refer to the optimum PA-LSSTC as OPA-LSSTC.

4.5 Complexity of OPA-LSSTC

It was observed that the optimum power allocation at high SNR provides a significant SNR gain with little increase in the complexity of the signal. The main parameters that will be affected by the OPA processing are the feedback load and the number of operations per unit time.

The BS analyzes the CSI data to optimize the performance by assigning the layer powers according to $\mathbf{K}_{opt}$. As a result, the number of operations will increase, and faster processors will be required. Observing the simulation results, the computational complexity was noted to be higher for small SNR values. The reason for that is hardware limitation, as the tiny difference between the optimum powers will require the step size δ to be very small. In such a case, finding the solution by numerical methods will require a huge number of operations. The minimum step size used to solve the optimum PA equations was 10^{-4}. Also it should be clear that finding the optimum PA in the low SNR range will not improve the performance much, and therefore no need to allocate powerful computational resources for it. For the high SNR range, few operations are enough to provide the optimum performance.

To speed up the convergence of $\mathbf{K}_{opt}$, The BS can have a database that contains the best initial guess of each SNR value. This way the number of operations required will be minimized and the system resources are used efficiently.

The feedback load does not increase much when using OPA-LSSTC since we

have assumed that the channel changes slowly, and the CSI need to be sent only if the channel state changes.

4.6 Numerical Results

In this section we illustrate the numerical results of the proposed PA scheme for LSSTC systems with different modulation schemes and transmitter configurations. Throughout this thesis, the following notation will be used:

- EPA-LSSTC will be used to denote equal power allocation LSSTC system in which all the layers are assigned the same amount of power.

- OPA-LSSTC will be used to denote optimum power allocation LSSTC system in which the layers are assigned different amounts of power according to $\mathbf{K}_{opt}$.

Figure 4.2 shows the SER of the individual layers of an 8×2 LSSTC using non-ordered SGIC detector employing BPSK modulation with $K = 2$ and $L = 2$ obtained from both the simulation and the analysis. The Figure compares the analytical results of the SER obtained in this chapter, denoted as "analysis 2", to that obtained in Chapter 3, denoted as "analysis 1". Also, the simulation results with equal power allocation is shown. It is clear that the simulation makes a nearly perfect match to the two analysis methods, which demonstrates the validity of the analysis methods we have proposed.
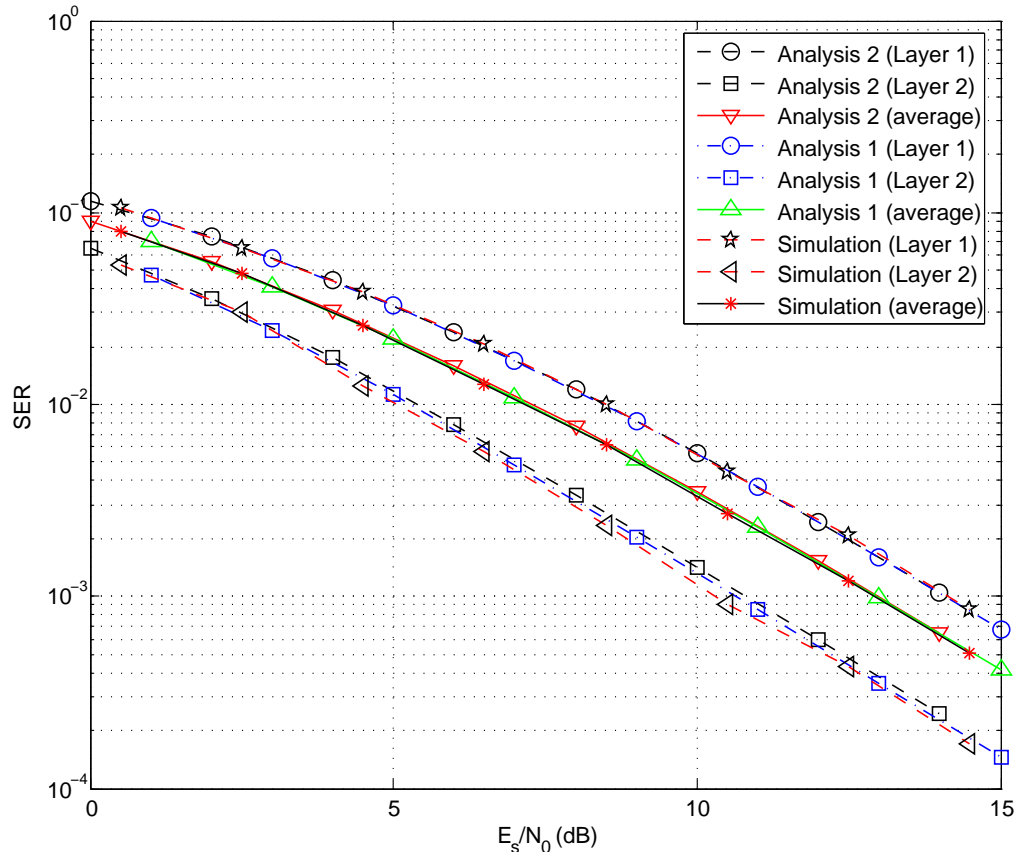
Figure 4.2: SER of the individual sub-streams of an 8×2 LSSTC employing SGIC without ordering and BPSK modulation with $K = 2$ & $L = 2$ (comparing analysis to simulation results).

Figure 4.3 compares the simulation results to the results of the two methods of analysis for SER of an LSSTC system employing non-ordered SGIC and BPSK modulation with $K = 2$ and $N_R = 2$ and different number of beamforming elements. It can be seen that the simulation and analysis results match quite well, which proves the validity of the analysis. Figure 4.4 shows the same results but with $K = 4$ and $N_R = 4$.
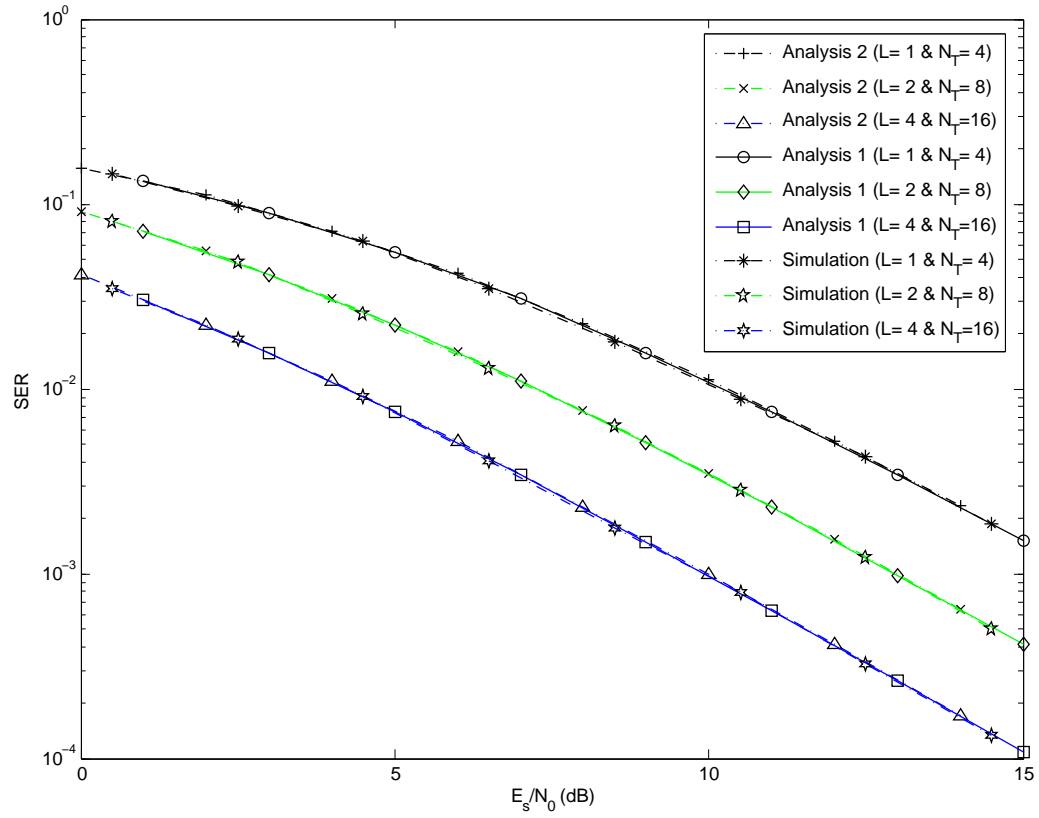
Figure 4.3: SER of LSSTC employing non-ordered SGIC and BPSK modulation with $K = 2$ & $N_R = 2$ (comparing analysis to simulation results).
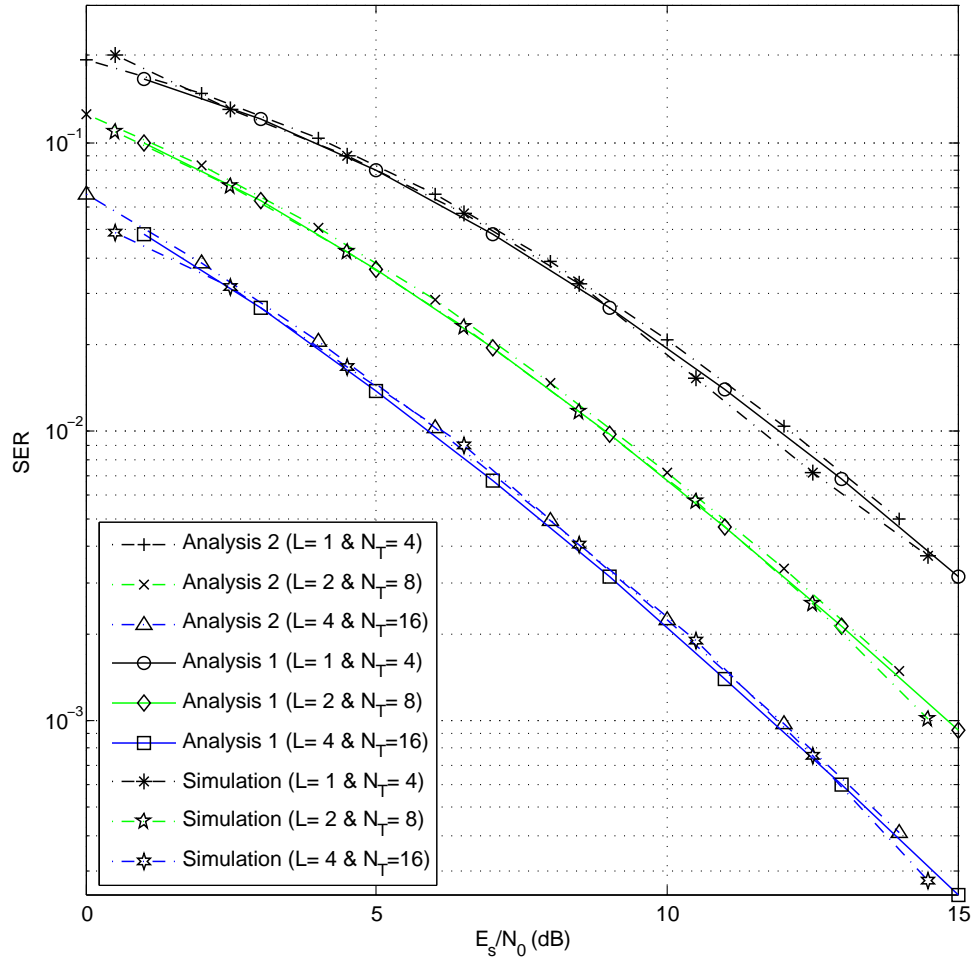
Figure 4.4: SER of LSSTC employing non-ordered SGIC and BPSK modulation with $K = 4$ & $N_R = 4$ (comparing analysis to simulation results).

Figure 4.5 shows a fair comparison between different transmitter configurations of the LSSTC system in terms of the SER, obtained from both the EPA-LSSTC analysis and simulation. The three configurations use a total number of transmit antennas, $N_T = 8$, and the receiver is equipped with 4 antennas. In this comparison a different modulation scheme is used such that the spectral efficiency would be the same for all of them, which is set to 4 bps/Hz.

Figure 4.6 shows the SER of the individual layers of an 8×4 LSSTC using non-ordered SGIC ordering employing BPSK modulation with $K = 4$ and $L = 1$ obtained using the PA-LSSTC analysis. From Figure 4.6 it can be seen that the first layer dominates the probability of error because it has the lowest diversity order of $(m_1(N_R - K + 1) = 2)$.

Figure 4.7 shows SER of the individual layers of an 8×4 LSSTC using non-ordered SGIC detector employing QPSK modulation with $K = 2$ and $L = 2$ obtained using the PA-LSSTC analysis.

Figure 4.8 shows the SER of a 2×1 LSSTC using SGIC detector employing BPSK modulation with $K = 1$ and $L = 1$ obtained using the PA-LSSTC analysis. This result is exactly the same result obtained by Alamouti in [4] for $2Tx \times 1Rx$ STBC, which is equivalent to the 2×1 LSSTC, and that proves the validity of our analysis.
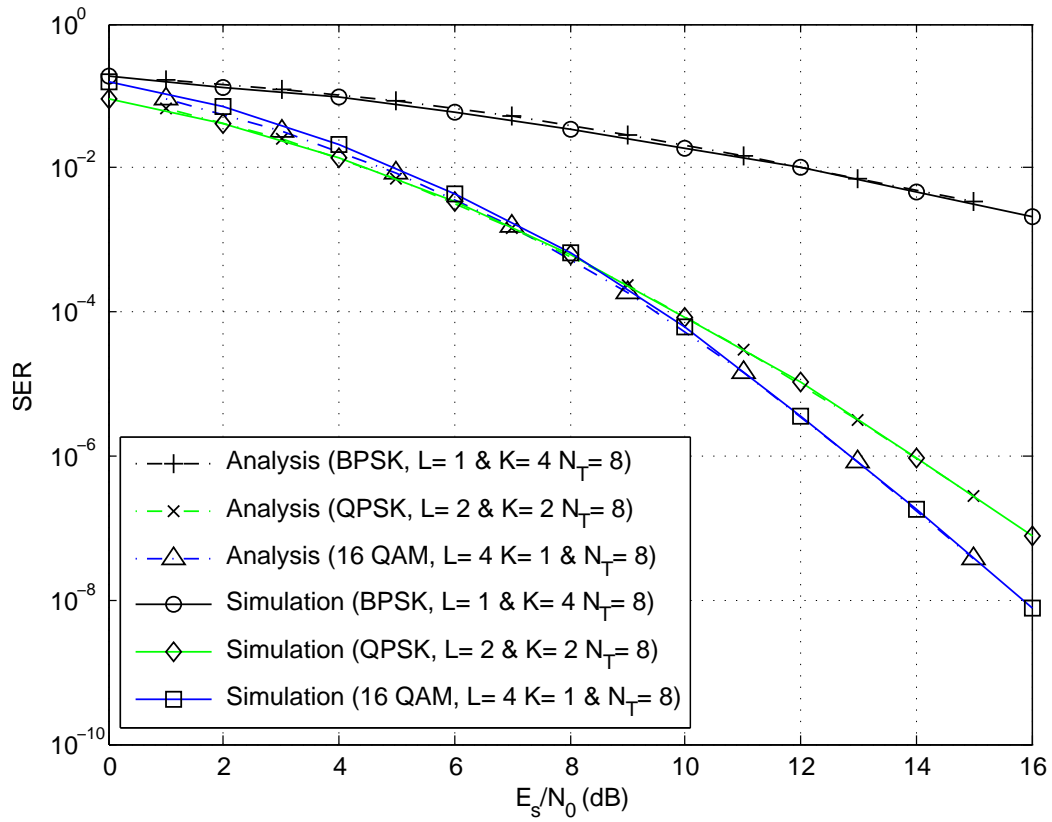
Figure 4.5: SER of LSSTC employing non-ordered SGIC and BPSK modulation with $K = 2$ & $N_R = 2$ (comparing analysis to simulation results).
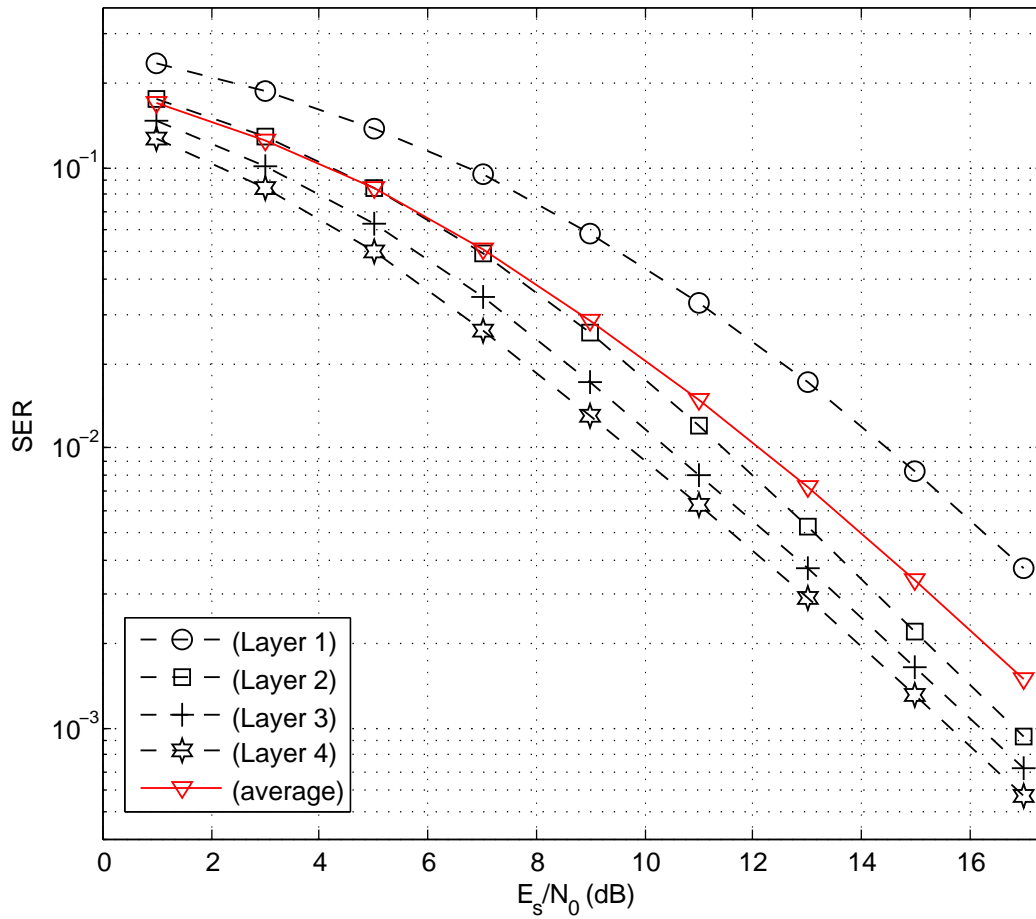
Figure 4.6: SER of the individual layers of an 8×4 LSSTC employing SGIC without ordering and BPSK modulation with $K = 4$ & $L = 1$.
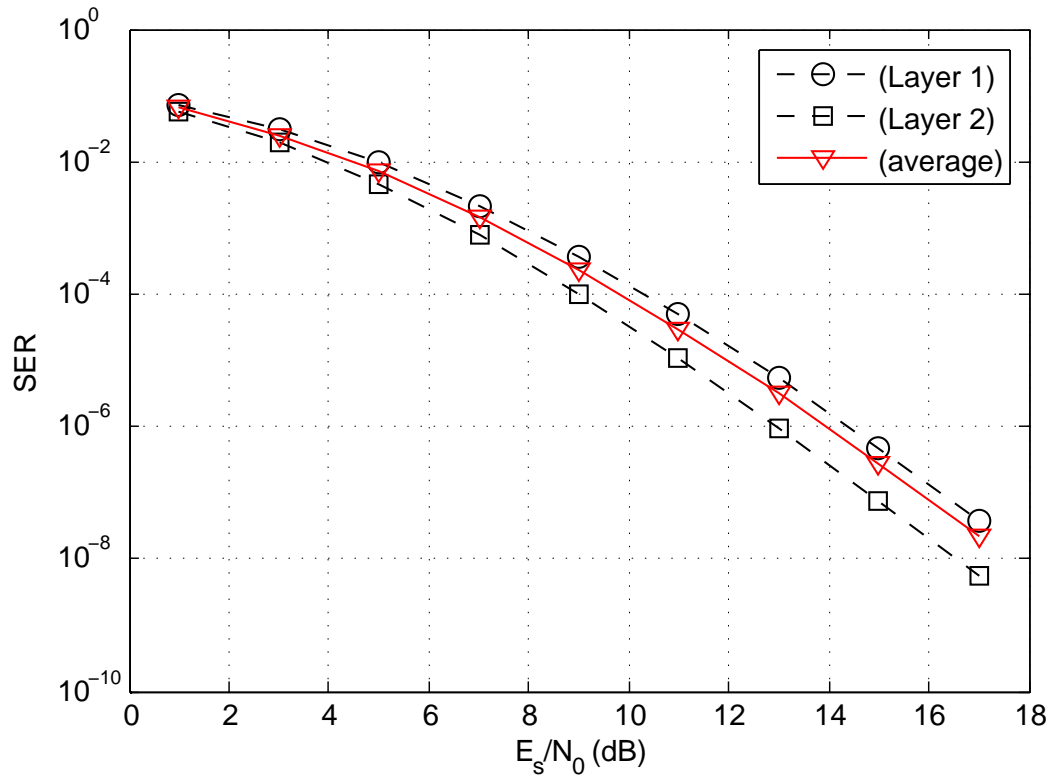
Figure 4.7: SER of the individual layers of an 8×4 LSSTC employing SGIC without ordering and QPSK modulation with $K = 2$ & $L = 2$.
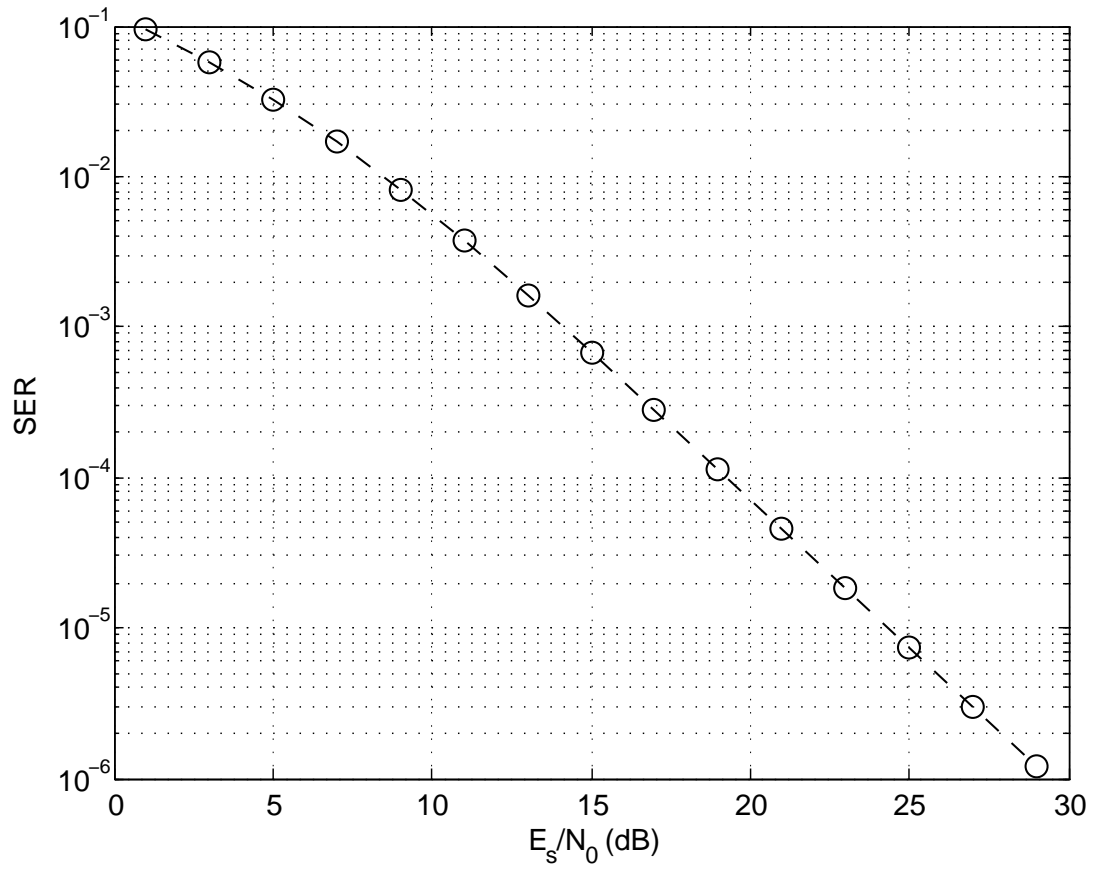
Figure 4.8: SER of a 2×1 LSSTC employing SGIC and BPSK modulation with $K = 1$ & $L = 1$.

A 16×4 OPA-LSSTC employing BPSK modulation with $K = 4$ and $L = 2$ is considered. The optimum PA for each layer versus E_s/N_0 is plotted in Figure 4.9, where it can be seen that at high SNR, the impact of error propagation is more dominant than the noise. It can be seen from Figure 4.9 that the SER is dominated by the first layer, and that the detection errors in the first layer would cause severe detection errors to the following layers, therefore, the optimum PA scheme suggests assigning the earlier layers higher power than the later ones as the SNR increases. Note that the first layer gets most of the transmit power at high SNR since it is the weakest layer that has the lowest diversity order among all layers. In Figure 4.10, we plot the SER of a 16×4 LSSTC system employing BPSK modulation with $K = 4$ and $L = 2$. We compare two cases, PA-LSSTC with equal power allocation (EPA-LSSTC), and the PA-LSSTC with optimum power allocation (OPA-LSSTC). Our SER analysis is shown to be very accurate as compared to simulation results. It is observed that the proposed OPA-LSSTC has about 2.5 dB gain at a SER of 10^{-4} compared to EPA-LSSTC. This shows the superior performance of the proposed scheme.
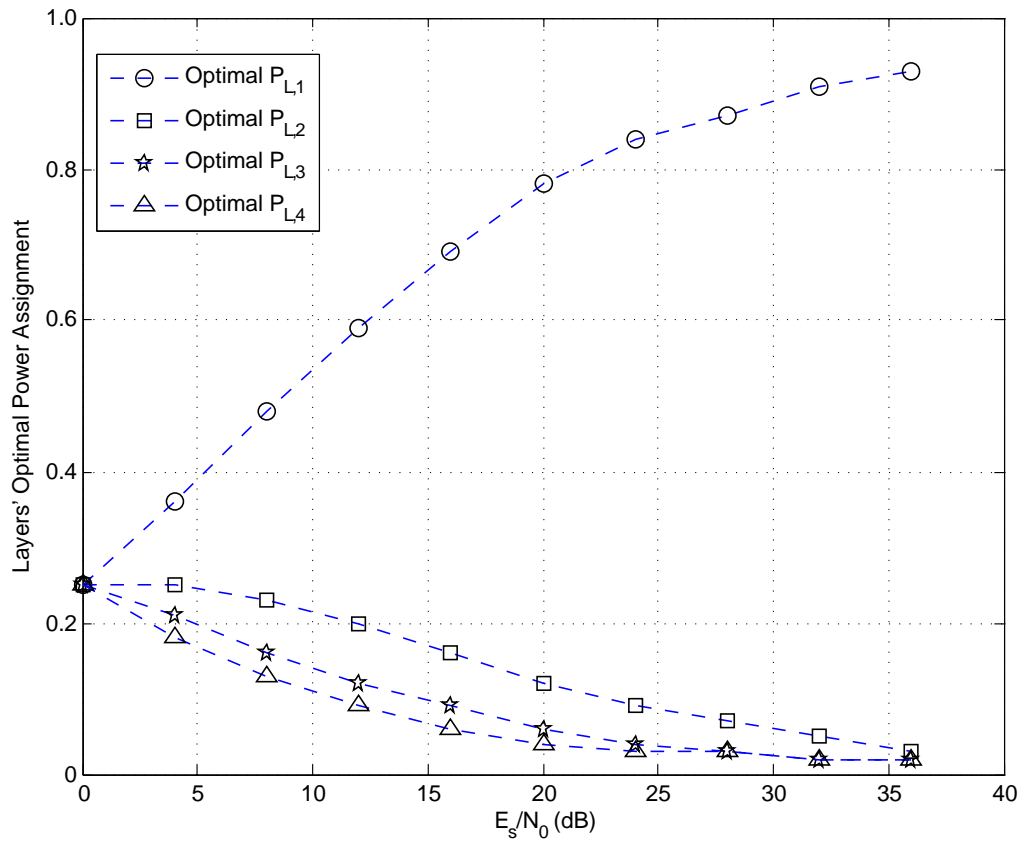
Figure 4.9: Optimum PA for each layer for a 16×4 PA-LSSTC employing BPSK modulation with $K = 4$ & $L = 2$.
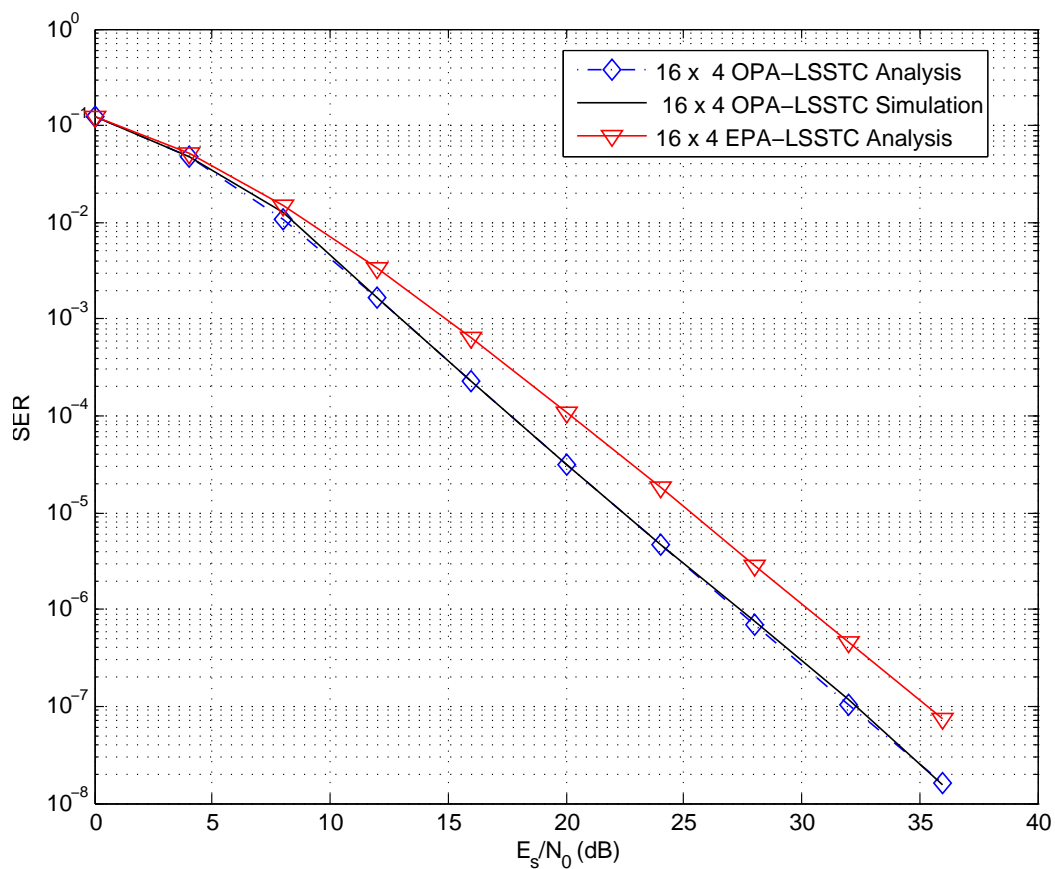
Figure 4.10: SER of 16×4 LSSTC system using PA-LSSTC scheme employing BPSK modulation with $K = 4$ & $L = 2$.

Next, we consider a 16×4 OPA-LSSTC employing QPSK, and 16-QAM modulation respectively with $K = 4$ and $L = 2$. Similar results to what have been described earlier for the case of BPSK have been obtained in the Figures 4.11, and 4.12 for QPSK, and in the Figures 4.13, and 4.14 for 16-QAM. It can be seen from the figures that the optimum power allocation provides about 2.7 dB gain at a SER of 10^{-4} in the case of QPSK, and about 2.8 dB gain at a SER of 10^{-4} in the case of 16-QAM. Regarding the layer optimum PA of QPSK and 16-QAM, the points in the low SNR range were discarded due to hardware limitations.

Figure 4.11: Optimum power assigned for each layer for a 16×4 OPA-LSSTC scheme employing QPSK modulation with $K = 4$ & $L = 2$.

Figure 4.12: SER of 16×4 LSSTC system using PA-LSSTC scheme employing QPSK modulation with $K = 4$ & $L = 2$.
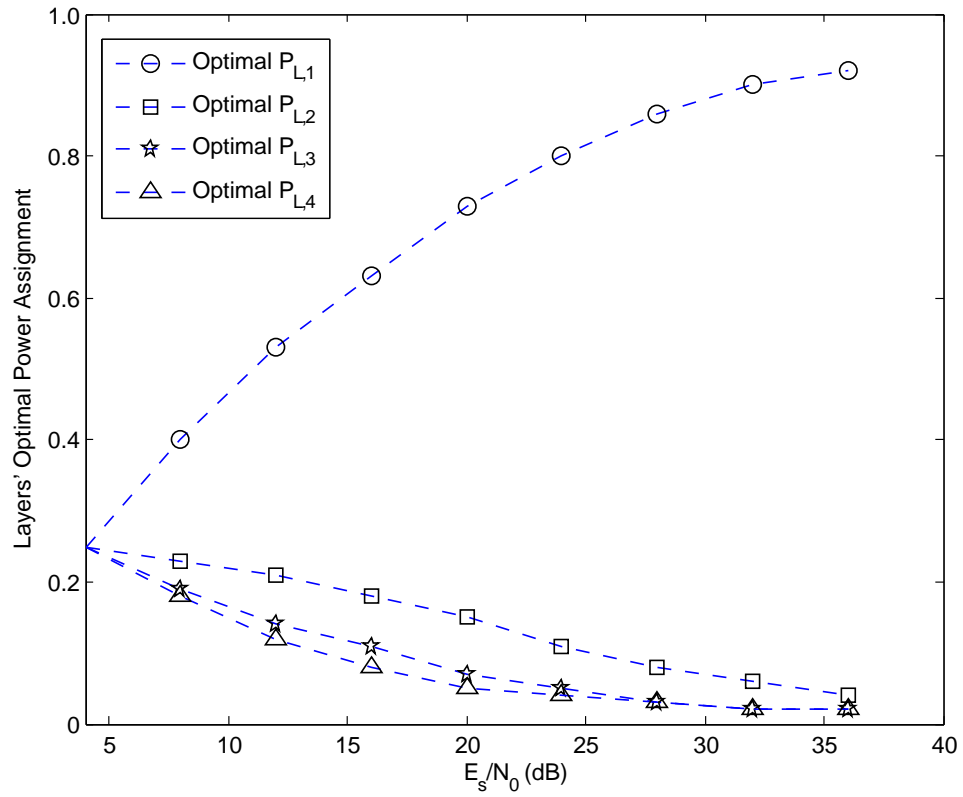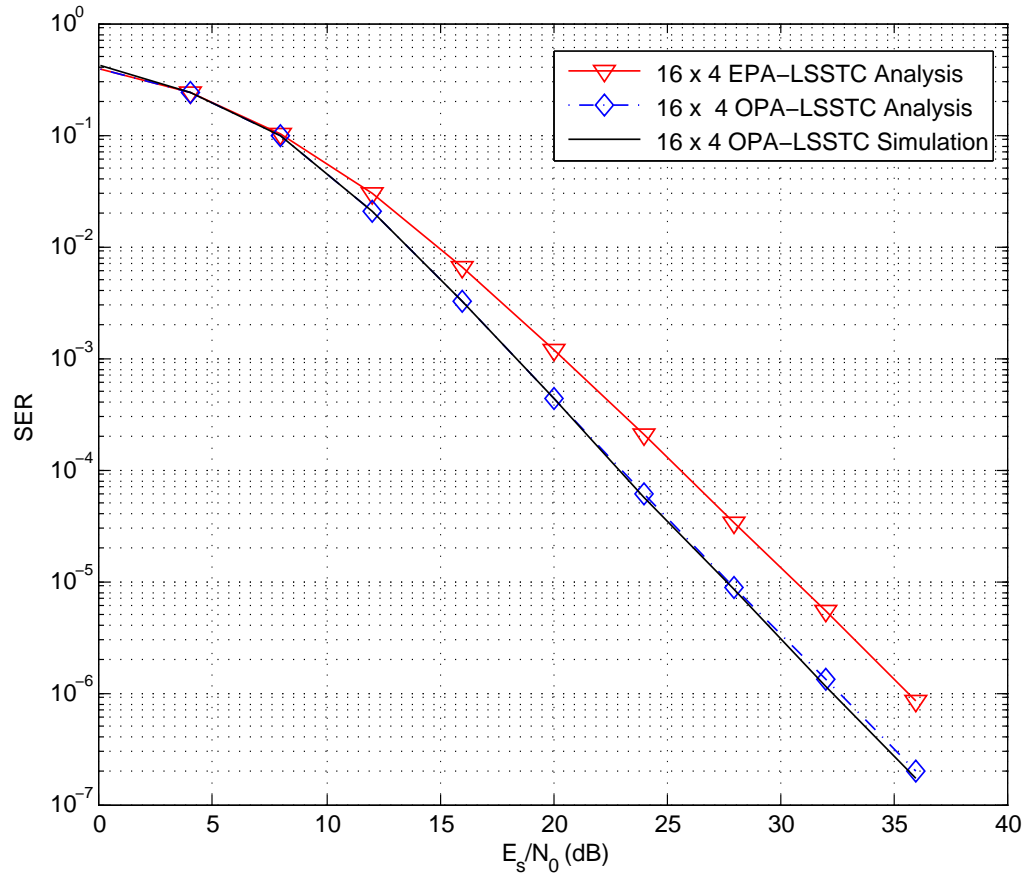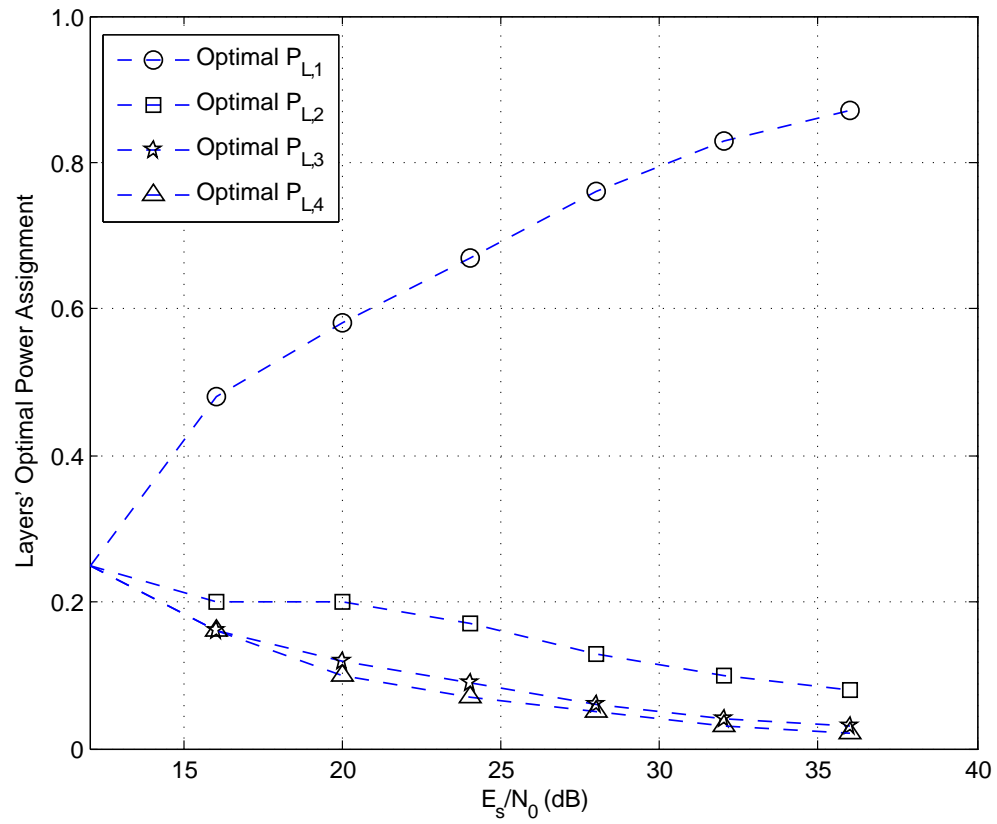
Figure 4.13: Optimum power assigned for each layer for a 16×4 OPA-LSSTC scheme employing 16-QAM modulation with $K = 4$ & $L = 2$.
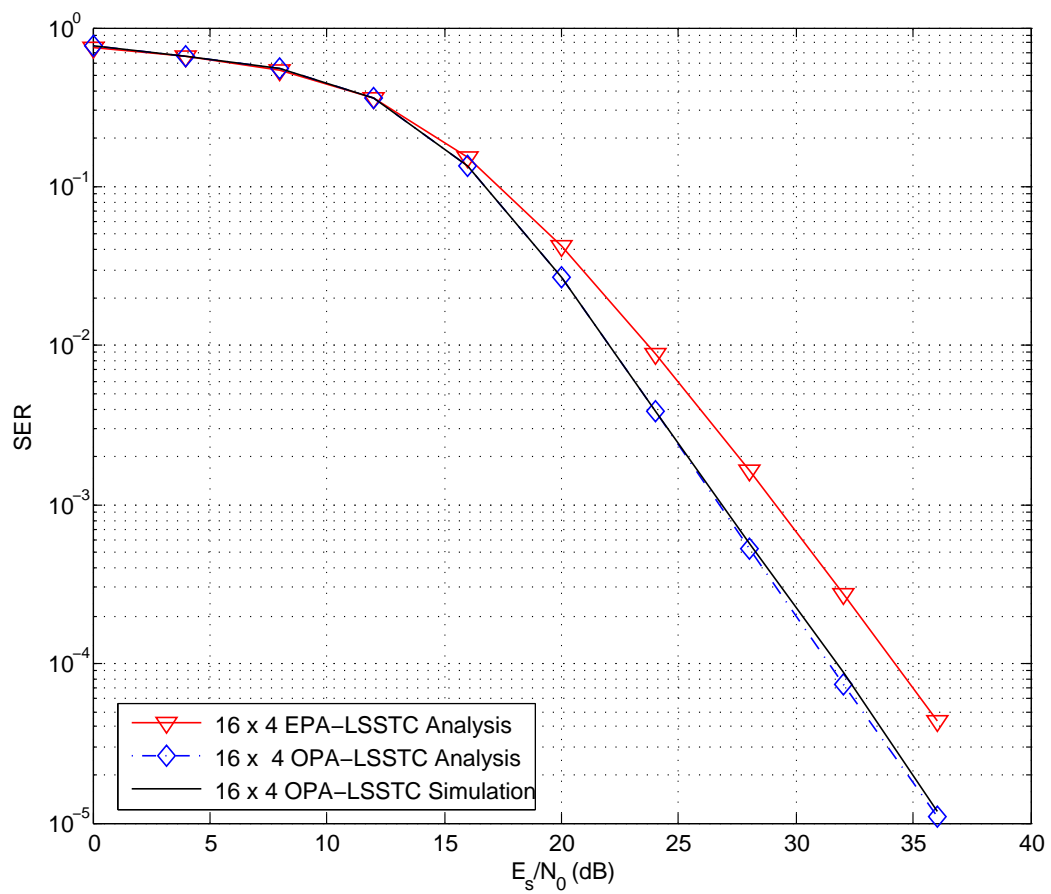
Figure 4.14: SER of 16×4 LSSTC system using PA-LSSTC scheme employing 16-QAM modulation with $K = 4$ & $L = 2$.

Now, we want to study the effect of changing the parameters of the LSSTC system on the PA gain. Figure 4.15 shows the SER of LSSTC versus the number of beam-steering elements (L) at an E_s/N_0 of 35 dB using SGIC and BPSK modulation with $K = 4$, $m_k = 2$, and $N_R = 4$. In Figure 4.16 we plot the PA gain, G_{PA} (dB) versus (L) at a SER of 10^{-6}. It is observed that the gain remains approximately constant and does not depend on L, which is actually expected since L is not related directly to the distribution of the power among the layers, i.e. if L increase or decrease the layer will still get the same amount of power.

Figure 4.17 shows the SER of LSSTC versus the number of AAs associated with each STBC encoder (m_k) at an E_s/N_0 of 35 dB using SGIC and BPSK modulation with $K = 4$, $L = 2$, and $N_R = 4$. In Figure 4.18 we plot the PA gain, G_{PA} (dB) versus m_k at a SER of 10^{-6}, where it can be seen that G_{PA} does not increase significantly with increasing m_k. The small increase can be related to the diversity order.

In Figure 4.19 we plot the power allocation gain, G_{PA} (dB) versus number of Layers (K) at a SER of 10^{-6} using SGIC employing BPSK modulation with $m_k = 2$, $L = 2$, and $N_R = 8$, where it can be seen that G_{PA} increases with increasing K, which is expected, since increasing the number of layers will lead to an increase in the degrees of freedom. Therefore a better distribution for the power can be found, since the total number of layers over which the power can be distributed is increased.
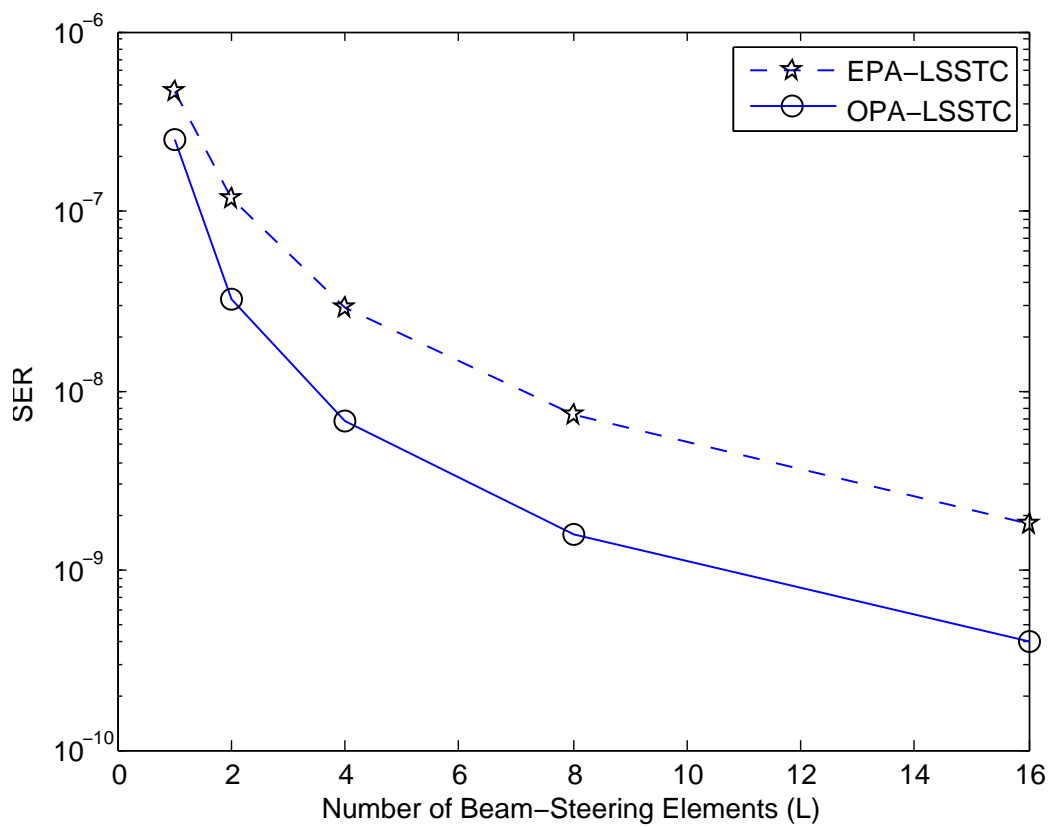
Figure 4.15: SER of LSSTC versus the number of beam-steering elements (L) using SGIC employing BPSK modulation with $K = 4$ & $m_k = 2$ & $N_R = 4$.

Figure 4.16: PA gain, G_{PA} versus the number of beam-steering elements (L) at a SER of 10^{-6} using SGIC employing BPSK modulation with $K = 4$ & $m_k = 2$ & $N_R = 4$.

Figure 4.17: SER of LSSTC versus the number of AAs associated with each STBC encoder (m_k) using SGIC employing BPSK modulation with $K = 4$ & $L = 2$ & $N_R = 4$.
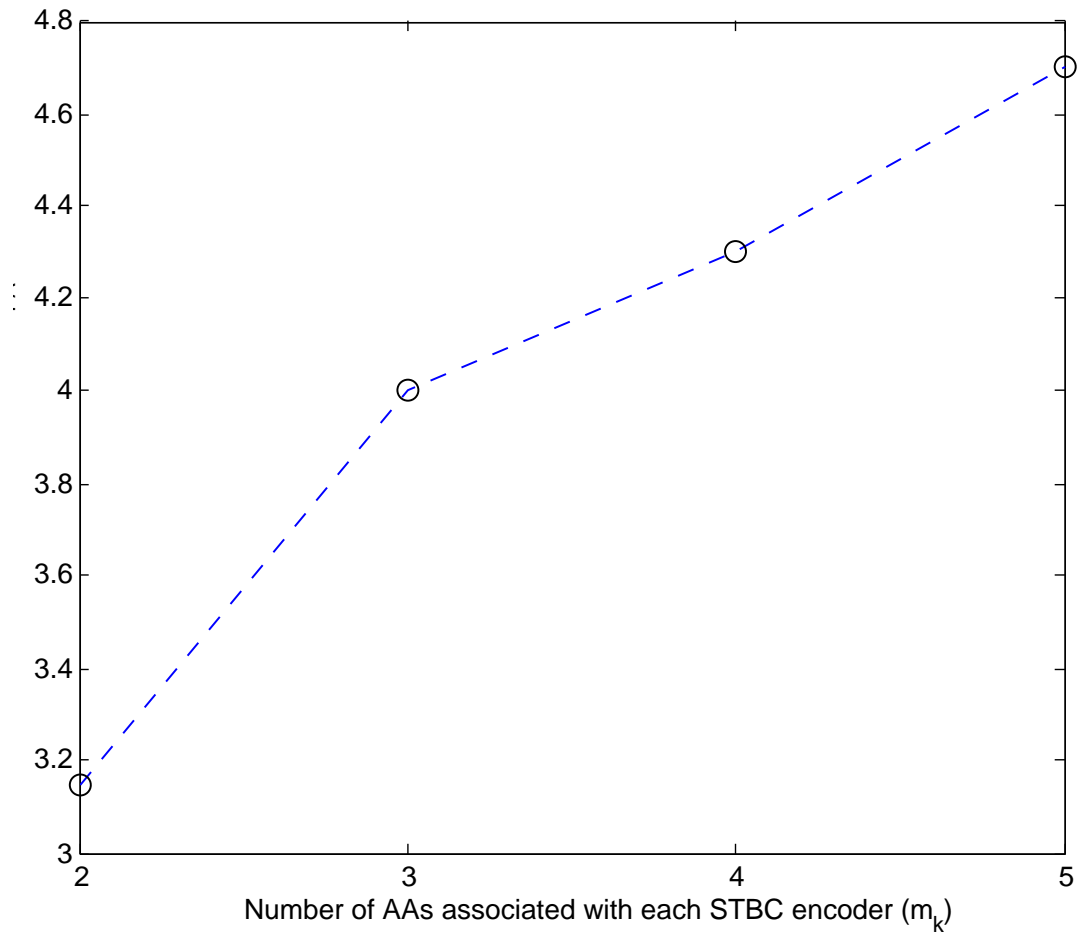
Figure 4.18: PA gain, G_{PA} versus the number of AAs associated with each STBC encoder (m_k) at a SER of 10^{-6} using SGIC employing BPSK modulation with $K = 4$ & $L = 2$ & $N_R = 4$.
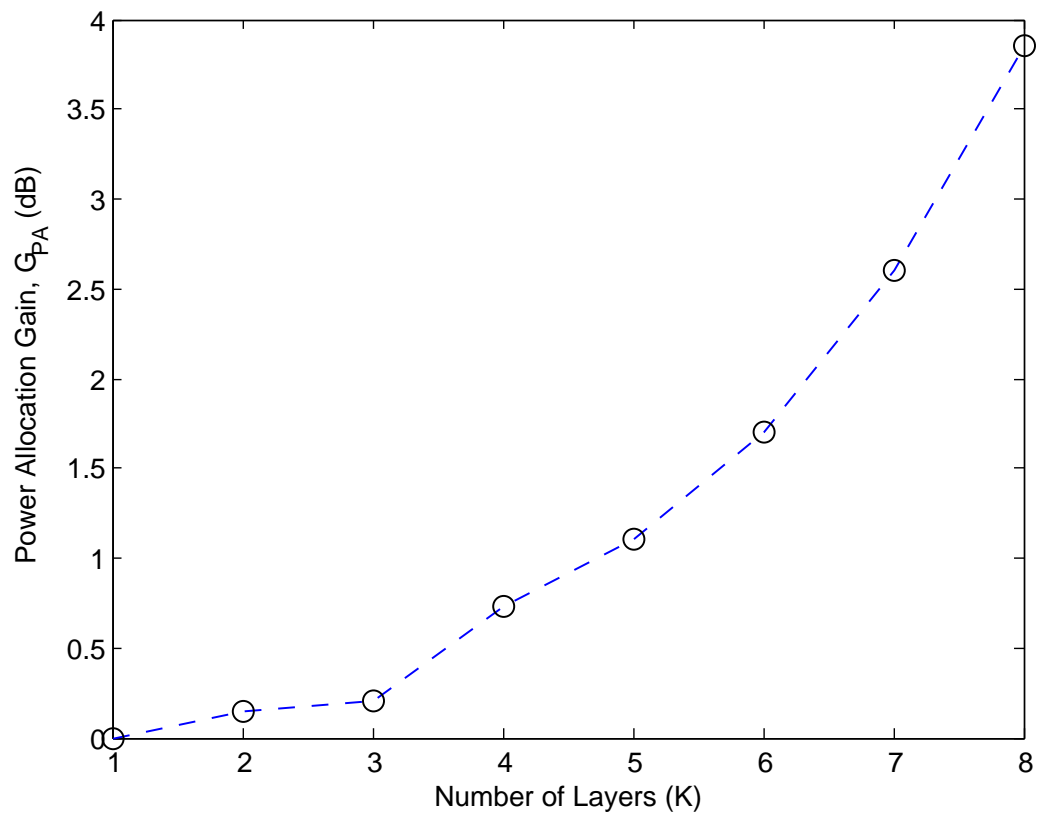
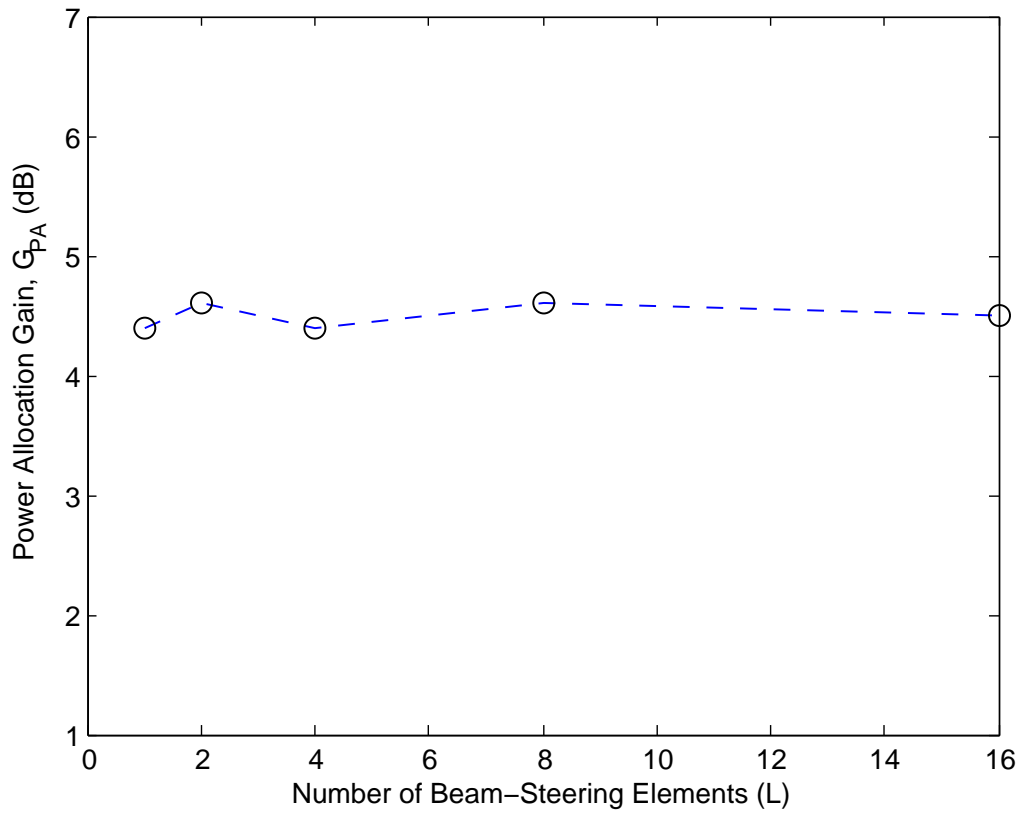Figure 4.19: PA gain, G_{PA} versus the number of Layers (K) at a SER of 10^{-6} using SGIC employing BPSK modulation with $m_k = 2$ & $L = 2$ & $N_R = 8$.
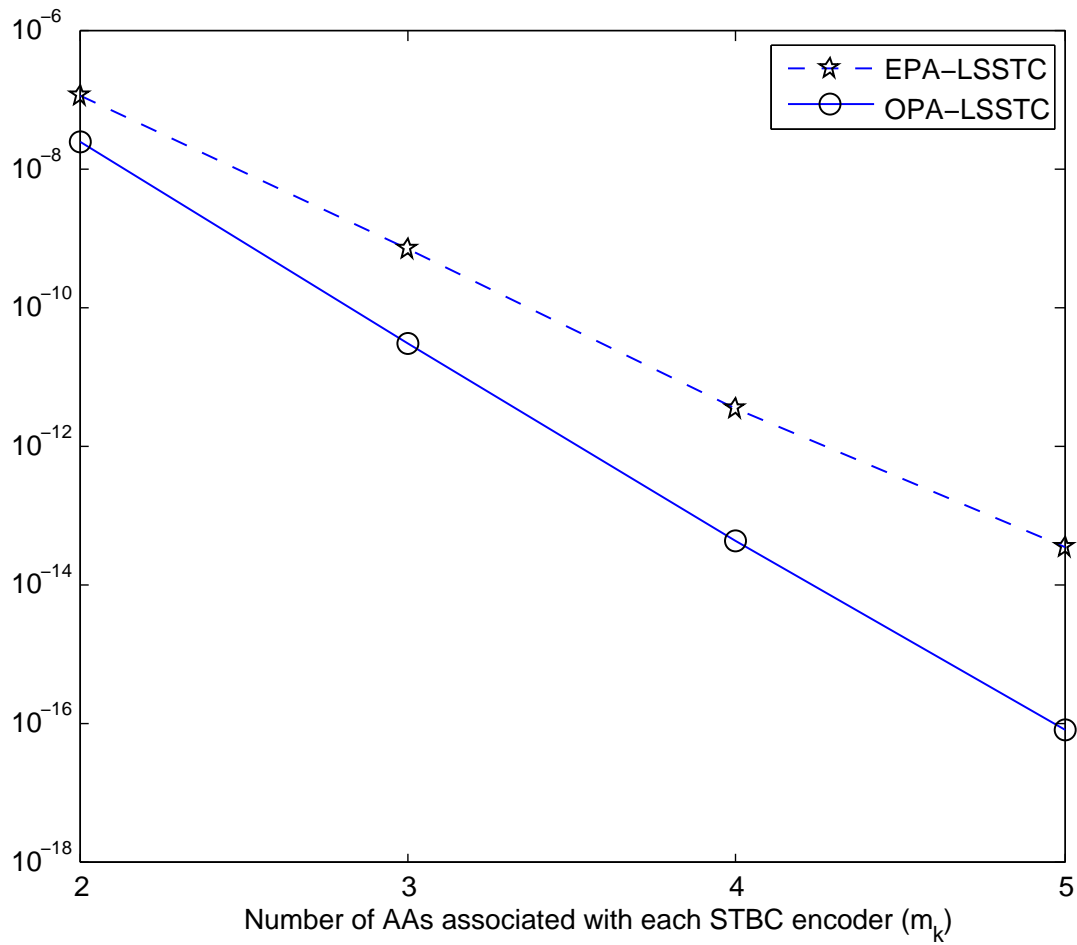
We can summarize four possible Transmitter-Receiver configurations for LSSTC in Table 4.1.

Table 4.1: Possible Transmitter-Receiver configurations for LSSTC.

Receiver / Transmitter	Non-ordered detector	Post-ordered detector
Equal Power Allocation	EPA-LSSTC with non-ordered detector	EPA-LSSTC with post-ordered detector
Optimum Power Allocation	OPA-LSSTC with non-ordered detector	OPA-LSSTC with post-ordered detector

Figure 4.20 plots the SER versus E_s/N_0 of the four possible configurations listed in Table 4.1. Looking at the SER around 10^{-5}, we can see that in the case of EPA using the post-ordered detector provides a gain of 1.2 dB compared to using the non-ordered detector, while in the case of OPA using the post-ordered detector provides a gain of 0.5 dB compared to using the non-ordered detector, because the OPA had already pre-ordered the detection of the sub-streams, therefore attempting to further order them by the post-ordered detector will not result in much gain. We can also note that the using the OPA is better than using the a post-ordered detector, since it provides about 2.8 dB gain compared to 2.1 dB for the latter, and also because using the post-ordered detector will require more processing at the user handset and that will consume the battery, on the other hand, the PA will be done at the base station where the processing and power is not an issue.
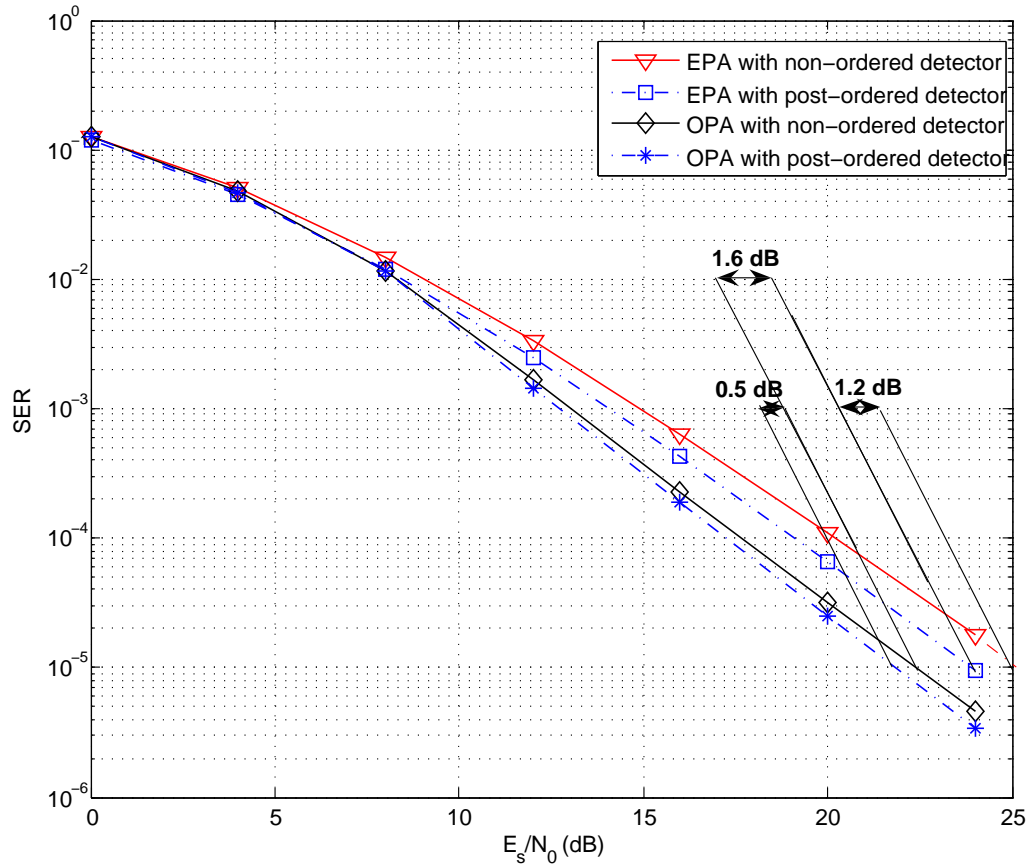
Figure 4.20: SER of 16×4 LSSTC employing SGIC and BPSK modulation with $K = 4$ & $L = 2$ (simulation results).

It has been mentioned earlier that the first layer dominates the probability of error, therefore we can approximate the probability of error of whole system by that of the first layer. In the following, we seek to further study the last statement, by comparing the SER of the first layer to the average SER, aiming to find which parameters or conditions will make this approximation much accurate.

Figure 4.21 shows the SER of LSSTC with varying the number of beamforming elements (L), where we can see that the gap between the first layer and the average doesn't change, and therefore it does not depend on L.

Figure 4.22 shows the SER of LSSTC with varying the number of layers (K), and we can see that the gap between the first layer and the average increases with increasing K.

In Figure 4.23 the SER of LSSTC is plotted with varying the STBC size (m_k) which corresponds to the number of AAs per layer. We can see that the gap between the first layer and the average decreases with increasing m_k. We can also note that the gap becomes constant when m_k becomes high, this is because the diversity order becomes high and the improvement doesn't change much after further increase in m_k.
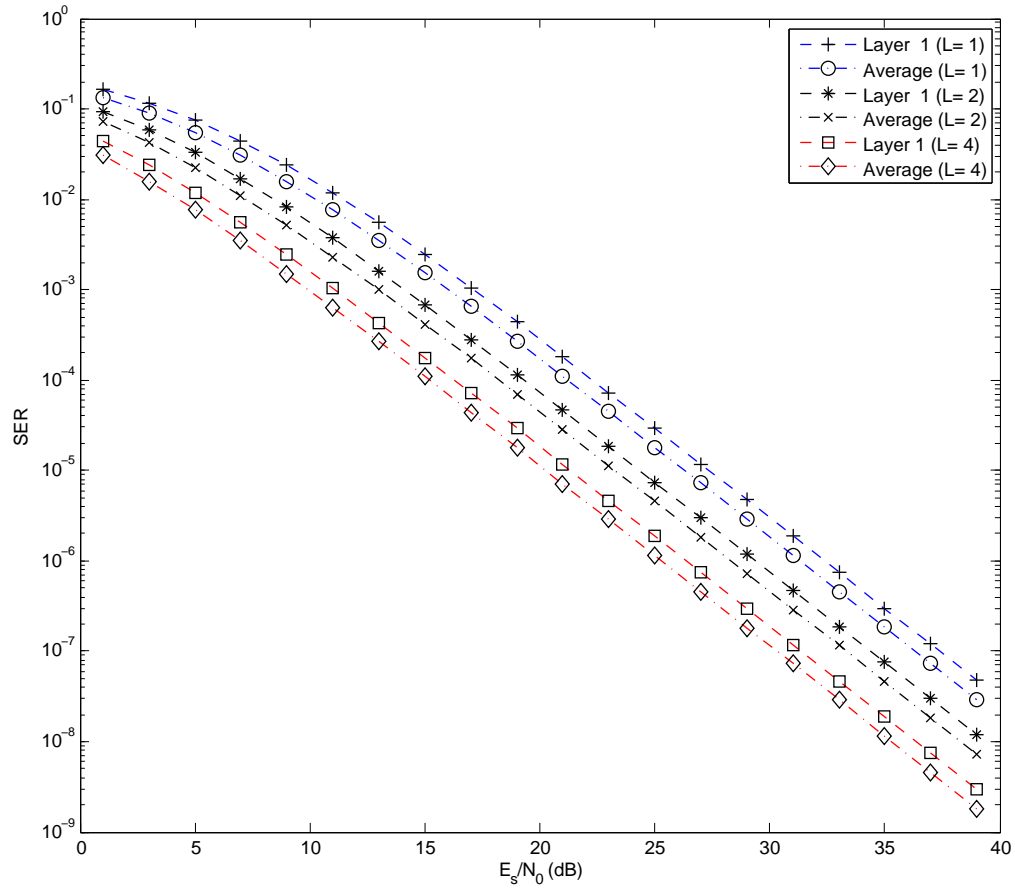
Figure 4.21: First layer & average SER of EPA-LSSTC employing SGIC and BPSK modulation with $K = 2$ & $N_R = 2$ & $m_k = 2$ (varying the number of beamforming elements (L)).
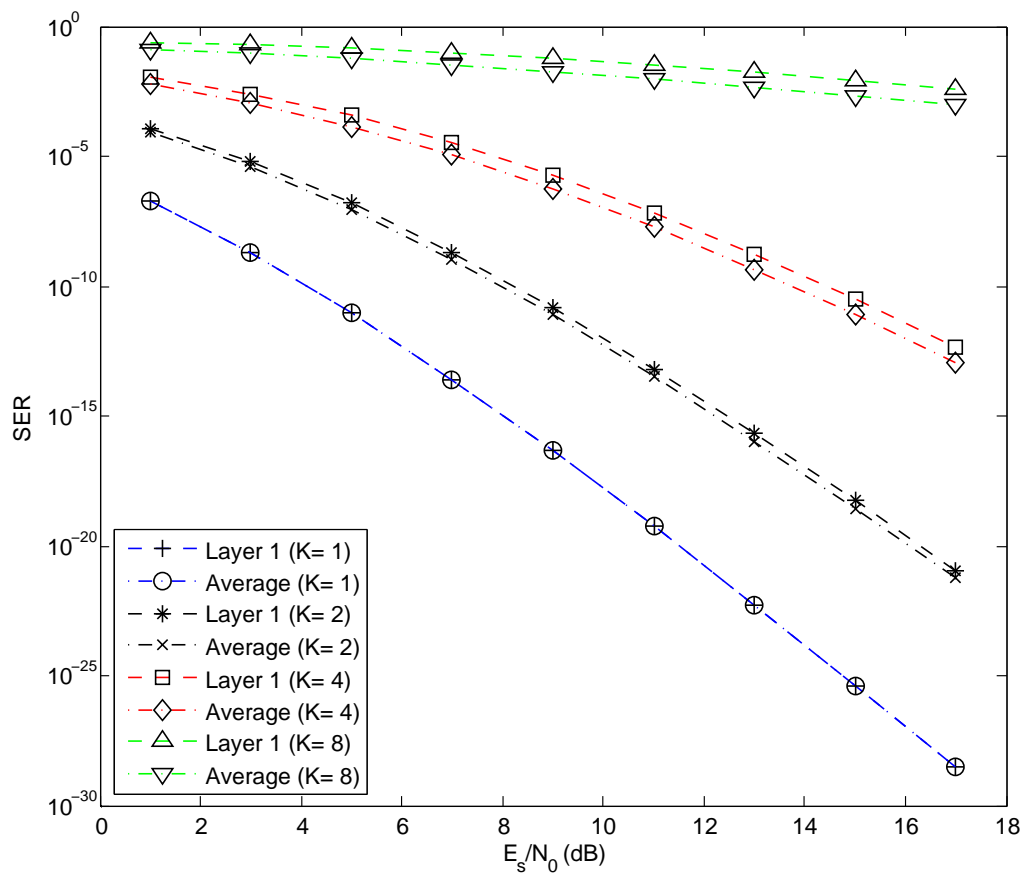
Figure 4.22: First layer & average SER of EPA-LSSTC employing SGIC and BPSK modulation with $L = 2$ & $m_k = 2$ & $N_R = 8$ (varying the number of layers (K)).
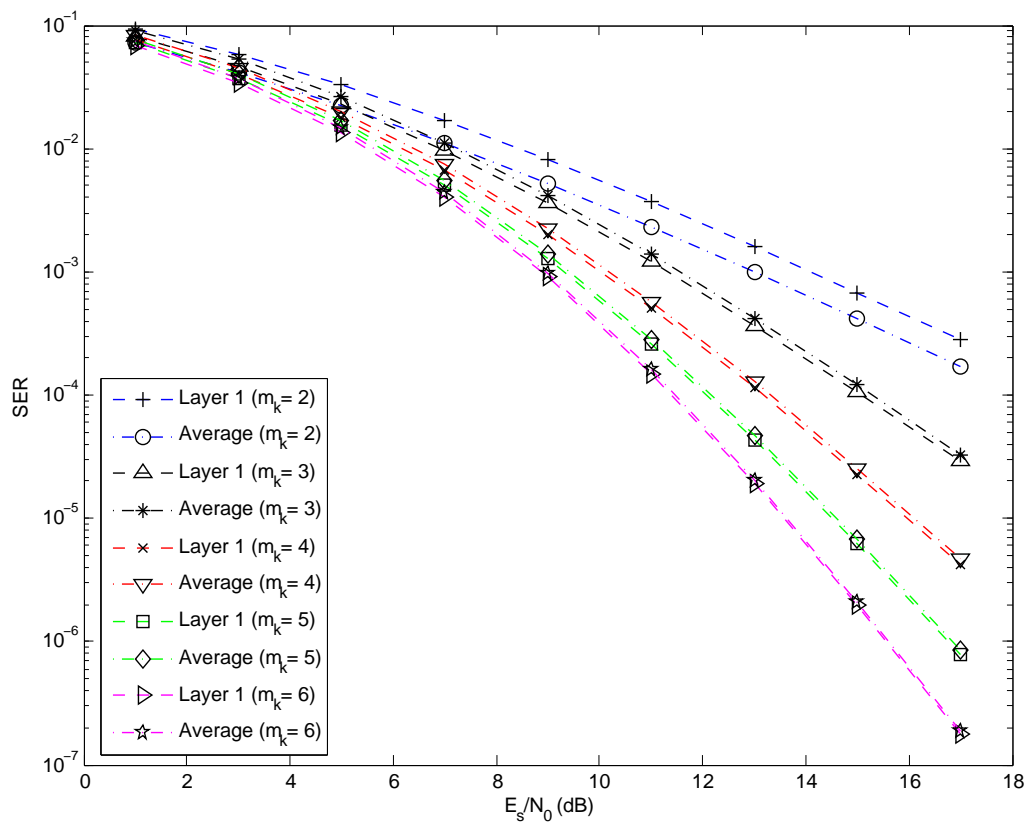
Figure 4.23: First layer & average SER of EPA-LSSTC employing SGIC and BPSK modulation with $L = 2$ & $K = 2$ & $N_R = 2$ (varying the STBC size (m_k)).

4.7   Chapter Conclusions

In this chapter we investigated the performance of single-user PA-LSSTC. We have derived an expression for the probability of error for PA-LSSTC employing BPSK by extending previously obtained results for VBLAST, such that it includes the diversity gain and SNR gain of beamforming. The results also included other modulation schemes, such as, M-ary PSK and M-ary QAM. The analytical results have shown merely a perfect match with simulation results, which proves their validity. Also from the numerical results, we have seen the benefits of PA-LSSTC in improving the performance. Finally, the optimum PA performance for LSSTC was derived using Newton's method, and we noted that choosing a small value for the step size will lead to convergence in just a few iterations.

Chapter 5

LSSTC in Multi-User Systems

The statistical randomness in the time-varying MIMO wireless channel across the different users results in creating the multiuser diversity gain. The multiuser diversity is harnessed by scheduling to enhance the average SNR and the sum-rate capacity [59]. In this chapter we investigate the use of LSSTC in a multi-user wireless network with applying scheduling technique to improve the performance of LSSTC systems.

The outline of this chapter is as follows. Section 5.1 gives a description of the system model for the Multi-User LSSTC. In Section 5.2, Scheduling is discussed along with presenting its definition, algorithms, criteria, and fairnes. In Section 5.3 we derive the PDF of the maximum pre-processing SNR for a Greedy-based multi-user LSSTC. Section 5.4 presents the simulation results conducted to evaluate the multi-user LSSTC system. Finally, Section 5.5 presents the chapter's

124

conclusions.

5.1 System Model

The model we consider applies to the downlink channel of a MlMO wireless cellular packet data system as illustrated in Figure 5.1. We assumed having a single BS equipped with multi antennas (M AAs) that provides data services to J users, each of which could be equipped with N_R antenna elements, where we should have $N_R \geq K$. Since the data rate that can be supported for each user is proportional to its received SNR, the instantaneous channel conditions are assumed to be known perfectly at the BS. That is each user reports his channel state information (CSI) every STBC block, using it and harnessing the unequal latency property of the service to serve multiple users with disparate SNRs. The scheduler at the BS may decide to schedule transmissions to one or more users based upon their reported CSI in the uplink channel. For simplicity purposes, we assume perfect channel tracking at the receiver and perfect feedback of the CSI to the base station. It is also assumed that the J users experience the same average SNR. Each MIMO link exhibits quasi-static frequency non-selective (flat) fading so that the channel gains remain constant throughout the transmission of an STBC block, which we refer to as a time slot, and the channel is assumed to vary independently between STBC blocks. The received baseband data matrix for the jth user,
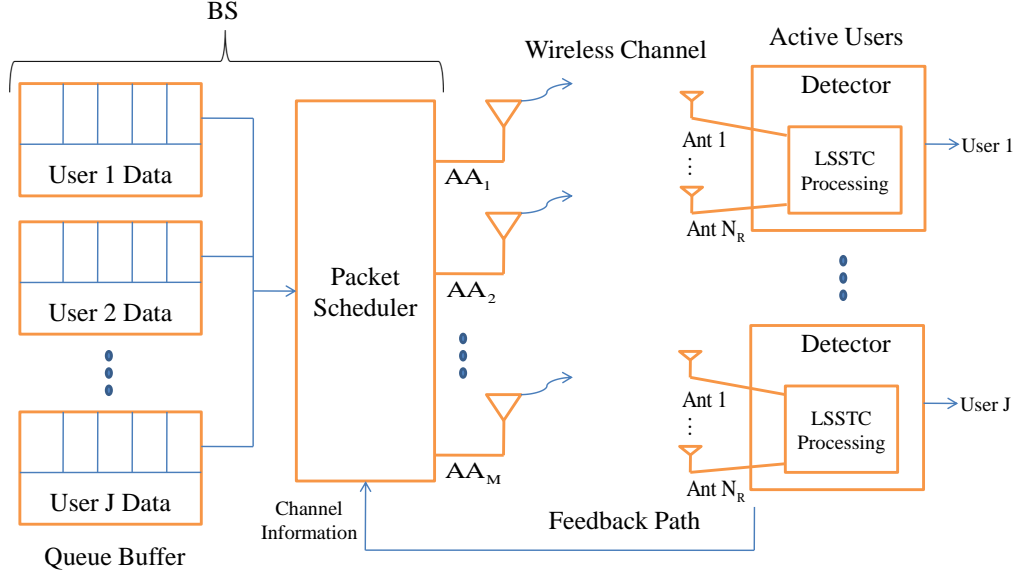
Figure 5.1: Block diagram of a multi-user LSSTC system.

$\mathbf{Y_j}$, can be expressed as

$$\mathbf{Y_j} = \mathbf{H_j W_j C_j} + \mathbf{N_j},\tag{5.1}$$

The parameters in (5.1) have been defined earlier for single-user system, the reader may refer to 3.1 for further details. Figure 5.2 shows the structure of the time frame considered in this Chapter where each frame consists of Q time slot, each time slot has a duration that is equal to that of the STBC block, this assumption is to ensure that the STBC block is sent to the same user, otherwise it will lose the advantage of time redundancy. In addition, we consider the case where the antennas of the base station are assigned to the same users in any time slot.
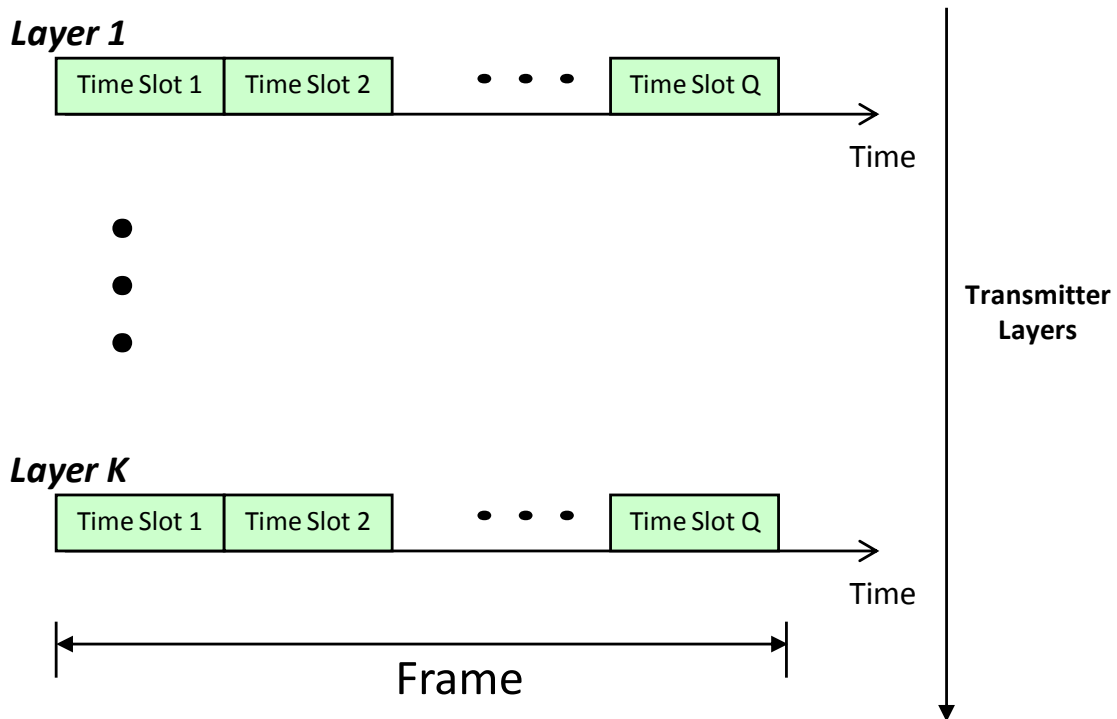
Figure 5.2: Proposed frame structure.

5.2 Scheduling for Packet Data

5.2.1 The Definition of Scheduling

Scheduling is a method of allowing multiple users to share a common resource. Scheduling allocates systems resources (e.g; transmit power, bandwidth, modulation scheme), to optimize a measure of goodness (e.g; throughput, delay) [73]. The scheduling process on the downlink of a wireless, time-slotted system answers two questions. The first one is related to user scheduling, i.e; "which user(s) should be served in a time slot?". The second question is related to selecting be-

tween different types of data [73], i.e; "If we have different types of traffic directed to a single-user, which traffic flow should get served first?". Unlike voice, data is typically delay insensitive. Exceptions to this statement are the cases of streaming live video or speech over data packets. Data systems can exploit fading channels by using scheduling algorithms. The best strategy to maximize system throughput is to transmit to users who have the best channel conditions by continuously monitoring fading coefficients at the receiver (as we are interested in the downlink) [74]. An important scheduling criterion is fairness, because if the base station always serves the user with the best channel, poor-channel users would be left with no service. Hence, algorithms need a way of balancing the scheduled users. As it is expected the scheduling algorithms are executed within the medium access control (MAC) layer, while the space-time processing is executed in the physical (PHY) layer [75].

5.2.2 Scheduling Algorithms

Scheduling on the downlink in MIMO and multiple-input single-output MISO systems can be employed in two methods. The first is by dedicating all the antennas of the BS to a single-user at any time slot. The second is by allocating the antennas of the BS to many users at any time slot. In our work we have used the former method where only one user is served in each time slot and so he will be given all the resources from all the transmission antennas. The reason for using

this method is that it has been proven in [76] that scheduling to more than one user at the same time will complicate the system without providing worthy advantages. Algorithms that do not take channel conditions into considerations are called non-opportunistic. An example of this algorithm is the the round robin (RR). On the other hand, opportunistic algorithms take channel conditions into consideration before allocating the resource to any user. Next, we will describe three opportunistic algorithms, along with the RR scheme which will be used as a benchmark for evaluating the opportunistic algorithms.

Round Robin

In RR users are chosen in cyclic order for transmission, regardless of their individual requested rates. This algorithm provides the highest degree of fairness with respect to the air interface, but suffers low average throughput [75], since channel conditions are ignored. The round robin scheduler is equivalent to the single-user case since all users are equally served in an orthogonal TDM-like manner, such as in TDMA.

Greedy Scheduling

In this scheme, the scheduler selects a user who reports the the best instantaneous channel conditions. This provides the maximum possible average throughput [75]. The "greedy" scheduler gives rise to multiuser diversity mechanism, where

the link with the best instantaneous SNR is selected out of many independent links on a per time slot basis.

Opportunistic Round Robin (ORR)

ORR guarantees that all the J users will be assigned a the time slot within a farme. The time slots are assigned opportunistically such that the users will be assigned the time slots that maximizes the total throughput within a frame [77]. The ORR algorithm works as follows. In the first time slot the scheduler selects the best user according to some scheduling criterion, after that this user will be excluded from the competition of the coming time slots, and the the process is repeated until the frame is finished and all the time slots have been assigned to users ranging from the best user to the worst one. This algorithm captures part of the available multiuser diversity [16], and provides the highest short term fairness when the number of time slots allocated in frames is equal to the number of users J [77].

Proportional Fair (PF)

In this scheme, the PF scheduler assigns a user for transmission when its instantaneous channel capacity is the highest relative to its average channel condition [76]. As such, the benefit of multiuser diversity can be exploited and fairness among users can be maintained. This scheme comes in the middle between two extremes, one is the RR that result in the maximum fairness, the other is

the greedy scheduling that result in maximum system capacity. Originally the PF scheme has been proposed for SISO and single-input multiple-output (SIMO) systems. When multiple input and multiple output systems achieve spatial multiplexing, multiple spatial links are created at each time slot. Different information symbols can be transmitted through these multiple spatial links during the same time slot. As a result, the data rate DRC_i is defined. $DRCi(t)$ is the instantaneous data rate experienced by user i if it is served by the packet scheduler. $DRCi(t)$ is represented by the sum of the data rates of the M spatial links for that user, and can be written as [76]:

$$DRC_i(t) = \sum_{n=1}^{M} R_{k,n}(t), \tag{5.2}$$

where $R_{k,n}(t)$ denotes the data rate of the nth spatial channel for the kth user at the tth time slot. In the PF scheme the scheduler selects the mobile with the highest ratio $DRC_i(t)/R_i(t)$ [76], where $R_i(t)$ is the average data rate received by the mobile over a window of an appropriate time duration. This can be expressed by:

$$k(t) = \arg\max_{i \in \{1,2,\cdots,K\}} \frac{DRC_i(t)}{R_i(t)} \tag{5.3}$$

where $k(t)$ denotes the index of the user selected to be served at the tth time slot. The computation of the user average data rate $R_i(t)$ is given from the following

equation [63]:

$$R_i(t) = \begin{cases} (1 - \frac{1}{t_c})R_i(t-1) & , i \neq k \\ (1 - \frac{1}{t_c})R_i(t-1) + \frac{1}{t_c}DRC_i(t) & , i = k \end{cases} \tag{5.4}$$

Further, $DRC_i(t)$ is given from the following equation in the case of a MIMO multiuser system [76]

$$DRC_i(t) = \sum_{n=1}^{M} \log_2\left(1 + \gamma_{k,n}(t)\right), \tag{5.5}$$

where $\gamma_{k,n}$ denotes the post-processing SNR for the channel corresponding to the nth transmit antenna and the kth user.

5.2.3 Time Slot Fairness

Fairness is an important measure in performance studies, especially in distributed systems where a set of resources is to be shared by a number of users [78]. For fairness comparison, we employ the Jain fairness index (JFI) [78, 77] which is defined as

$$F_J(T) = \frac{(E_T[X])^2}{E_T[X^2]}, \tag{5.6}$$

where X is a random variable describing the amount of resources allocated to a user and $E_T[\cdot]$ is the expectation calculated over T time-slots. JFI is bounded between zero and one, where zero means total unfairness and one means total fairness. It should be noted that total unfairness will occur when we have an

infinite number of user and one user dominates over all the resources [77].

5.2.4 Scheduling Criteria

A scheduling criterion is defined as the condition that the scheduling algorithm consider to differentiate between users. Throughout this chapter we will use the following scheduling criteria:

1. *MaxSNR*

2. *MaxSNR$_{WL}$*

3. *MinES*

4. *MaxMinSV*

5. *MaxLSSTCCap*

In this section, we illustrate and evaluate the above scheduling criteria when applied to the downlink channel of a multi-user LSSTC system. When applying the *MaxSNR* criteria the scheduler selects the user that has the maximum received SNR [16], thus, the selected user satisfies:

$$\max_{k=1,2,\ldots,J}\left\{\text{trace}(\mathbf{H}_k\mathbf{H}_k^{H})\right\} \tag{5.7}$$

For the *MaxSNR$_{WL}$* criterion, the subscript $'WL'$ refers to the worst layer. Since the performance is dominated by the worst layer (group), then choosing the user that

has the best worst layer in terms of the squared Frobenius norm corresponding to that group, will result in a better performance. In this case, the scheduler will select the user with

$$\max_{k=1,2,\dots,J} \min_{i=1,2,\dots,K} \left\{ \|\mathbf{h}_i^{(k)}\|^2 \right\}, \tag{5.8}$$

where $\|\tilde{\mathbf{H}}_i^{(k)}\|^2$ is the squared Frobenius norm of the ith group of $\tilde{\mathbf{H}}$ corresponding to the kth user.

In case of the *MinES*, the scheduler selects the user with the minimum eigenspread of $(\mathbf{H}\mathbf{H}^H)$ [79]. On the other hand, the *MaxMinSV* criterion selects the user that has the largest minimum singular value of $(\mathbf{H}_k)$ [16], mathematically

$$\max_{k=1,2,\dots,J} \left\{ \rho_{min}(\mathbf{H}_k) \right\}. \tag{5.9}$$

For the *MaxLSSTCCap* criterion, the scheduler selects the user that maximizes the LSSTC capacity, i.e.

$$\max_{k=1,2,\dots,J} \left\{ C_{LSSTC}^{(k)} \right\}, \tag{5.10}$$

where $C_{LSSTC}^{(k)}$ is the LSSTC capacity of the kth user. Substituting the value of $C_{LSSTC}^{(k)}$ in (5.10) will lead to

$$\max_{k=1,2,\dots,J} \left\{ K \cdot R_s \cdot \min_{i=1,2,\dots,K} \left\{ \log_2 \left(1 + \frac{L^2 \cdot P_T}{M \cdot N_0} \cdot \|\mathbf{H}_{PP,i}^{(k)}\|^2 \right) \right\} \right\}, \tag{5.11}$$

where $\mathbf{H}_{PP,i}^{(k)}$ is the post-processing matrix corresponding to the ith group of the the kth user. As stated in Section 3.4, the LSSTC capacity is dominated by the worst group, therefore, we can say that choosing the best user according to the *MaxLSSTCCap* criterion is equivalent to choosing the user that has the best worst post-processing group. In other words choosing the user whose worst post-processing group is the maximum among all users. Therefore, 5.11 can be reduced to:

$$\max_{k=1,2,\ldots,J} \min_{i=1,2,\ldots,K} \left\{ \|\mathbf{H}_{PP,i}^{(k)}\|^2 \right\} \tag{5.12}$$

Note that the slight difference between the *MaxSNR_{WL}* and the *MaxLSSTCCap* criteria is just that the former uses the pre-processing SNR (received SNR), while the latter uses the post-processing SNR, but actually, that leads to a huge difference in the performance as we will show in the simulation results. Throughout this chapter we will be using several combinations of scheduling algorithms and criteria, thus it is useful to define the *algorithm − criteria* configuration as the combination of using the specified algorithm with the specified criteria to schedule the users, for instance, the *ORR − MaxSNR* configuration indicates that the scheduler will apply the *ORR* algorithm with the *MaxSNR* criteria as the merit of goodness to schedule the users.

5.3 PDF of the *Greedy* Algorithm with *MaxSNR* Criteria

In this Section we derive the PDF of the maximum pre-processing SNR for a Greedy-based multi-user LSSTC, i.e., *Greedy − MaxSNR* LSSTC. For a MIMO system the pre-processing SNR can be defined in terms of the squared FN $\tilde{\mathbf{H}}$ is an $(N_R \times M)$ matrix whose entries are $\alpha_{n,m}$. Therefore, the squared FN of $\tilde{\mathbf{H}}$ can be written as

$$
\begin{aligned}
\|\tilde{\mathbf{H}}\|^2 &= \sum_{n=1}^{N_R} \sum_{m=1}^{M} \|\alpha_{n,m}\|^2 \\
&= \sum_{n=1}^{N_R} \sum_{m=1}^{M} \|\alpha_{n,m\,R}\|^2 + \|\alpha_{n,m\,I}\|^2,
\end{aligned} \tag{5.13}
$$

where both $\alpha_{n,m\,R}$ and $\alpha_{n,m\,I}$ are complex Gaussian random variables with zero mean and variance σ^2. This shows that $\|\tilde{\mathbf{H}}\|^2$ is a central Chi-squared random variable with $n = 2MN_R$ degrees of freedom, which has the following PDF [80]:

$$
f_{\Gamma}(\gamma) = \frac{1}{\bar{\gamma} \cdot (m-1)!} \left(\frac{\gamma}{\bar{\gamma}} \right)^{m-1} \exp\left(-\frac{\gamma}{\bar{\gamma}} \right), \tag{5.14}
$$

where $\bar{\gamma}$ is the mean of $\|\tilde{\mathbf{H}}\|^2$, $\bar{\gamma} = 2\sigma^2$, and $m = \dfrac{n}{2}$. Given the power constraints stated in 3.3, $\bar{\gamma}$ for the case of LSSTC can be written as $\bar{\gamma} = \dfrac{(L^2 P_T / N_T)}{N_0}$. On the

other hand, the CDF of $\|\tilde{\mathbf{H}}\|^2$ is given by [80]:

$$F_{\Gamma}(\gamma) = 1 - exp\left(-\frac{\gamma}{\bar{\gamma}}\right) \sum_{k=0}^{m-1} \frac{1}{k!} \left(\frac{\gamma}{\bar{\gamma}}\right)^k. \tag{5.15}$$

The *Greedy − MaxSNR* scheduler selects the best user out of J users. Thus, from order statistics theory [75], the PDF the maximum pre-processing SNR will be

$$\begin{aligned} g_{\Gamma}(\gamma) &= J f_{\Gamma}(\gamma) F_{\Gamma}(\gamma)^{J-1} &\tag{5.16} \\ &= \frac{J}{\bar{\gamma} \cdot (m-1)!} \left(\frac{\gamma}{\bar{\gamma}}\right)^{m-1} exp\left(-\frac{\gamma}{\bar{\gamma}}\right) \left(1 - exp\left(-\frac{\gamma}{\bar{\gamma}}\right) \sum_{k=0}^{m-1} \frac{1}{k!} \left(\frac{\gamma}{\bar{\gamma}}\right)^k\right)^{J-1}. \end{aligned}$$

The last result is compared to simulation results for verification.

5.4 Numerical Results

In all the simulations conducted in this section, unless otherwise mentioned, we assume a multi-user 16×4 LSSTC system with BPSK modulation. The base station sends the data to a single-user per time slot, so all the antennas are dedicated to that user. The average SNR is set to $15\ dB$, and the B.S. transmits via $K = 4$ layers each of which is equipped with alamouti STBC encoder and transmit using $M_s = 2$ AAs, and each AA is composed of $L = 2$ antennas that are responsible for beamforming. On the other hand, the receiver of each user employs post-ordered SGIC, and is equipped with $N_R = 4$ antennas.

Figure 5.3 shows a sample of scheduling 30 users over 30 time slots using several combinations of scheduling algorithms and criteria. The Y-axis represents the percentage of time the user takes the channel, while the abscissa marks the user indices. In *RR* all users takes the channel for equal time periods, the same happens in the case of *ORR* − *MaxSNR* this might have been caused from the assumption of equal average power among users. The other subfigures of Figure 5.3 show the effect of scheduling on a group of 30 users.
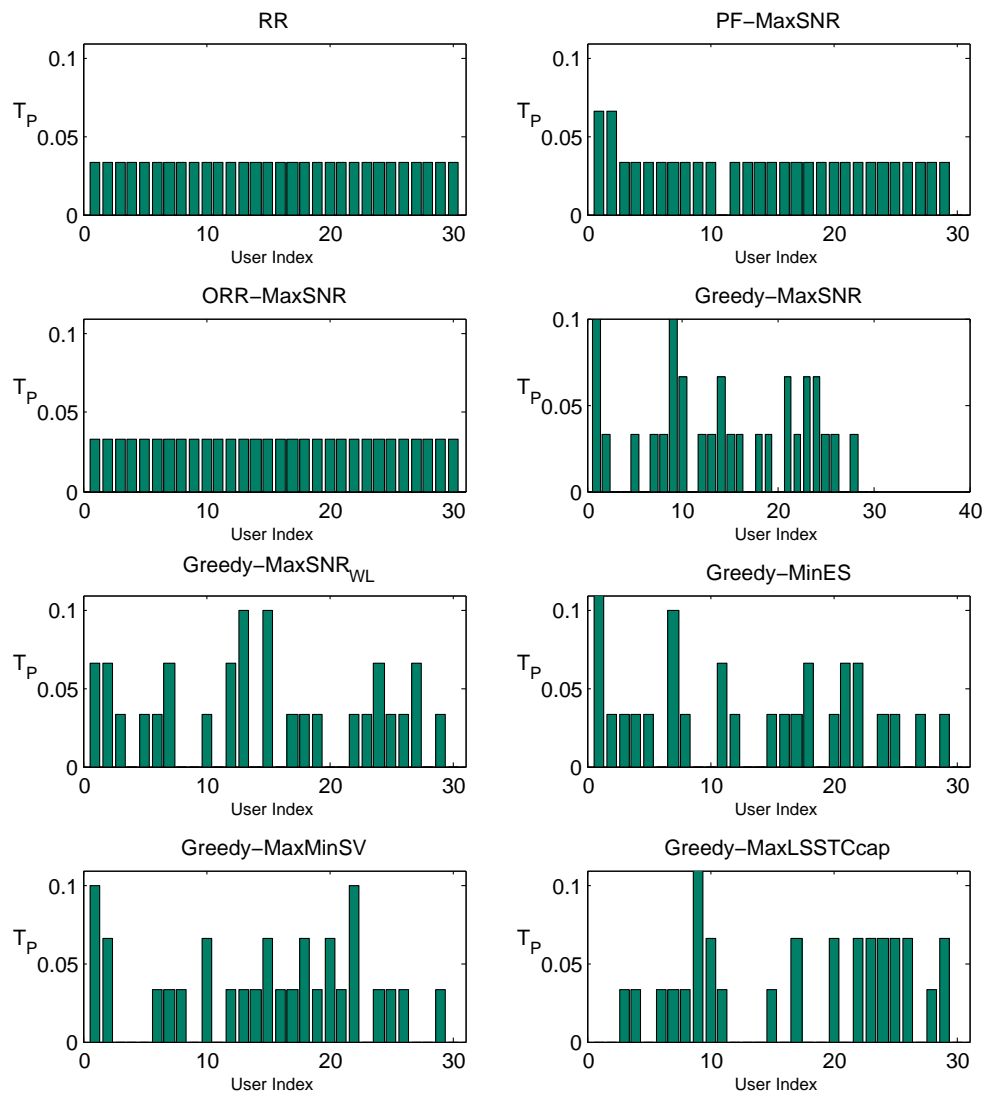
Figure 5.3: Percentage of time the user takes the channel (T_P) using several scheduling algorithms.

Figure 5.4 plots Jain's Fairness Index vs. the number of time Slots of a 16×4 LSSTC system serving 5 users at 15 dB average SNR for several scheduling algorithms and criteria. It can be seen that if the number of the time slots becomes high, Jain's fairness index for all the tested methods gradually approaches 1, that means it is highly probable that all the users will be able to use the channel if the number of time slots is large compared to the number of users, this is because the channel is assumed independent and uncorrelated. Also, it should be observed that the fairness of the *RR* and the *ORR* algorithms is perfect when all the users are served equally within the frame, which results if the number of time slots is a multiple of the number of users. In our case, where $J = 5$, the perfect fairness is when the number of time slots per frame is 5, 10, 15, etc. Figure 5.4 shows that the fairness does not depend on the scheduling criteria and depends solely on the scheduling algorithm. Figure 5.4 shows that *RR* provides the highest fairness followed by *PF*, and the worst fairness is experienced with the greedy algorithm.
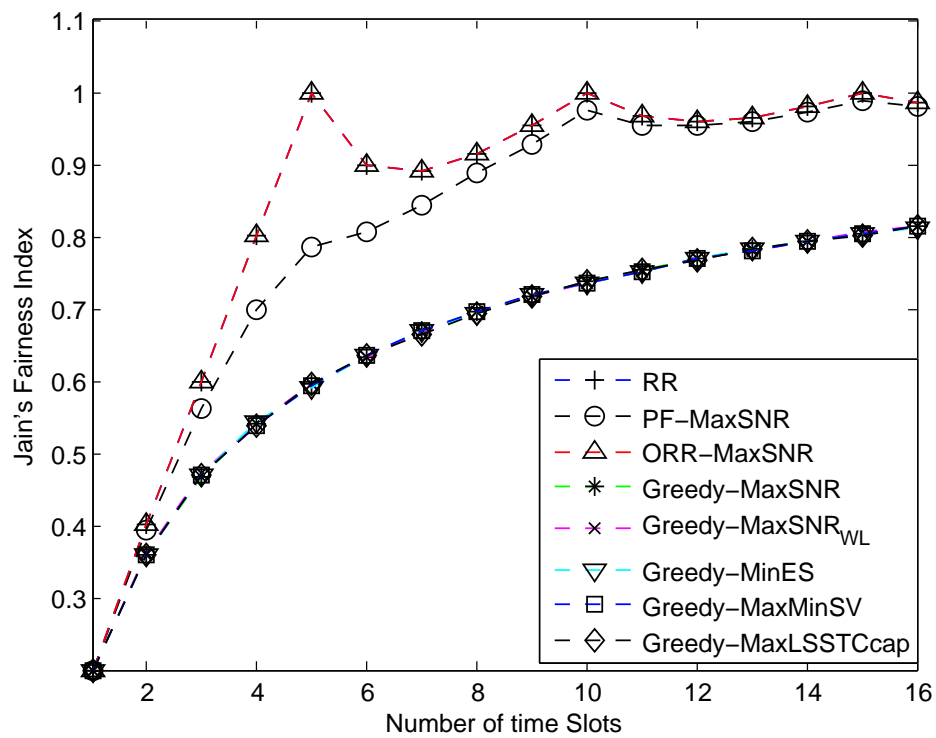
Figure 5.4: Jain's Fairness Index vs. the Number of time Slots of a 16×4 LSSTC serving 5 users at 15 dB average SNR for several cases.

In Figure 5.5, we compare the supported system capacity of different scheduling schemes versus the number of users at 10% Outage probability. As expected, for the Round Robin Scheduler the capacity doesn't increase with increasing J, while in the Greedy scheme, we see that it is increasing with J, as while we're increasing the number of users there will be a higher possibility of getting a high channel coefficient. Among the scheduling criteria, The *MaxLSSTCCap* is the best because it directly coincides with the detection mechanism, i.e. interference nulling at the receiver, and it doesn't matter whether ordering is used or not. The *MaxMinSV* is second best, since it takes into account both the user's instantaneous power and the eigenspread of the user's channel matrix as $\rho_{min} = \frac{\rho_{max}}{\sqrt{s}}$, though, *MaxMinSV* is inferior to *MaxLSSTCCap* since it doesn't coincide with the detection mechanism of LSSTC. Figure 5.5 also shows that the *ORR* algorithm doesn't increase the capacity much compared to the simple *RR* algorithm.
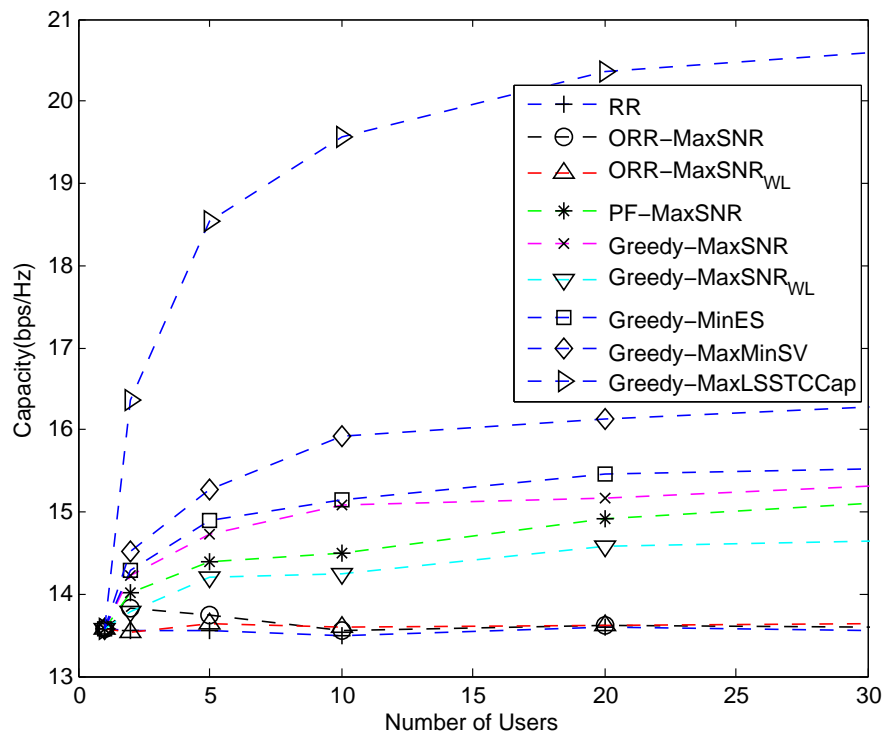
Figure 5.5: Capacity vs. number of users for a 16×4 LSSTC at 10% Outage probability and 15 dB SNR.

Figure 5.6 shows the capacity of the forementioned configuration plotted versus E_s/N_0, and in all cases, the system serves 30 users. As it can be seen from the figure, the capacity is approximately linearly increasing with increasing E_s/N_0. the different configurations behave in a similar manner to that in 5.5.
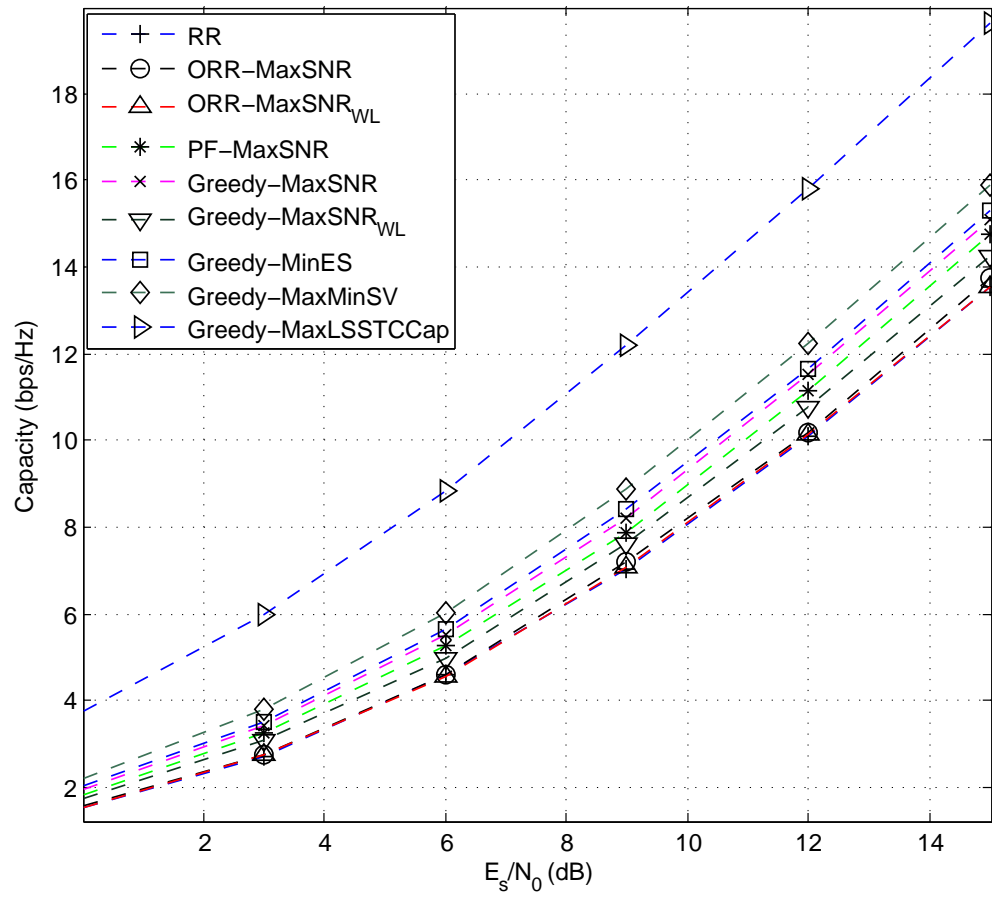
Figure 5.6: Capacity vs. E_s/N_0 for a 30 user 16×4 LSSTC at 10% Outage probability.

Figure 5.7 shows the SER versus E_s/N_0 for a 20 user 16×4 LSSTC system. Figure 5.7 shows the performance superiority of the *MaxLSSTCCap* criteria as it provides a gain of 7.5 *dB* compared to *RR* at a SER of 10^{-3}. While one might have good expectations about *Greedy − MaxSNR*, it is clear that it doesn't perform well in the case of LSSTC, where it only provides 1.9 *dB* over RR, this might be caused from the fact that STBC, which is a component of LSSTC, tends to average the channel while the *MaxSNR* scheduler tends to take the maximas of the channel. Thus, we can conclude that *MaxSNR* criteria and LSSTC is not a very good combination. Most of the tested configurations have a similar behaviour to *Greedy − MaxSNR*. The gain for several algorithm-criteria combinations over the *RR* algorithm at a SER of 10^{-3} is summarized in Table 5.1. The gains are ordered descendingly.

Table 5.1: Gain of several configurations over *RR* at $SER = 10^{-3}$.

Configuration	Gain over *RR*
Greedy − MaxLSSTCCap	7.5 *dB*
Greedy − MaxMinSV	2.4 *dB*
Greedy − MinES	2.2 *dB*
Greedy − MaxSNR	1.9 *dB*
PF − MaxSNR	1.8 *dB*
Greedy − MaxSNR$_{WL}$	1.7 *dB*
ORR − MaxSNR$_{WL}$	0.8 *dB*
ORR − MaxSNR	0.6 *dB*
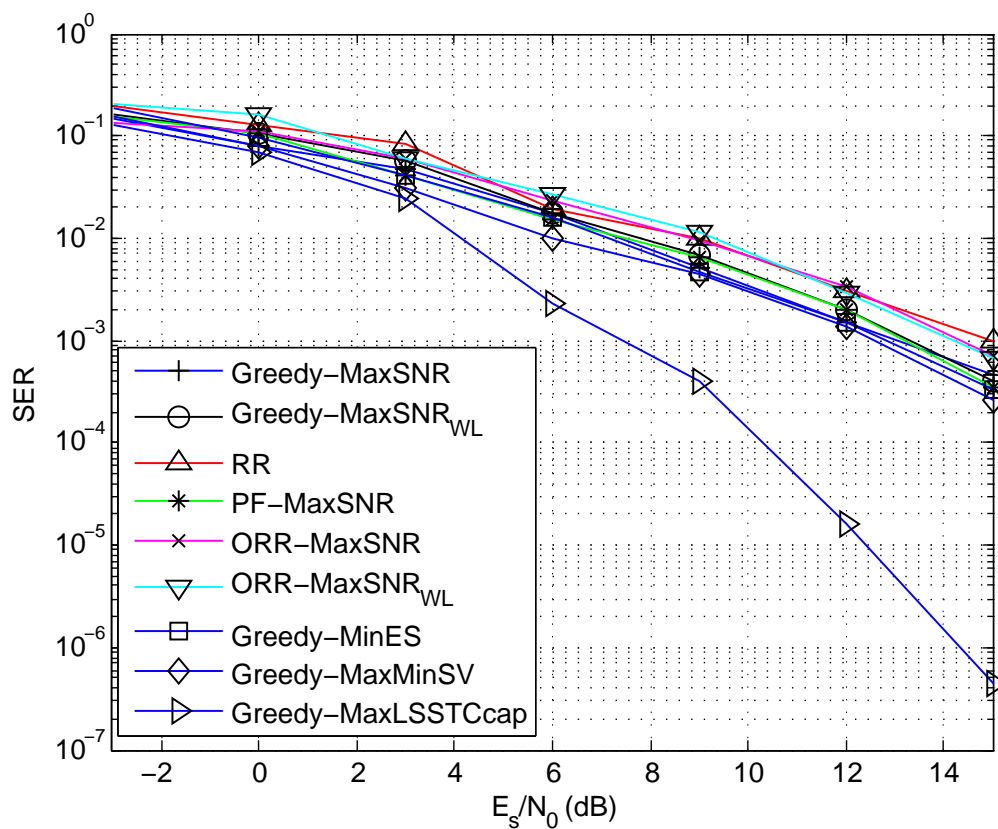
Figure 5.7: SER versus E_s/N_0 for a 20 user 16×4 LSSTC (comparing several scheduling configurations).

In Figure 5.8, we compare the SER versus E_s/N_0 for a 16×4 LSSTC serving different number of users using the *MaxLSSTCCap* criterion. As expected, the diversity gain increases with increasing the number of users, as the plot becomes more steep while increasing the number of users. It seems that the rate of the slope increase will be slower with increasing number of users. Figure 5.9 shows similar results for the case of the *MaxMinSV*, for the other configurations, the diversity gain was very small, and the performance of the system with increasing the number of users was close to the single-user case, therefore, there were no need to include their plots.
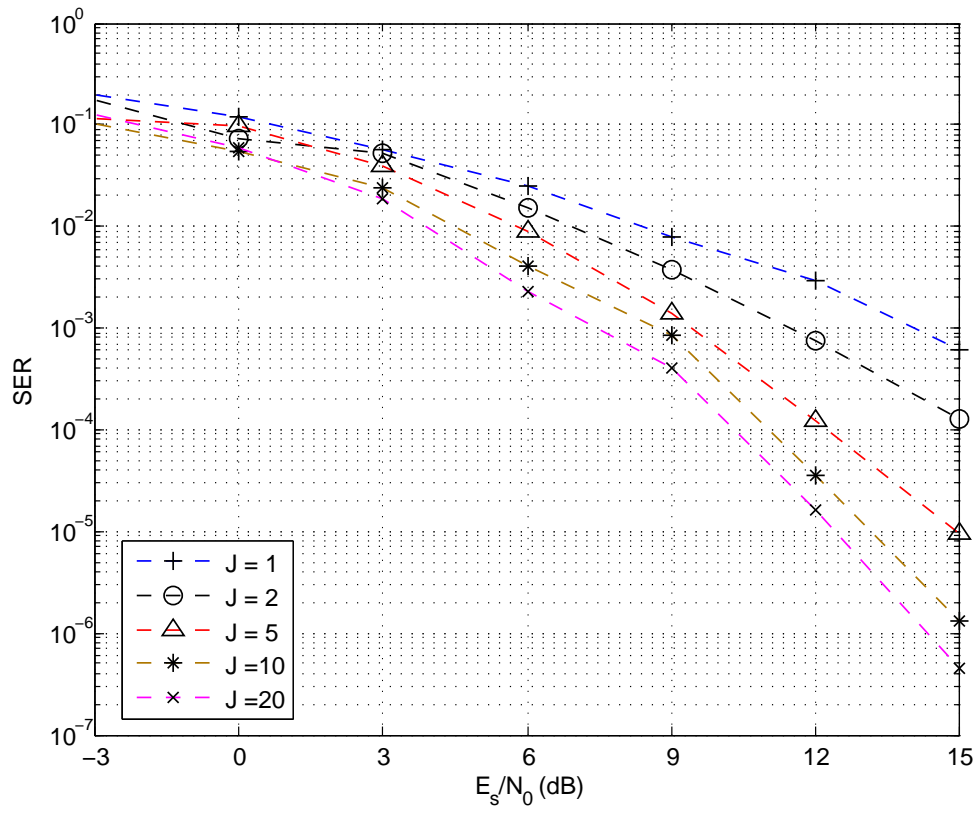
Figure 5.8: SER vs. E_s/N_0 for a 16×4 LSSTC serving different number of users using the *MaxLSSTCCap* criterion.
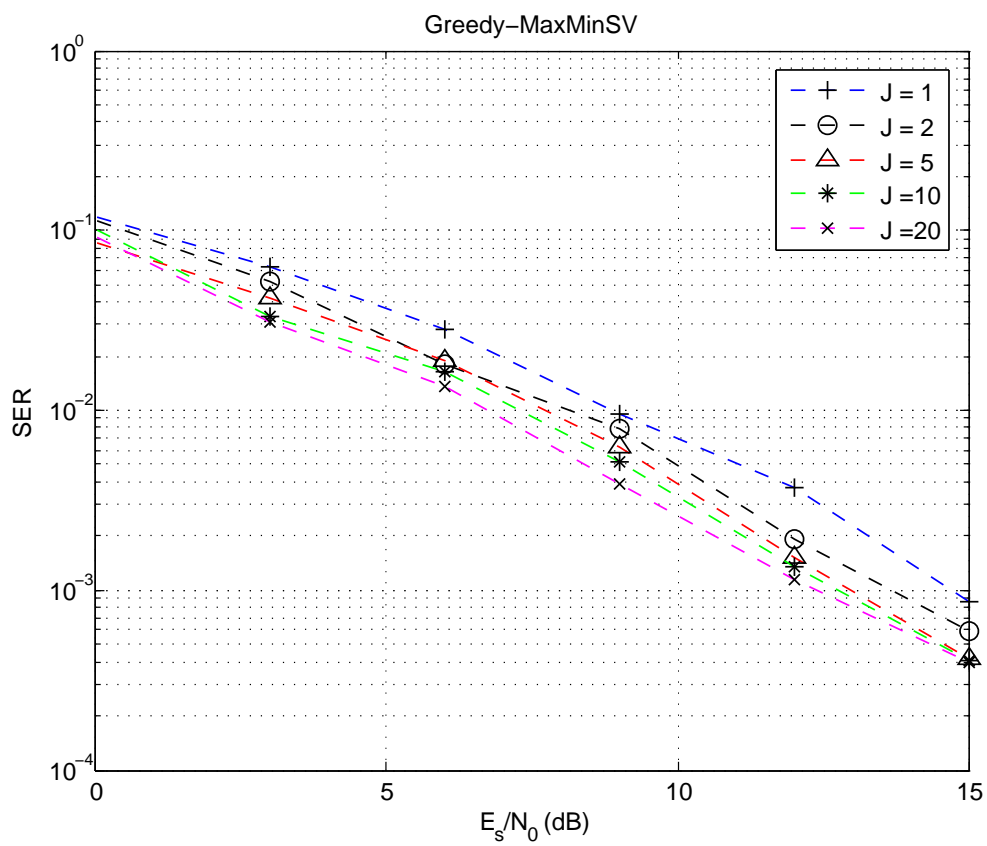
Figure 5.9: SER vs. E_s/N_0 for a 16×4 LSSTC serving different number of users using the *MaxMinSV* criterion.

Next we examine the cumulative distribution function (CDF) for some of the forementioned the scheduling criteria. Figure 5.10 shows the CDF of the pre-processing SNR of the best user for a 16×4 LSSTC serving 20 users. The scheduling is conducted using the proposed configurations. It can be inferred that the pre-processing SNR (received SNR) of the $Greedy - MaxSNR$ criterion has the best behaviour (highest values) but this doesn't necessarily mean that it will result in the best system performance, since the latter depends on the post-processing SNR rather than the the pre-processing SNR.
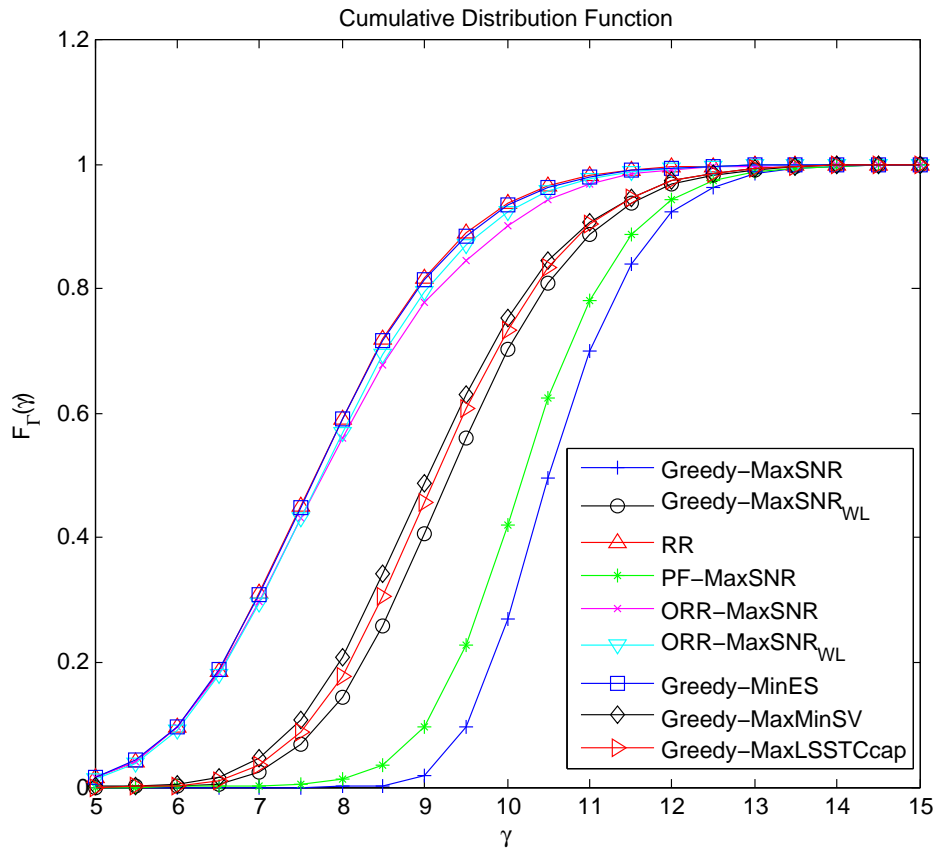
Figure 5.10: CDF of the pre-processing SNR of the best user for a 16×4 LSSTC serving 20 users (comparing several scheduling configurations).

Figure 5.11 shows the PDF of the maximum pre-processing SNR of a 16×4 LSSTC serving 20 users. Figure 5.11 compares the analytical results derived in 5.3 to simulation results, also the PDF for the single-user case is included for reference. It is clear that the Monte Carlo simulation makes a nearly perfect match to the analytical results, which demonstrates the validity of the analytical results.
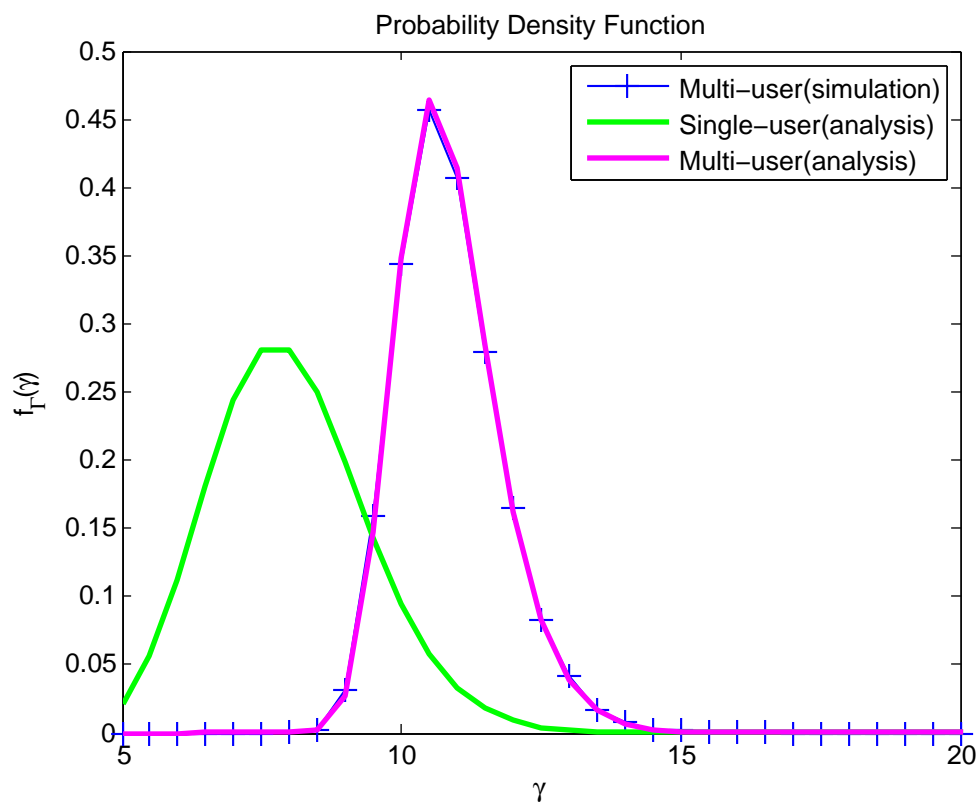
Figure 5.11: PDF of the maximum pre-processing SNR of a 16×4 LSSTC serving 20 users (comparing analysis to simulation results).

Figure 5.12 compares the post-processing PDFs of the worst layer. Unlike Figure **??**, Figure 5.12 coincides directly with the results of Figure 5.5 for the capacity, and Figure 5.7 for the SER. Figure 5.12 shows the PDF of the post-processing SNR of the best user for a 16×4 LSSTC serving 20 users. where the scheduling is conducted using the proposed configurations. where the scheduling are from best to worst as in Table which reflects the actual performance of the system since the worst group is the one dominating the performance whether we are talking about capacity or SER.
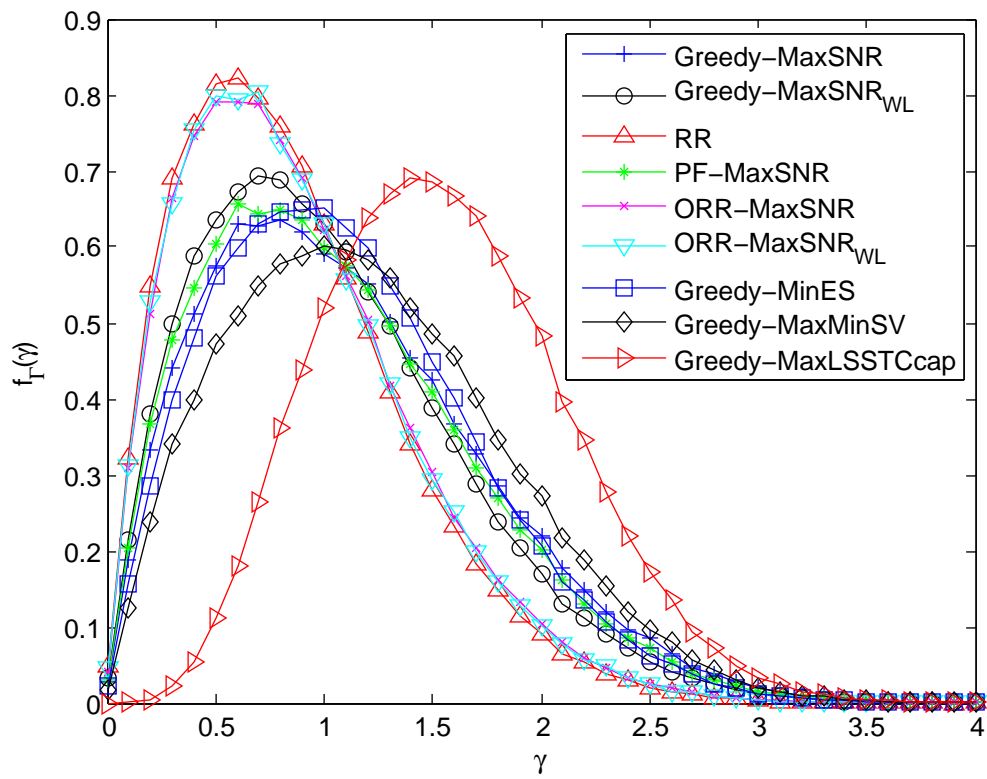
Figure 5.12: PDF of the post-processing SNR corresponding to the weakest layer of the scheduled user for a 16×4 LSSTC serving 20 users (comparing several scheduling configurations).

Figure 5.13 shows the PDF of the post-processing SNR of the scheduled user according to the *MaxLSSTCCap* criterion when used with a 16×4 LSSTC employing post-ordered SGIC and serving 20 users. Figure 5.13 also shows the PDF of each group, where the 4th layer is the worst layer since ordering is used.

5.5 Chapter Conclusions

In this chapter we investigated the performance of multi-user LSSTC. The work of this chapter depends mainly on simulations in which we have used to evaluate the system with several combinations of scheduling algorithms and criteria. The main result of this chapter is finding that the most suitable scheduling criteria to multi-user LSSTC is the one that maximizes its capacity, namely, the *MaxLSSTCCap* criteria. This is because it directly coincides with the detection mechanism at the receiver, which means that it will result in the highest possible post-processing SNR per layer, which will result in improving the capacity and SER of multi-user LSSTC. Additionally, other configurations were studied, and plots of the PDF, CDF, and CCDF were generated to illustrate the differences. Finally, we derived a formula for the PDF of the maximum pre-processing SNR for a Greedy-based multi-user LSSTC.
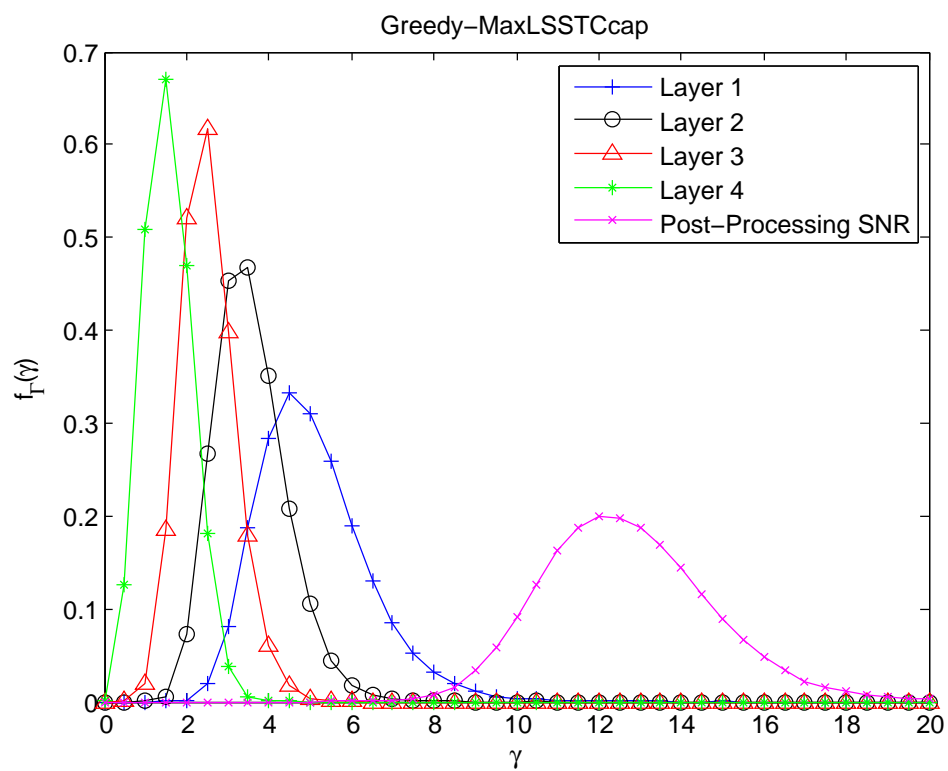
Figure 5.13: PDF of the post-processing SNR according to the *MaxLSSTCCap* criterion for a 16×4 LSSTC employing post-ordered SGIC and serving 20 users.

Chapter 6

Conclusions and Future Research

In this concluding chapter, we summarize the content of the thesis and we discuss some of the possible future research directions.

6.1 Conclusions

In Chapter 2 we describe STBC, VBLAST, and beamforming, these systems are the components of LSSTC, therefore, the system model of each of those systems was introduced.

In Chapter 3 we investigated the analytical error performance of single user LSSTC, and we were able to obtain recursive expressions for the probability of error. The analytical results were verified by comparing to simulation results. In addition, a formula for the instantaneous capacity of single-user LSSTC is derived. Also, we obtained the diversity, multiplexing, and beamforming tradeoff

curve for LSSTC. which links the extremes of beamforming gain, diversity gain, and the multiplexing gain. Finaly we proposed a multi-configuration transmission scheme based on LSSTC and VBLAST systems that suggests the configuration and the modulation scheme in order to improve the performance, where it was noted that LSSTC has a better performance than VBLAST at high SNR range.

In Chapter 4 we proposed the PA-LSSTC scheme that enhances the performance and capacity. Also, we investigated the performance of this scheme for BPSK, M-ary PSK and M-ary QAM. In addition, we obtained the optimum PA performance by using numerical methods.

In Chapter 5, we evaluated the multi-user LSSTC system, this was done by comparing the capacity and the probability of error for different $algorithm - criteria$ configurations. Also we derived a formula for the PDF of the maximum preprocessing SNR for a Greedy-based multi-user LSSTC.

6.2   Future Research

The advantages of using LSSTC in wireless systems calls to further research on the topic, as there is a lot possibilities of what can be done. In the following we list some suggested points:

- Conducting complexity analysis for the LSSTC system in single and multi-user environment.

- Designing a system that combines VBLAST, beamfoming, and space-time trellis code (STTC), and studying the error performance,capacity, and optimum power allocation in both single and multi-user environments. This scheme replaces STBC in our LSSTC system with STTC. The motivation for proposing is that STBC has a fixed performance while STTC can improve its performance by increasing the number of states [81]. On the other hand, STTC is not always reliable to implement because of the detection complexity.

- Finding formulas for the probability of error for multi-user LSSTC for the different *algorithm − criteria* configurations used in Chapter 5, this can be done by first finding the PDF of the post-detection SNR, and then integrating the error probability conditioned on a certain SNR over the obtained PDF.

- Proposing a new scheduling criteria, *MaxOptPA*, in which we schedule the

user that has the best optimum PA performance, i.e. the user that has the best performance given his optimum PA vector $\mathbf{K}_{opt}$.

- Finding formulas for the average feedback load for the different *algorithm − criteria* configurations used in Chapter 5.

- Extending the multi-user LSSTC model to the case where the antennas of the base station can be assigned to different users at the same time. Although it seems complicated, the proposed scheme is expected to improve the performance of the multi-user LSSTC system.

Appendices

Appendix A: The covariance matrix of $\mathbf{N}^{i,k}$

The covariance matrix of $\mathbf{N}^{i,k}$ can be written as

$$\Sigma_{mn} = Cov\left[\mathbf{N}_m^{i,k}, \mathbf{N}_n^{i,k}\right] = \mathrm{E}\left[\left(\mathbf{N}_m^{i,k} - \mu_m\right)\left(\mathbf{N}_n^{i,k} - \mu_n\right)\right], \tag{A.1}$$

where μ_m and μ_n are the mean values of $\mathbf{N}_m^{i,k}$ and $\mathbf{N}_n^{i,k}$ respectively, and they are both zeros. Therefore, we may write the covariance matrix of $\mathbf{N}^{i,k}$ as

$$\begin{aligned}
\Sigma_{mn} &= \mathrm{E}\left[\left(\mathbf{N}_m^{i,k}\right)\left(\mathbf{N}_n^{i,k}\right)\right] \\
&= \mathrm{E}\left[\left(\mathbf{n}_m + \sum_{j=1}^{i} \mathbf{h}_{g_{k,m}}(j) \cdot \left(s_{g_{k,m}}(j) - \hat{s}_{g_{k,m}}(j)\right)\right) \cdot \left(\mathbf{n}_n + \sum_{j=1}^{i} \mathbf{h}_{g_{k,n}}(j) \cdot \left(s_{g_{k,n}}(j) - \hat{s}_{g_{k,n}}(j)\right)\right)\right] \\
&= \mathrm{E}\left[\mathbf{n}_m \mathbf{n}_n\right] \\
&\quad + \mathrm{E}\left[\mathbf{n}_m \sum_{j=1}^{i} \mathbf{h}_{g_{k,n}}(j) \cdot \left(s_{g_{k,n}}(j) - \hat{s}_{g_{k,n}}(j)\right)\right] \\
&\quad + \mathrm{E}\left[\mathbf{n}_n \sum_{j=1}^{i} \mathbf{h}_{g_{k,m}}(j) \cdot \left(s_{g_{k,m}}(j) - \hat{s}_{g_{k,m}}(j)\right)\right] \\
&\quad + \mathrm{E}\left[\sum_{j_m=1}^{i} \sum_{j_n=1}^{i} \mathbf{h}_{g_{k,m}}(j_m) \mathbf{h}_{g_{k,n}}(j_n) \left(s_{g_{k,m}}(j_m) - \hat{s}_{g_{k,m}}(j_m)\right) \left(s_{g_{k,n}}(j_n) - \hat{s}_{g_{k,n}}(j_n)\right)\right].
\end{aligned} \tag{A.2}$$

In the following, we will find each term of the last equation separately, then

we'll add them up as follows

$$
\begin{aligned}
E\left[\mathbf{n}_m\mathbf{n}_n\right] &= \mathrm{Cov}\left[\mathbf{n}_m\mathbf{n}_n\right]+E\left[\mathbf{n}_m\right]+E\left[\mathbf{n}_n\right]\\
&= N_0\mathbf{I}_{N\times N}.
\end{aligned}
\tag{A.3}
$$

$$
\begin{aligned}
E\left[\mathbf{n}_m\sum_{j=1}^{i}\mathbf{h}_{g_{k,n}}(j)\cdot\left(s_{g_{k,n}}(j)-\hat{s}_{g_{k,n}}(j)\right)\right] &= E\left[\mathbf{n}_m\right]\cdot E\left[\sum_{j=1}^{i}\mathbf{h}_{g_{k,n}}(j)\cdot\left(s_{g_{k,n}}(j)-\hat{s}_{g_{k,n}}(j)\right)\right]\\
&= 0.
\end{aligned}
\tag{A.4}
$$

And the same applies for the third term

$$
\begin{aligned}
E&\left[\sum_{j_m=1}^{i}\sum_{j_n=1}^{i}\mathbf{h}_{g_{k,m}}(j_m)\mathbf{h}_{g_{k,n}}(j_n)\left(s_{g_{k,m}}(j_m)-\hat{s}_{g_{k,m}}(j_m)\right)\left(s_{g_{k,n}}(j_n)-\hat{s}_{g_{k,n}}(j_n)\right)\right]\\
&= E\left[\sum_{j_m=1}^{i}\mathbf{h}_{g_{k,m}}^2(j_m)\left(s_{g_{k,m}}(j_m)-\hat{s}_{g_{k,m}}(j_m)\right)^2\right]\\
&\quad + E\left[\sum_{\substack{j_m=1\\j_m\neq j_n}}^{i}\sum_{j_n=1}^{i}\mathbf{h}_{g_{k,m}}(j_m)\mathbf{h}_{g_{k,n}}(j_n)\left(s_{g_{k,m}}(j_m)-\hat{s}_{g_{k,m}}(j_m)\right)\left(s_{g_{k,n}}(j_n)-\hat{s}_{g_{k,n}}(j_n)\right)\right]\\
&= \sum_{j_m=1}^{i}E\left[\mathbf{h}_{g_{k,m}}^2(j_m)\left(s_{g_{k,m}}(j_m)-\hat{s}_{g_{k,m}}(j_m)\right)^2\right]\\
&\quad + \sum_{\substack{j_m=1\\j_m\neq j_n}}^{i}\sum_{j_n=1}^{i}E\left[\mathbf{h}_{g_{k,m}}(j_m)\mathbf{h}_{g_{k,n}}(j_n)\left(s_{g_{k,m}}(j_m)-\hat{s}_{g_{k,m}}(j_m)\right)\left(s_{g_{k,n}}(j_n)-\hat{s}_{g_{k,n}}(j_n)\right)\right]\\
&= \sum_{j_m=1}^{i}E\left[\mathbf{h}_{g_{k,m}}^2(j_m)\right]E\left[\left(s_{g_{k,m}}(j_m)-\hat{s}_{g_{k,m}}(j_m)\right)^2\right]\\
&\quad + \sum_{\substack{j_m=1\\j_m\neq j_n}}^{i}\sum_{j_n=1}^{i}E\left[\mathbf{h}_{g_{k,m}}(j_m)\mathbf{h}_{g_{k,n}}(j_n)\left(s_{g_{k,m}}(j_m)-\hat{s}_{g_{k,m}}(j_m)\right)\left(s_{g_{k,n}}(j_n)-\hat{s}_{g_{k,n}}(j_n)\right)\right]
\end{aligned}
\tag{A.5}
$$

Since $\mathbf{h}_{g_{k,m}}(j_m)$ and $\mathbf{h}_{g_{k,n}}(j_n)$ are independent, and both of their expected values are equal to zero, then the second term in (A.5) will vanish. Therefore we are left with following

$$\mathrm{E}\left[\mathbf{h}^2_{g_{k,m}}(j_m)\right] = \mathrm{E}\left[\left(L \cdot \tilde{\mathbf{h}}_{g_{k,m}}(j_m)\right)^2\right] = L^2 \mathbf{I}_{N \times N}, \tag{A.6}$$

where $\mathrm{E}\left[\left(\tilde{\mathbf{h}}_{g_{k,m}}(j_m)\right)^2\right]$ is the power of a Rayleigh-distributed random variable that have been assumed unity. The last term to be found is

$$\mathrm{E}\left[\left(s_{g_{k,m}}(j_m) - \hat{s}_{g_{k,m}}(j_m)\right)^2\right] = Var\left[s_{g_{k,m}}(j_m) - \hat{s}_{g_{k,m}}(j_m)\right] + \mathrm{E}\left[s_{g_{k,m}}(j_m) - \hat{s}_{g_{k,m}}(j_m)\right]^2$$

$$= Var\left[s_{g_{k,m}}(j_m) - \hat{s}_{g_{k,m}}(j_m)\right] + \left(\mathrm{E}\left[s_{g_{k,m}}(j_m)\right] - \mathrm{E}\left[\hat{s}_{g_{k,m}}(j_m)\right]\right)^2 \tag{A.7}$$

$$= Var\left[s_{g_{k,m}}(j_m)\right] + Var\left[\hat{s}_{g_{k,m}}(j_m)\right] + 2Cov\left[s_{g_{k,m}}(j_m), \hat{s}_{g_{k,m}}(j_m)\right].$$

The first and second terms of A.7 can be found by

$$Var\left[s_{g_{k,m}}(j_m)\right] = \frac{1}{2}\left(\left(\sqrt{\frac{P_t}{M}} - 0\right)^2 + \left(-\sqrt{\frac{P_t}{M}} - 0\right)^2\right)$$

$$= \frac{P_t}{M} = Var\left[\hat{s}_{g_{k,m}}(j_m)\right], \tag{A.8}$$

to find the third term in A.7 we write

$$Cov\left[s_{g_{k,m}}(j_m), \hat{s}_{g_{k,m}}(j_m)\right] = \mathrm{E}\left[s_{g_{k,m}}(j_m)\hat{s}_{g_{k,m}}(j_m)\right] - \mathrm{E}\left[s_{g_{k,m}}(j_m)\right] \cdot \mathrm{E}\left[\hat{s}_{g_{k,m}}(j_m)\right]$$

$$= \mathrm{E}\left[s^2_{g_{k,m}}(j_m)\right] = Var\left[s_{g_{k,m}}(j_m)\right] = \frac{P_t}{M}. \tag{A.9}$$

Thus A.7 can be written as

$$\mathrm{E}\left[\left(s_{g_{k,m}}(j_m) - \hat{s}_{g_{k,m}}(j_m)\right)^2\right] = \frac{4P_t}{M}. \tag{A.10}$$

Therefore, the fourth term in (A.2) is equal to $\frac{4P_t i L^2}{M}$. collecting the above terms,

we can write the covariance as

$$\mathrm{Cov}\left[\mathbf{N}_m^{i,k}, \mathbf{N}_n^{i,k}\right] = \left[N_0 + \frac{4P_t i L^2}{M}\right] I_{N \times N}, \tag{A.11}$$

Appendix B: Calculation of $\mathrm{Prob}\{A_{k-1}^i\}$

In this section we derive in a similar way as [57] the $\mathrm{Prob}\{A_{k-1}^i\}$ for three cases:

Case I $(\mathbf{i} = \mathbf{0})$:

If there are no detection errors up to layer $(k-1)$, that can be translated into hav-

ing a correct decision in detecting the layer $(k-1)$, along with having no errors

up to the layer $(k-2)$, mathematically,

$$
\begin{aligned}
\mathrm{Prob}\{A_{k-1}^0\} &= \mathrm{Prob}\{S_{k-1} = \hat{S}_{k-1}, A_{k-2}^0\} \\
&= \mathrm{Prob}\{S_{k-1} = \hat{S}_{k-1} \mid A_{k-2}^0\}\mathrm{Prob}\{A_{k-2}^0\} \\
&= \left[1 - \mathrm{Prob}\{S_{k-1} \neq \hat{S}_{k-1} \mid A_{k-2}^0\}\right]\mathrm{Prob}\{A_{k-2}^0\} \tag{B.1} \\
&= \left[1 - P_e\left(m_{k-1}(N-K+k), \frac{P_T L^2}{MN_0}\right)\right]\mathrm{Prob}\{A_{k-2}^0\}
\end{aligned}
$$

Case II ($i = k - 1$):

In this case all the sub-streams up to and including the currently detected layer are in error, we may write

$$\text{Prob}\{A_{k-1}^{k-1}\} = \text{Prob}\{S_{k-1} \neq \hat{S}_{k-1}, A_{k-2}^{k-2}\}$$

$$= \text{Prob}\{S_{k-1} \neq \hat{S}_{k-1} \mid A_{k-2}^{k-2}\}\text{Prob}\{A_{k-2}^{k-2}\} \quad \text{(B.2)}$$

$$= P_e\left(m_{k-1}(N-K+k), \frac{P_T L^2}{MN_0 + 4P_T(k-2)L^2}\right)\text{Prob}\{A_{k-2}^{k-2}\}$$

Case III ($i = 1, \ldots, k - 1$):

This case come between the two extremes of zero or all error. Here some of the detected sub-streams are detected correctly, while the others are detected erroneously, it can be written as

$$\text{Prob}\{A_{k-1}^i\} = \text{Prob}\{S_{k-1} \neq \hat{S}_{k-1}, A_{k-2}^{i-1}\} + \text{Prob}\{S_{k-1} = \hat{S}_{k-1}, A_{k-2}^i\}$$

$$= \text{Prob}\{S_{k-1} \neq \hat{S}_{k-1} \mid A_{k-2}^{i-1}\}\text{Prob}\{A_{k-2}^{i-1}\}$$

$$+ \text{Prob}\{S_{k-1} = \hat{S}_{k-1} \mid A_{k-2}^i\}\text{Prob}\{A_{k-2}^i\} \quad \text{(B.3)}$$

$$= \text{Prob}\{S_{k-1} \neq \hat{S}_{k-1} \mid A_{k-2}^{i-1}\}\text{Prob}\{A_{k-2}^{i-1}\}$$

$$+ \left[1 - \text{Prob}\{S_{k-1} \neq \hat{S}_{k-1} \mid A_{k-2}^i\}\right]\text{Prob}\{A_{k-2}^i\}$$

Bibliography

[1] C. E. Shannon, "A mathematical Theory of Communication," *Junior Faculty Research Grants Project*, vol. 27, pp. 379–423 and 623–656, July and October 1948.

[2] P. W. Wolniansky, G. J. Foschini, G. D. Golden, and R. A. Valenzuela, "V-BLAST : An Architecture for Realizing Very High Data Rates Over the Rich-Scattering Wireless Channel," *URSI International Symposium on Signals, Systems and Electronics*, pp. 295–300, October 1998.

[3] T. Rappaport, *Wireless Communications: Principles and Applications*. Singapore: Pearson Education, Inc., 2nd ed., 2002.

[4] S. Alamouti, "A Simple Transmit Diversity Technique for Wireless Communications," *Selected Areas in Communications, IEEE Journal on*, vol. 16, pp. 1451–1458, Oct 1998.

[5] V. Tarokh, A. Naguib, N. Seshadri, and A. Calderbank, "Combined Array Processing and Space-Time Coding," *Information Theory, IEEE Transactions*

on, vol. 45, pp. 1121–1128, May 1999.

[6] M. Mohammad, S. Al-Ghadhban, B. Woerner, and W. Tranter, "Comparing Decoding Algorithms for Multi-Layered Space-Time Block Codes," *IEEE SoutheastCon Proceedings*, pp. 147–152, August 2004.

[7] J. H. Chong, S. Khatun, N. K. Noordin, B. M. Ali, and M. J. Syed, "Joint Optimal Detection of Ordering SIC ZF and SIC ZF MAP for V-BLAST/STBC Wireless Communication Systems," pp. 84–89, 2008.

[8] M. El-Hajjar and L. Hanzo, "Layered steered space-time codes and their capacity," *IEEE Electronics Letters*, pp. 680–682, June 2007.

[9] J. Heath, R.W., M. Airy, and A. Paulraj, "Multiuser Diversity for MIMO Wireless Systems with Linear Receivers," *Conference Record of the Thirty-Fifth Asilomar Conference on Signals, Systems and Computers*, vol. 2, pp. 1194–1199 vol.2, 2001.

[10] K. Pahlavan and P. Kishnamurthy, *Principles of Wireless Networks - A Unified Approach*. New Jersey, USA: Prentice Hall Inc, 2002.

[11] A. Goldsmith, *Digital Beamforming in Wireless Communications*. Cambridge, UK: Cambridge University Press, 2005.

[12] B. Sklar, "Rayleigh Fading Cannel in Mobile Digital Communication Systems Part II: Mitigation," *IEEE Communications Magazine*, vol. 35, pp. 102 – 109, July 1997.

[13] J. Proakis, *Digital Communications*. New York, USA: McGraw-Hill, 4th ed., 2000.

[14] W. C. Jakes, *Microwave Mobile Communications*. USA: Wiley-IEEE Press, 1994.

[15] I. E. Telatar, "Capacity of Multi-Antenna Gaussian Channels," *European Transactions on Telecommunications*, vol. 10, pp. 585–595, 1999.

[16] S. Al-Ghadhban, *Multi-Layered Space Frequency Time Codes*. PhD thesis, Virginia Polytechnic Institute and State University, Virginia, USA, November 2005.

[17] V. Tarokh, H. Jafarkhani, and A. R. Calderbank, "Space-Time Block Codes from Orthogonal Designs," *IEEE Trans. Inform. Theory*, vol. 45, pp. 1456–1467, 1999.

[18] V. Tarokh, H. Jafarkhani, and A. Calderbank, "Space-Time Block Coding for Wireless Communications: Performance Results," *Selected Areas in Communications, IEEE Journal on*, vol. 17, pp. 451–460, Mar 1999.

[19] G. J. Foschini, "Layerd Space-Time Architecture for Wireless Communications in a Fading Environment when Using Multi-Element Antennas," *Bell Labs Technical Journal*, pp. 1–19, Autumn 1996.

[20] G. J. Foschini and M. J. Gans, "On limits of wireless communications in a fading environment when using multiple antennas," *Wireless Personal Communications*, pp. 311–335, March 1998.

[21] G. D. Golden, G. J. Foschini, R. A. Valenzuela, and P. W. Wolniansky, "Detection Algorithm and Initial Laboratory Results Using V-BLAST Space-Time Communication Architecture," *IEE Electronic Letters*, pp. 14–16, January 1999.

[22] S. Baro, G. Bauch, A. Pavlic, and A. Semmler, "Turbo-BLAST for High-Speed Wireless Communications," *GLOBECOM 2000*, vol. 2, 2000.

[23] M. Sellathurai and S. Haykin, "A Simplified Diagonal BLAST Architecture with Iterative Parallel-Interference Cancelation Receivers," *IEEE International Conference on Communications*, vol. 10, 2001.

[24] M. Sellathurai and S. Haykin, "Turbo-Blast for High-Speed Wireless Communications," *Wireless Communications and Networking Conference*, 2000.

[25] R. Gozali, *Improving BLAST Performance Using Space-Time Block Codes and Turbo Decoding*. PhD thesis, Virginia Polytechnic Institute and State University, 2002.

[26] J. Litva and T. K. Lo.

[27] T. Haynes, "A Primer on Digital Beamforming," *Spectrum Signal Processing*, March 1998.

[28] "Applications of Antenna Arrays to Mobile Communications, Part I: Performance Improvement, Feasibility, and System Considerations," *Proceedings of the IEEE*, vol. 85, pp. 1029–1030, Jul 1997.

[29] L. Godara, "Application of Antenna Arrays to Mobile Communications. Part II. Beam-Forming and Direction-of-Arrival Considerations," *Proceedings of the IEEE*, vol. 85, pp. 1195–1245, Aug 1997.

[30] W. Gabriel, "Adaptive Processing Array Systems," *Proceedings of the IEEE*, vol. 80, pp. 152–162, Jan 1992.

[31] A. LLC, "Multi-Antenna Signal Processing in Practice," *http://www.arraycomm.com/serve.php?page=practice*.

[32] R. Roy, "An Overview of Smart Antenna Technology: The Next Wave in Wireless Communications," *Aerospace Conference, Proceedings, IEEE*, vol. 3, pp. 339–345 vol.3, Mar 1998.

[33] R. Kohno, "Spatial and Temporal Communication Theory Using Adaptive Antenna Array," *Personal Communications, IEEE*, vol. 5, pp. 28–35, Feb 1998.

[34] A. J. Paulraj and B. C. Ng, "Space-Time Modems for Wireless Personal Communications," *IEEE Personal Communications*, vol. 5, pp. 36–48, 1998.

[35] J. Winters, "Smart Antennas for Wireless Systems," *Personal Communications, IEEE*, vol. 5, pp. 23–27, Feb 1998.

[36] J. Liberti and T. S. Rappaport, *Smart Antennas for Wireless Communications: IS-95 and Third Generation CDMA Applications*. New Jersey: Prentice Hall Communications Engineering and Emerging Technologies Series, 1999.

[37] S. Choi, D. Shim, and T. K. Sarkar, "A Comparison of Tracking-Beam Arrays and Switching-Beam Arrays Operating in a CDMA Mobile Communication Channel," *IEEE Antennas Propagation Magazine*, vol. 41, pp. 10–56, Dec. 1999.

[38] B. Pattan, *Robust Modulation Methods and Smart Antennas in Wireless Communications*. New Jersey: Prentice Hall Inc., 2000.

[39] M. Er and Y. Sng, "A New GSC Beamformer Employing DOA Estimation and Null Steering," *Singapore ICCS/ISITA. 'Communications on the Move'*, pp. 816–820 vol.2, Nov 1992.

[40] Y. Sng, M. Er, and Y. Soh, "Partially Adaptive Array Design Using DOA Estimation and Null Steering," *Radar, Sonar and Navigation, IEE Proceedings -*, vol. 142, pp. 1–5, Feb 1995.

[41] A. El Zooghby, C. Christodoulou, and M. Georgiopoulos, "A Neural Network-Based Smart Antenna for Multiple Source Tracking," *Antennas and Propagation, IEEE Transactions on*, vol. 48, pp. 768–776, May 2000.

[42] A. Zooghby, H. Southall, and C. Christodoulou, "Experimental Validation of a Neural Network Direction Finder," *Antennas and Propagation Society International Symposium, IEEE*, vol. 3, pp. 1592–1595 vol.3, Aug 1999.

[43] S. Sensorer, P. Zetterberg, and B. Ottersten, "The Spectrum Efficiency of a Basestation Antenna Array System for Spatially Selective Transmission," *IEEE Transactions on Vehicular Technology*, vol. 44, Aug 1995.

[44] S. Ponnekanti and S. Sali, "Application of Antenna Arrays for Spatial Separation in Wireless Systems," *IEEE International Conference on Personal Wireless Communications*, pp. 243–246, Feb 1996.

[45] R. Kozick, F. Elmer, and V. Nalbandian, "Phased Arrays Composed of Antennas With Steerable Patterns," *Record of the IEEE International Radar Conference*, pp. 737–741, May 1995.

[46] M. Kim, W. cheol Lee, J. Choi, and S. Choi, "Adaptive Beamforming Technique Based on Eigen-Space Method for a Smart Antenna in IS2000 1X Environment," *Antennas and Propagation Society International Symposium, IEEE*, vol. 1, pp. 118–121 vol.1, 2002.

[47] W.-C. Lee and S. Choi, "Adaptive Beamforming Algorithm Based on Eigen-Space Method for Smart Antennas," *Communications Letters, IEEE*, vol. 9, pp. 888–890, Oct. 2005.

[48] M. Tao and R. Cheng, "Low Complexity Post-Ordered Iterative Decoding for Generalized Layered Space-Time Coding Systems," *IEEE International Conference on Communications*, vol. 4, pp. 1137–1141 vol.4, 2001.

[49] S. Baro, G. Bauch, A. Pavlic, and A. Semmler, "Improving Blast Performance Using Space-Time Block Codes and Turbo Decoding," *Global Telecommunications Conference, IEEE*, vol. 2, pp. 1067–1071 vol.2, 2000.

[50] S. Al-Ghadhban, R. Buehrer, and B. Woerner, "Outage Capacity Comparison of Multi-Layered STBC and V-BLAST Systems," *Vehicular Technology Conference, IEEE 62nd*, vol. 1, pp. 24–27, Sept., 2005.

[51] S. Al-Ghadhban and B. Woemer, "Iterative Joint and Interference Nulling/Cancellation Decoding Algorithms for Multigroup Space Time Trellis Coded Systems," *Wireless Communications and Networking Conference, IEEE*, vol. 4, pp. 2317–2322 Vol.4, March 2004.

[52] F. Shu, L. Lihua, T. Xiaofeng, and Z. Ping, "A Spatial Multiplexing MIMO Scheme with Beamforming for Downlink Transmission," *IEEE Vehicular Technology Conference*, pp. 700–704, October 2007.

[53] Z. Lei, F. Chin, and Y.-C. Liang, "Orthogonal Switched Beams for Downlink Diversity Transmission," *Antennas and Propagation, IEEE Transactions on*, vol. 53, pp. 2169–2177, July 2005.

[54] F. Zhu and M. Lim, "Combined Beamforming with Space-Time Block Coding Using Double Antenna Array Group," *Electronics Letters*, vol. 40, pp. 811–813, June 2004.

[55] L. lin Wang, S. xun Wang, X. ying Sun, and F. ye Hu, "Combined Beamforming and Space-Time Block Coding for Wireless Communications," *14th IEEE Proceedings on Personal, Indoor and Mobile Radio Communications*, vol. 1, pp. 607–611 Vol.1, Sept. 2003.

[56] G. Jongren, M. Skoglund, and B. Ottersten, "Combining Beamforming and Orthogonal Space-Time Block Coding," *IEEE Transactions on Information Theory*, vol. 48, pp. 611–627, Mar 2002.

[57] C. Shen, Y. Zhu, S. Zhou, and J. Jiang, "On the Performance of V-BLAST with Zero-Forcing Successive Interference Cancellation Receiver," *IEEE Global Telecommunications Conference*, pp. 2818–2822, December 2004.

[58] S. Loyka and F. Gagnon, "On BER Analysis of the BLAST without Optimal Ordering Over Rayleigh Fading Channel," *IEEE Vehicular Technology Conference*, vol. 2, pp. 1473–1477 Vol. 2, Sept. 2004.

[59] R. Knopp and P. Humblet, "Information Capacity and Power Control in Single-Cell Multiuser Communications," *IEEE International Conference on Communications*, vol. 1, pp. 331–335 vol.1, Jun 1995.

[60] D. Tse, "Multiuser Diversity in Wireless Networks," *Wireless Communications Seminar, Stanford University, www.eecs.berkeley.edu/ dtse/ima810.pdf*, April 2001.

[61] L. Technologies, "Throughput Simulations for MIMO and Transmit Diversity Enhancements to HSDPA," *www.3gpp.org/ftp/tsg ran/wg1 rl1/TSGR1 17/Docs/PDFs/R1-00-1388.pdf*.

[62] O.-S. Shin and K. B. Lee, "Packet Scheduling for MIMO Cellular Systems," *The 57th IEEE Semiannual on Vehicular Technology Conference*, vol. 3, pp. 1694–1698 vol.3, April 2003.

[63] P. Viswanath, D. Tse, and R. Laroia, "Opportunistic Beamforming Using Dumb Antennas," *Information Theory, IEEE Transactions on*, vol. 48, pp. 1277–1294, Jun 2002.

[64] M. Sharif and B. Hassibi, "On the Capacity of MIMO Broadcast Channels with Partial Side Information," *Information Theory, IEEE Transactions on*, vol. 51, pp. 506–522, Feb. 2005.

[65] T. Eriksson and T. Ottosson, "Compression of Feedback for Adaptive Transmission and Scheduling," *Proceedings of the IEEE*, vol. 95, pp. 2314–2321, Dec. 2007.

[66] H.-Y. Chen, C.-H. Chuang, P.-C. Yeh, and S. Zummo, "Performance Analysis and Application of Power Allocation Scheme for Vblast Systems under Rayleigh Fading." Paper Accepted for Publishing.

[67] R. T. Compton, *Adaptive Antennas: Concepts and Performance*. New Jersey, USA: Prentice Hall, 1988.

[68] L. Hanzo, O. Alamri, M. El-Hajjar, and N. Wu, *Near-Capacity Multi-Functional MIMO Systems*. UK: Wiley Press, 2009.

[69] S. Loyka, "V-BLAST Outage Probability: Analytical Analysis," *Vehicular Technology Conference, Proceedings, IEEE 56th*, vol. 4, pp. 1997–2001 vol.4, 2002.

[70] S. Sandhu and A. Paulraj, "Space-Time Block Codes: a Capacity Perspective," *Communications Letters, IEEE*, vol. 4, pp. 384–386, Dec 2000.

[71] L. Zheng and D. N. C. Tse, "Diversity and Multiplexing: a Fundamental Tradeoff in Multiple-Antenna Channels," *IEEE Transactions on Information Theory*, vol. 49, no. 5, pp. 1073–1096, 2003.

[72] F. Al-Shalan, *Performance of Quadrature Amplitude Modulation in Nakagami Fading Channels with Diversity*. PhD thesis, King Fahd University of Petroleum and Minerals, Dhahran, Saudi Arabia, March 2000.

[73] J. Jiang, *Downlink Throughput Optimization for Wireless Packet Data Networks*. PhD thesis, Virginia Polytechnic Institute and State University, Virginia, USA, July 2004.

[74] D. N. C. Tse and S. V. Hanly, "Multi-access fading channels - part i: Polymatroid structure, optimal resource allocation and throughput capacities," *IEEE Transactions on Information Theory*, vol. 44, pp. 2796–2815, 1998.

[75] R. Gozali, R. Buehrer, and B. Woerner, "The Impact of Multiuser Diversity on Space-Time Block Coding," *Communications Letters, IEEE*, vol. 7, pp. 213–215, May 2003.

[76] H. Bang, T. Ekman, and D. Gesbert, "A Channel Predictive Proportional Fair Scheduling Algorithm," *IEEE 6th Workshop on Signal Processing Advances in Wireless Communications*, pp. 620–624, June 2005.

[77] V. Hassel, M. Hanssen, and G. Oien, "Spectral Efficiency and Fairness for Opportunistic Round Robin Scheduling," in *Communications, 2006. ICC '06. IEEE International Conference on*, vol. 2, pp. 784–789, June 2006.

[78] R. Jain, D. Chiu, and W. Hawe, "A Quantitative Measure Of Fairness And Discrimination For Resource Allocation In Shared Computer Systems," *ArXiv Computer Science e-prints*, Sept. 1998.

[79] S. Al-Ghadhban, R. Buehrer, and M. Robert, "Uplink Scheduling Criteria Comparison for V-BLAST Users," in *Signal Processing and Its Applications, 2007. ISSPA 2007. 9th International Symposium on*, pp. 1–4, Feb. 2007.

[80] M. K. Simon, *Probability Distributions Involving Gaussian Random Variables: A Handbook for Engineers, Scientists and Mathematicians*. Secaucus, NJ, USA: Springer-Verlag New York, Inc., 2006.

[81] J. Cheng, H. Wang, M. Chen, and S. Cheng, "Performance Comparison and Analysis between STTC and STBC," in *Vehicular Technology Conference, 2001. VTC 2001 Fall. IEEE VTS 54th*, vol. 4, pp. 2487–2491 vol.4, 2001.

Vita

Ahmad Salim was born in 1984 in Saudi Arabia. He received his B.Sc. degree in electrical engineering from the University of Jordan, Amman, Jordan, in 2006. He has achieved the eighth place in the University Qualifying Examination held in Jordan in the year 2005/2006 in the field of electrical engineering covering all the Jordanian universities. In 2007, Mr. Salim joined the M.Sc. program in Telecommunication Engineering at King Fahd University of Petroleum Minerals (KFUPM), Dhahran, Saudi Arabia. His research interests include MIMO systems, iterative receivers, interference modeling and analysis, cooperative communication, and multiuser diversity via scheduling. He has specific interest in some MIMO systems that includes LSSTC, STBC, VBLAST, and WiMAX.

Nationality: Jordanian

Present and Permanent Addresses: Bayader Wadisair P.O.Box 141772, Amman 11184, Jordan.

Telephone No.: +962777971148

E-mail: asalim@live.com